Computational Insights
into
Zebrafish Brain Development
during
Gastrulation

Zur Erlangung des akademischen Grades eines

DOKTORS DER NATURWISSENSCHAFTEN

bei der Fakultät für Physik des
Karlsruher Instituts für Technologie

genehmigte

DISSERTATION

von

Dipl.-Phys. Claude Sinner
aus Ettelbrück

Tag der mündlichen Prüfung: 03.02.2017
Referent: Prof. Dr. Wolfgang Wenzel
Korreferent: Prof. Dr. G. Ulrich Nienhaus

To my sister,
Corinne Sinner

Introduction

Science is the art of observing, rationalizing, and understanding. If we as humans take a step outside, we observe a multitude of different organisms that we commonly refer to as *nature*. One of the greatest achievements in the early days of 19^{th} century was the observation that all of these living organisms have a mutual, smallest unit of organization, the *cell*. These results lead in their most prominent way to the rationalization of the theory of Evolution by Darwin and Wallace, the understanding of the origin of the complexity that we are faced with in any ecological environment. Leaving aside the complexity of macroscopic organisms and their mutual interactions, we understand that each of these organisms itself is formed by a multitude of tissues; groups of cells living next to each other, performing a collective task to ensure the well-being of the organism. In an analogous process to the rationalization of the atom, and the discovery of smaller and smaller elementary particles, we dwell deeper into the understanding of life and matter. Developmental biology has taken on the task to elucidate these developmental processes of organisms. Nowadays, this process and the resolution of the employed microscopy techniques have become so well-resolved that developmental biologists need the help of physicists to further rationalize the observed processes. The boundaries, differentiating biology and physics, are presently being obliterated.

At the beginning of every higher-order multicellular organism stands a complex process known as *embryogenesis*. In this key process, the early organism will develop from a single fertilized cell into a multitude of tissues of various forms, shapes, and ultimately tasks. The earliest and most important result of developmental biology is that the processes taking place during embryogenesis are similar for any vertebrate animal (which are also known as the phylum Chordata). This explains the interest of man in these processes. It is not a self-forgetting quest for knowl-

edge, but just one of the many facets of man to overcome its limitations. Every cell in the organism contains the complete set of DNA that encodes the organism. But in every tissue, we find different types of cells. These cells differentiate by the pattern of which genes they express and produce. These patterns shape and define the task of any cell. Thus, the common mechanics to embryogenesis is *gene expression*. Gene expression is one of the many intercept points where biology and physics meet, the former interested in the consequences of the expression, and the latter interested in the physical and molecular means to achieve this goal.

Depending on the size of the organism embryogenesis can take from several hours only to several weeks. The results in developmental biology are usually obtained from a few fast-growing model organism. The most notable ones are *Drosophila melanogaster* (a fly), *Xenopus laevis* (a frog), or *Danio rerio* (a fish). The results presented in this study have been experimentally observed in *Danio rerio*, commonly known as zebrafish by the group of Steffen Scholpp, from the Institute of Toxicology and Genetics (ITG) at the Karlsruhe Institute of Technology (KIT).

In this work, I want to showcase two interdisciplinary projects in which computer simulations greatly enhanced the understanding of involved physical and biological concepts. The introductory chapter focuses on a large number of concepts new to the general physicist as the computational models and the necessary physical concepts are heavily reliant on the biological systems in question. Both of these works take place in the early developmental stages of zebrafish and elucidate the early stages of brain development.

In the methods chapter I explain in thorough detail the physical models that I either developed or used in a novel context. For both of the works introduced in this study dynamical as well as statistical features were available. Therefore two hybrid simulation schemes have been chosen, as they were the best adapted to the experimentally available parameters. For the first work I developed a computationally inexpensive grid-based tissue simulation scheme using discrete-event simulations. The full parametrization from novel high-resolution microscopy results is explained in detail. The second work modified and parametrized a cellular Potts model and employed it in the novel context of notochord formation.

The first work clarifies whether or not a novel short-range transport method via specialized filopodia is able to form the necessary long-range gradient for the hindbrain, midbrain, and forebrain differentiation. The second work employs a cellular Potts model to clarify whether a single strongly adhesive progenitor cell group is able to shape the early notochord. Furthermore, the work aims at clarifying the formation of the notochord as several competing ideas have currently been formed with the experimental results at hand. I was able to obtain crucial results in regards to the current debate of the role of the LPM cells in notogenesis.

Contents

List of Figures

1 Chapter 1. Embryogenesis

Computer simulations are advancing to become the third pillar of science besides theory and experiment. In this work, I want to showcase two interdisciplinary projects in which computer simulations greatly enhanced the understanding of novel experimental results. This introductory chapter focuses on a large number of concepts new to the general physicist as the computational models and the necessary physical concepts are heavily reliant on the biological systems in questions. Both of these works cover events during the early developmental stages of zebrafish and elucidate the early stages of brain development.

The first work clarifies whether or not a novel short-range transport method via specialized filopodia is able to form the necessary long-range gradient for the hindbrain, midbrain, and forebrain differentiation. The second work employs a cellular Potts model to clarify if a single strongly adhesive progenitor cell group is able to shape the early notochord.

The chapter introduces the necessary nomenclature important in the early embryonal development phases. Furthermore, it gives an overview over the most important parameters of the reactive agents that form the basis of tissue differentiation, the so-called morphogens. Afterward, the most important stages of embryonal development are introduced along with the cellular movements that take place, necessary to understand the role and the formation of the notochord. A short introduction to

the physical sampling methods and computer simulations is given at the end of the chapter.

1.1. Overview

The early phases of the development are completed in just a couple of hours in zebrafish [12]. As each event must be located in a timewise manner, it has become common practice in zebrafish to locate an event at the hours past fecundation (hpf). Initially, the fertilized egg cell divides into two different cells, one of which becomes the embryo, and the other which transforms into the yolk. To not only locate things in a timewise manner, but also spatially, the **animal pole**, the side where the embryo develops, and the **vegetal pole**, the side where the yolk develops are introduced. As the embryo is growing from the animal pole towards the vegetal pole in a thin layer in the early developmental stages, an alternative naming scheme is the % epiboly, the percentage of yolk's surface coverage by the embryo. In figure 1.1, these results are recapped. In this study, I will talk about two different processes. The first one taking place during 30% (4.6 hpf [12, 13]) to 75% (8 hpf [12, 13]) epiboly, and the second during 50% (5.25 hpf [13]) to 100% (10.33 hpf [13]) epiboly. The latter is so peculiar that it has received its own name, the **gastrulation phase**. I will explain gastrulation in more detail in a separate chapter 1.5.

Having explained all the necessary phases of embryogenesis, we can take a further look at what is happening during these phases. In each and every phase the tissue will grow, and it will do so at specific speeds and directions. The cells will start to differentiate into different types of tissues. This differentiation is known as **morphogenesis**. Morphogenesis is a direct reaction of cells towards morphogens, molecules that alter the gene expression in cells. This introduces the next physical question of interest that will be further investigated in this study. How can these morphogens be transported? In chapter 1.2 I will go more into detail on the various means of transport within a cellular environment, and I will lay the foundations to understand a novel way of morphogen transport that we were investigating in the first study that I will introduce in chapter 3.

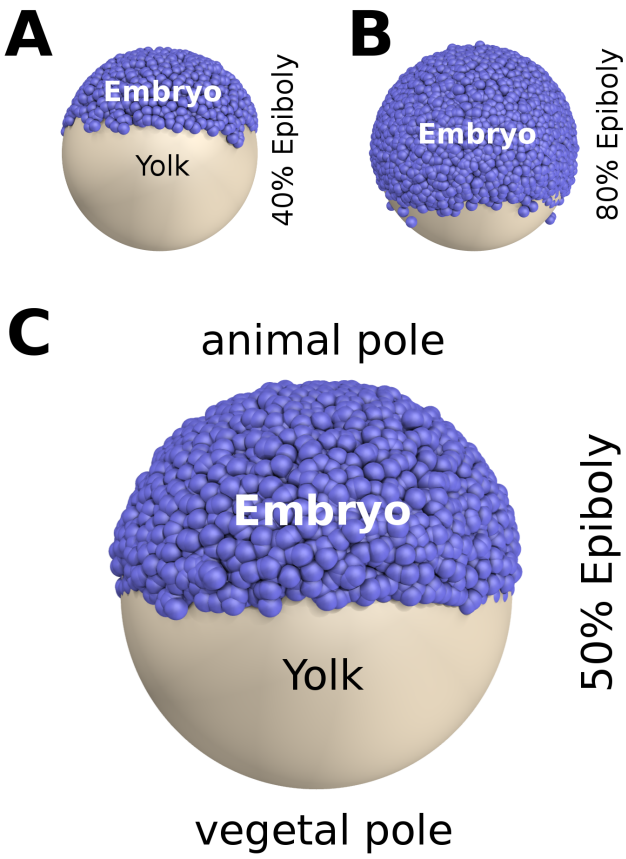

Figure 1.1.: Developmental stages. *During the early developmental stages, the embryo grows from one side of the egg over the yolk. The side of the embryo is known as the animal pole, the opposite side is known as the vegetal pole. The time axis of this progress can either be expressed in hpf (hours past fecundation), or in % epiboly, which describes the percentage of the yolk's surface coverage by the embryo.*

Along with the changes of gene expression, the physical properties of a cell will change [14]. During embryogenesis, the cells are highly motile, and large rearrangements of cells and tissues take place [15]. The most basic parameters in the context of cell motility are the size of a cell and its adhesiveness. The changes of cell adhesiveness and the organization of tissue by differential cell adhesiveness

will lay the foundation for the second study that I will introduce in this work. In this second work, we investigated notochord formation. **The notochord** is the precursor of several parts of the embryo, the most notable one being the vertebral column, the distinctive element of all Chordata. I will further describe the creation of the notochord, notogenesis, in chapter 1.6.

The results presented in this work find their foundations in new experimental approaches that were able to increase the spatial, and timewise resolution of molecular processes in zebrafish embryos [2, 10, 11]. As these experiments still face a resolution limit, only certain cellular properties were accessible. I chose statistical simulation schemes based on the well established Monte Carlo simulation schemes to further investigate these highly complex systems with the parameters that were available to me. I explain the basics of these schemes in chapter 1.7.

1.2. Morphogens and Cellular Signaling

During the early phases of embryonal development, a whole array of molecules is being transported throughout the embryo. The most notable of these molecules are **morphogens**. From a molecular viewpoint, one can classify these molecules as a type of hormone. As such they can either be small molecular compounds, or fully developed proteins. The role of these molecules is to start or alter the expression of different genetic pathways in a cell. A genetic pathway is a set of genes that encode for new proteins that will perform various functions within the cell. The most interesting case is when these proteins themselves act as morphogens, thus providing a self governing and replicating unity. This already attracted the interest of Alan Turing towards this class of molecules [16].

Morphogens can be locally expressed within the cell where it is acting, but are most commonly produced in a source cell or source tissue. During embryogenesis, specific well located tissues will initially form at specific places, and generate a large morphogenetic field that is acting on a large amount of cells, forming larger tissues. One example of such a morphogenetic source would be the Spemann organizer, a cellular organizer that marks the beginning of gastrulation [17, 18], and will be

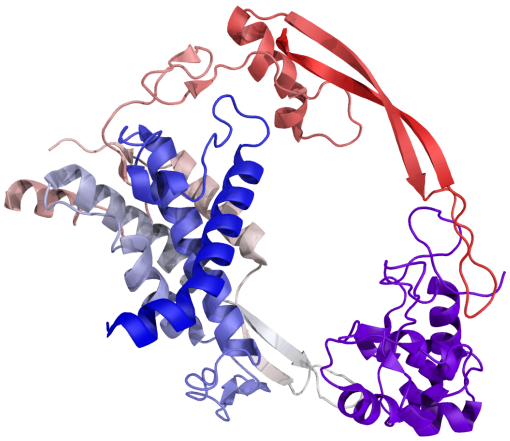

Figure 1.2.: Crystal structure of XWnt8 in complex with its receptor, the cysteine-rich domain of Frizzled 8. *Wnts are lipid-modified morphogens that bind to the Frizzled receptor. XWnt8 in blue and red, Frizzled 8 in violet. Rendering obtained from the structure deposited in the PDB [7] under the ID: 4F0A [8].*

further explained in chapter 1.5.

The morphogen poses several questions from a physical viewpoint. The most interesting physical question for this study is the mode of transport that the newly formed morphogen will take from its source cell towards the target cell where it will be acting [19]. The transport of these molecules can be done in various different ways that will give the organism different means of control over their action and reach [20, 21].

In this regard, one differentiates between different types of transport. Transport can be an active or an inactive process, along with being directed or undirected. The most straightforward mode of transport is diffusion. Diffusion is an inactive, and undirected mode of transport. The organism has no further abilities to alter the reach of the morphogen other than changing the key parameter of the diffusion, the diffusion constant. The diffusion constant depends entirely on geometric properties, e.g., the radius, of the molecule that is transported. Even though diffusion has only this parameter, the organism has a whole range of possibilities to alter this

parameter. One common case, also found in the Wnt pathway, are larger lipid transport vesicles [22, 23]. These vesicles can contain a varying amount of the morphogen, which has a strong effect on the turnover rate of the process [24, 25]. As diffusion is the most basic long-range mode of transport, I will compare my theoretical predictions to results obtained by modeling a diffusive transport. Diffusive transport types for morphogens have been identified in several instances [26], and also in zebrafish [27].

Diffusion is an inactive mode of transport. After the release not much can be done by the body to distribute the molecules. However, there is a whole range of active modes of transport. These modes of transport are very important within an organism to expand the range of stochastic processes towards a deterministic outcome. Often, molecules have to reach precise places. For this, the cell has an array of protein made tubules, so-called actin tubules that are surrounding it and can reach several cellular diameters. These actin protrusions are known as **cytonemes**.

Cytonemes have different modes of action again, an excellent review is found in [21]. They can either form a permanent bond with surrounding cells, in which different molecules can be exchanged, or they can bridge a larger distance and only form a temporary bond. In the first study that I present in this work, I focus on a special subclass of cytonemes that have shown an interesting behavior during zebrafish brain development and in Drosophilia [28, 29]. These special actin protrusions are known as **filopodia** and play an important role in cellular signaling [30, 31]. They grow from a morphogen active cell and can reach in average one cellular diameter. At the tip of these filopodia, morphogens are located. Upon reaching a target, the tip breaks off and the morphogen is transmitted. The formation of these filopodia takes only several minutes as shown in figure 1.3.

In this study, we are interested in the morphogen class known as Wnt. Communication of cells by paracrine signaling is essential for developmental processes, tissue regeneration and stem cell regulation and is also a major cause of diseases such as cancer when this type of communication becomes deregulated. The highly conserved Wnt proteins are important regulators of all of the above-mentioned pro-

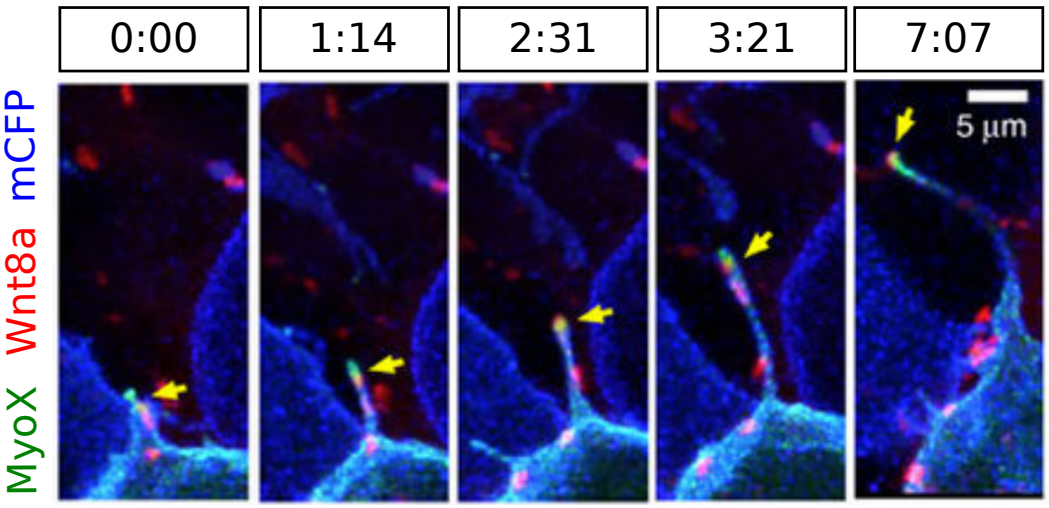

Figure 1.3.: Filopodia growing from a cell. *Filopodia are actin protrusions that grow from the cell. Experimental results suggest that these cellular actin protrusions are not only used for cellular movement but also have an important role in cellular signaling. Time in (minutes:seconds). Text and figure [2].*

cesses reviewed in [32, 33]. Wnt proteins are secreted as palmitoylated glycoproteins and can act as morphogens to induce responses in a concentration-dependent manner [34, 35]. The secretion of Wnt ligand and its presentation at the plasma membrane depends on the function of Evi/Wls [36, 37], the retromer complex [38] and a functional microtubule network [39]. However, there is still considerable debate with respect to the cellular mechanisms, which ensure the controlled release and spreading of Wnt morphogens thereafter. Different transport mechanisms such as diffusion with the aid of carrier proteins [40–42] or exovesicles [43] and more specifically exosomes [22, 44] have been proposed for the passage of hydrophobic Wnt molecules through a tissue. In those models, however, the source tissue has no control over direction and range of the signal after release and indeed these transport mechanisms do not appear to be essential for Wnt gradient formation [44].

1.3. French Flag Model

After having explained how the morphogen is transported, the next interesting question is how cells will react to the morphogen [45]. It would be highly uneconomical and difficult for an organism to have a specific morphogen for each and every tissue. It is much more economical, and therefore more likely, to have a single source of morphogen and several layers of tissues reacting to this single morphogen. The prevailing model that explains this is known as the French Flag Model. Introduced by Lewis Wolpert in 1969 [46], it states that tissues will react differently to different concentrations of morphogens. In this model, the morphogen is produced at a source and forms a gradient. Depending on the gradient of the morphogen that the cells experience, they will differentiate into different types of tissue.

In the first study of this work, we are interested in gradient formation of Wnt8a. This morphogen is produced from 30% to 75% epiboly [47]. The gradient is at the basis of the first large segmentation of the future zebrafish brain into three distinct layers: the hindbrain, the midbrain, and the forebrain [48]. Figure 1.4 illustrates a hypothetical gradient based entirely on diffusion, along with different cells. Furthermore, I show a top view of an early zebrafish embryo head, with the

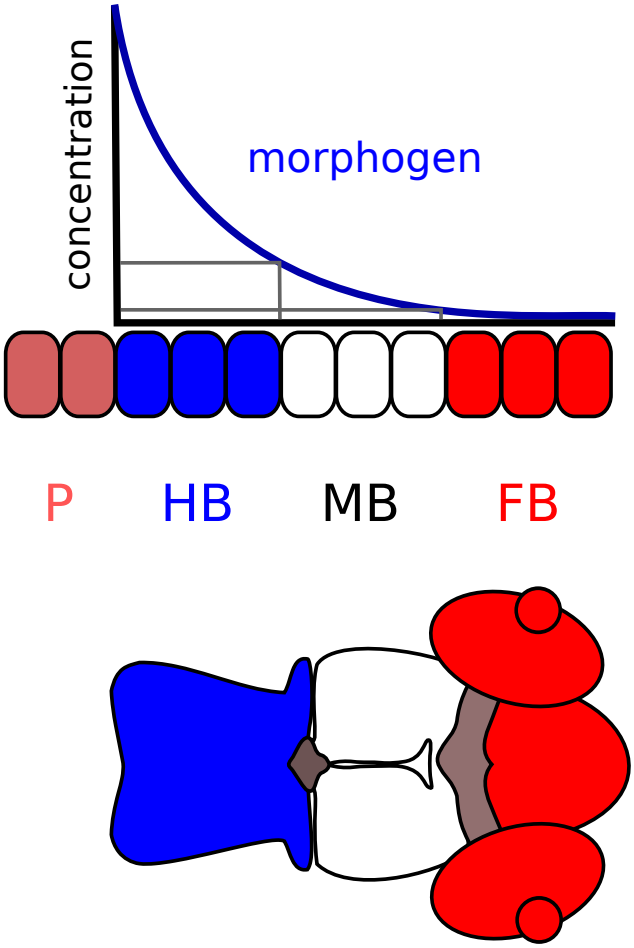

Figure 1.4.: French Flag Model. *French Flag model of a hypothetical gradient. Shown is one cellular layer with morphogen producing cells in violet, the hindbrain (HB) in blue, the midbrain (MB) in white, and the forebrain (FB) in red. The second picture shows a top down (dorsal) view of a zebrafish embryo's head with the different brain section in the same color coding. The embryo is facing to the right, and the very large eyes are part of the forebrain section.*

different brain sections colored with the same color coding.

1.4. Cell Adhesion and Motility

Cells are self-replicating systems with metabolism and represent the smallest units of life. They are composed of organelles and have a whole array of actions they can perform. In the previous chapters, I already explained how important cellular signaling is for cells in a multicellular environment. These are long-range means of communication, in which a signaling molecule is released into a so-called **morphogenetic field**. The morphogenetic field is the part of a tissue in which cells react to the morphogen in question.

But, cells do not only have these long-range modes of communication, they also have direct interaction with their surrounding environment. These interactions are driven by a cell's ability to form and break bonds with next neighbors, along with changing its own shape, hence **cell motility** and speed. The physical properties of a complete tissue are emergent properties of the basic cells that compose it [49]. One of the key parameters in this is **cell adhesiveness**, which is directly influenced by a cell's ability to perform bonds and links with neighboring cells. These interactions are transmitted by the actin network that we have already described in chapter 1.2. Cells also have the ability to sense their surroundings and form preferential attachments due to chemotaxis as a response to signaling molecules. The ability to change its shape, and therefore move or attach to other objects, is defined by its ability to change the surrounding actin network.

The molecular basis for adhesion and therefore also motility of cells are cadherins. Cadherins accumulate at cell-cell contact sites to regulate cell migration and cell adhesion [50]. The main functions of cadherins are reducing interfacial tension of the actin network at a forming cell–cell contact and stabilizing the contact by resisting mechanical forces [51] in a zipper-like fashion. The release of cellular contacts is controlled by deregulating cadherins and inhibiting their function. Protocadherins influence homophilic and heterophilic interactions of cadherins [52] and have been observed to play a role in cadherin recycling [53]. Thus, cellular adhesion is an

interplay between cadherins that promote cellular adhesion and protocadherin that inhibit cellular adhesion. Coupling both produces synergetic effects in cell motility.

The second study presented in this work focuses on the next step of embryogenesis: the organogenesis of the progenitor of the vertebral column, the notochord. Differential cell adhesion and cell motility play a crucial role in the formation of the notochord. A simulation scheme based on the Glazier-Graner-Hogeweg model that only needs relative adhesion strengths and relative motilities is found to be sufficient for explaining the behavior and forms witnessed in experimental results by Steffen Scholpp (ITG, KIT).

1.5. Gastrulation

"It is not birth, marriage, or death, but gastrulation, which is truly the most important time in your life" - is a famous quote by the leading developmental biologist Lewis Wolpert. Gastrulation is the most important phase in embryonal development, when the previously singular sheeted embryo, folds and transforms into a double sheeted layer. This stage starts at 50% (5.25 hpf [13]) and ends at 100% (10.33 hpf [13]) epiboly in zebrafish. By folding, the embryo consists of two distinct layers, each a few cells thick, and the inner and outer body plan comes into existence. The inner layer divides again and a three-fold organization emerges. The outer layer, the ectoderm, transforms into the skin and tissues that later constitute the nervous system. The innermost layer, the endoderm, transforms into most inner organs. The middle layer, known as *mesoderm* gives rise to muscles and the notochord, our target system in the second study. The gastrula is the onset of organogenesis, it is at this stage when the whole body plan of the future organism is defined [54].

The onset of gastrulation is marked by formation of the Spemann organizer [17]. An organizer is a group of cells that actively produce morphogens and determine the fate of a large group of cells. The Spemann organizer forms between the animal pole and vegetal pole at 50% epiboly. As soon as cells from the animal pole reach this point, they receive a signal to move inwards. This inward movement is known

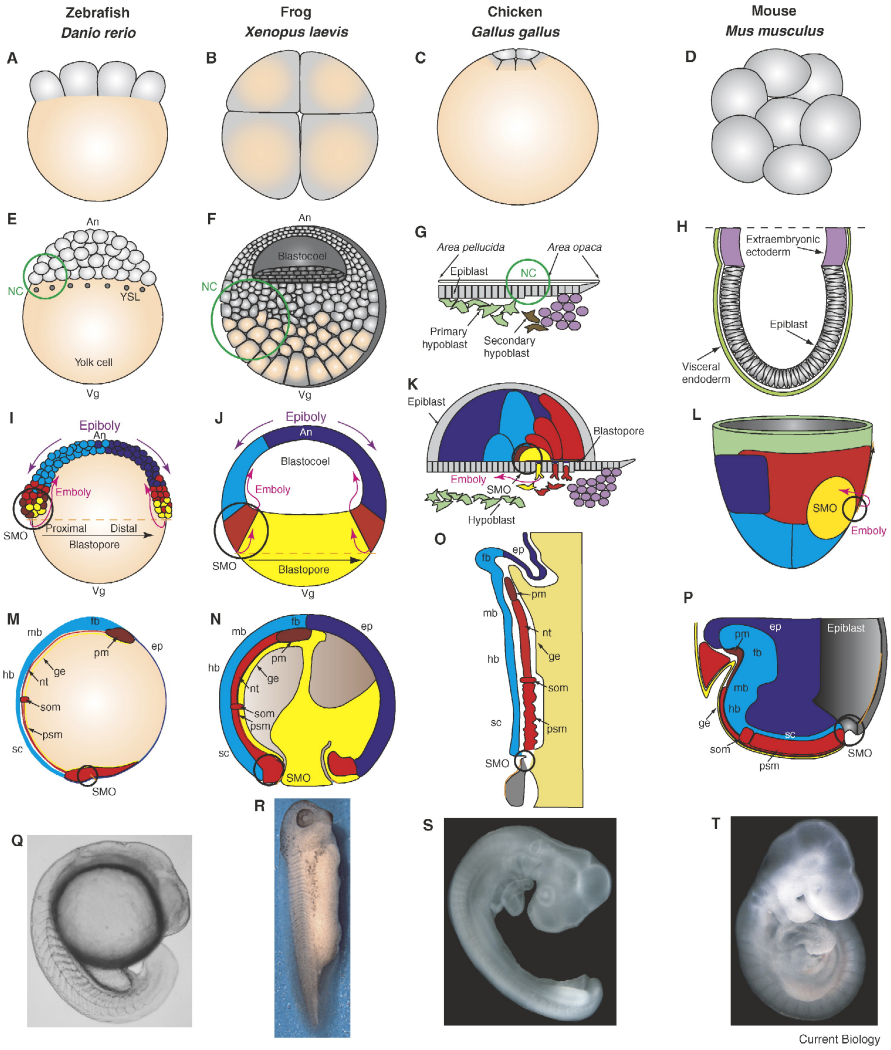

Figure 1.5.: Cleavage, blastula and gastrula stages of four vertebrate model organisms. *Developmental stages of zebrafish (A,E,I,M,Q), the frog Xenopus laevis (B,F,J,N,R), the chick (C,G,K,O,S) and the mouse (D,H,L,P,T). Cleavage, 8-cell stages (A-D). Note the incomplete cleavage in zebrafish (A) and chick (C) and the complete cleavage with differently sized blastomeres in Xenopus (B), and uniformly sized blastomeres in the mouse (D). Early blastula (E–H), late blastula–early gastrula (I–L), late gastrula (M–P) and pharyngula (Q–T). The position of the Nieuwkoop center (NC) and its equivalents is shown at cleavage stages and the position of the Spemann-Mangold organizer region (SMO) at early and late gastrula stages. Colors: light gray, cytoplasm; beige, yolk; dark gray, epiblast region of amniote embryos; red, mesoderm and its precursors; dark red, prechordal mesendoderm; yellow, definitive endoderm and its precursors; dark blue, epidermis; lighter blue, neuroectoderm; green, brown and violet, various extraembryonic tissues; orange, blastopore. Abbreviations: ep, epidermis; fb, forebrain; mb, midbrain; hb, hindbrain; sc, spinal cord; nt, notochord; pm, prechordal mesendoderm; som, somite; psm, presomitic mesoderm; ge, gut endoderm; an, animal; vg, vegetal.* ***Reprinted from Conserved patterns of cell movements during vertebrate gastrulation, 15(6), Solnica-Krezel, Lilianna: 213-228, ©2005, with permission from Elsevier*** *[9].*

as *ingression*. Subsequently, the cells change direction and use the outer layer as a substrate to move back upwards toward the animal pole. This backward growing layer is known as hypoblast and transforms as already said into two distinct layers, the endoderm and the middle layer, the *mesoderm*.

The mesoderm is nearly a cell monolayer and the starting point for most muscular tissues, and most notably the notochord. The notochord is the most prominent hallmark of the phylum Chordata and serves as common embryonic midline structure for all of their members, including humans. It plays a central role in the genesis of the vertebral body, as it serves as an embryonic scaffold for the surrounding mesoderm to subsequently form the skull, the membranes of the brain, and, most importantly, the vertebral column [55]. The notochord is an organ of a rod-like structure. Later in embryonal development, this rod-like structure induces the formation of the neural tube. Differential cell adhesion and cell motility play a crucial role in the formation of the notochord.

1.6. Notogenesis

The process in which the notochord forms is known as *notogenesis*. The notochord defines the axial structure of all vertebrates during development. Notogenesis is a result of immense cell rearrangements in the mesoderm, the convergence of the lateral cells, and the elongation of the axial cells. From a physical viewpoint, it is an interesting system, as it is only defined by the interaction of four different cell types [56]. In figure 1.6, these four cell types are shown at the onset of gastrulation, and at the end of gastrulation. The outer epithelial layer (yellow) is known as the prechordal plate mesoderm (PPM). The adhesive forces of the PPM are the strongest in this system as it acts as a skin layer. The PPM serves as a front towards the animal pole of the growing mesoderm. The cell group labeled in green is the most important of the four cell groups. We define them as notochord tip cells (NTC). They have a higher motility than any of the other groups, coupled with a higher cell adhesiveness. Therefore, we hypothesize that these cells are crucial for the exact formation of the notochord. In red and gray we have the lateral plate

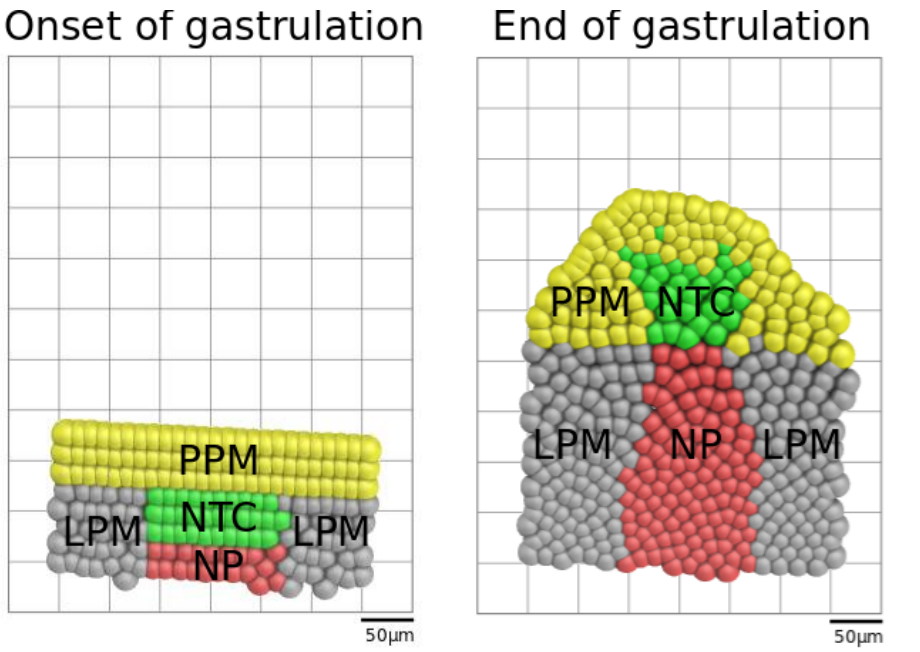

Figure 1.6.: Notochord at the onset and end of gastrulation. *The notochord is a cellular system composed of four cell types: prechordal plate mesoderm (PPM) (yellow), notochord tip cells (NTC) (green), lateral plate mesoderm (LPM) (gray), and the axial notochordal plate (NP) (red).*

mesoderm and the axial notochordal plate. Physically, these two cell types do not differ from each other, but their cellular fate does, as only the axial notochordal plate cells (red) turn into the notochord. Prior to this study, the formation of the notochord was highly debated.

It is unclear if the axial notochord forms by the LPM (gray) pushing inwards, or if the physical behavior of the NTC is sufficient for notogenesis. I implemented a modification of the cellular Potts model (CPM) [57], a so-called Glazier-Graner-Hogeweg model (GGH) [58], as a minimal system to test whether the physical properties of the NTC are sufficient for the shaping of the notochord or not.

1.7. Computer Simulations

The last 50 years brought incredible progress and the ubiquitous availability of computational power established computer simulations, that is, "in silico experiments", as a new paradigm or "third fundamental pillar" besides theory and experiment. Nowadays, scientific progress in fields as diverse as high-energy physics, automotive or airplane engineering, materials sciences, climate simulations, or the aforementioned quantum chemistry is driven by computer simulations, which allow calculations and predictions with high accuracy. For different situations and types of inputs, different simulation schemes have been developed. Not every parameter of the system in question is always accessible, nor do we necessarily know the exact time evolution of a system. Statistical physics expanded the array of possible simulations through the introduction of phase space. With the tools provided by statistical physics, it is possible to sample a system through the knowledge of its energy function. It is the opposing extreme of dynamical simulations.

For both of the works introduced in this study, dynamical as well as statistical features were available. Therefore, two hybrid simulation schemes have been chosen, as they were the best adapted to the experimentally available parameters. In the first study related to the deposition and spread of a morphogen, the dynamical boundary conditions were quite clear. The system can be parametrized into different time steps in which a specific amount of events are possible. For this,

a *discrete-event simulation* (DES) was a good choice. In the second study, the parametrization of an energy function to describe relative velocities and adhesive forces is straight forward, but the system needs to be extended by a force term. The GGH model was the best choice for achieving this as it was the only model that could be parametrized with the available measurements. It is an extension of the CPM. Both of these models are further explained in chapters 2.5 and 2.6.

Discrete-Event Simulation For the spread of morphogen, it was relatively easy to describe the behavior of the involved cells in single cell experiments. These experiments were capable of determining for every cellular behavior a probability of occurrence per second. In a discrete-event simulation (DES) a system jumps from one state to the next, after the occurence of a specific event. As I coupled this with the experimentally obtained probabilities, the time scale of the simulation was conserved.

The simulation cycles through each cell of a tissue and attempts the possible cellular events, i.e., cell division, cell migration, filopodium generation. Consecutively, it models the behaviors of producing layer and receiving morphogenetic field. The producing layer respects the rates for morphogen deposition and the morphogenetic field respects rates for tissue growth and cellular motility.

Events are accepted with a probability p_{event}

$$p_{\text{event}} = \begin{cases} 1 & \text{r} < p_{\text{effect}} \\ 0 & p_{\text{effect}} \leq \text{r} \end{cases} \tag{1.1}$$

Even though the number of cells is large in these simulations, the nature of these equations keeps the computational effort at a minimum. The probabilities are stored in a lookup table, and one only has to cycle trough these events and only do a relatively cheap random number generation.

Metropolis-Monte-Carlo By describing the system through a Hamiltonian H, it becomes possible to describe the statistics of a system through Monte-Carlo methods. In a Monte-Carlo scheme, the system hops randomly between any admissible state of the system. This is of computational interest if it is easy to generate a new conformation, but impossible of finding the next lowest energy in rugged landscapes. One example for the application of Monte-Carlo sampling would be the use in protein folding [59]. If it is easy to find the next lowest conformation in very smooth landscapes, the Metropolis acceptance criterion is of interest as acceptance rates for proposed moves are high.

The probability $p(\gamma \to \gamma')$ for switching from a state γ to a state γ' reads as

$$p(\gamma \to \gamma') = \begin{cases} e^{-\frac{\Delta H_{\mathrm{Tot}}}{T}}, & \text{if } \Delta H_{\mathrm{Tot}} \geq 0, \\ 1, & \text{if } \Delta H_{\mathrm{Tot}} < 0. \end{cases} \tag{1.2}$$

with the 'difference of energies' between old and new conformation ΔH_{Tot} [60] and the temperature T.

The parametrization of cells by an energy function to describe relative velocities and adhesive forces is straight forward. For our applications of notogenesis this basic system, known as cellular Potts model needs to be extended. The Glazier-Graner-Hogeweg model, an extension of the CPM, was the best choice for achieving this. It is an extension of the CPM. Both of these models are further explained in chapters 2.5 and 2.6.

Chapter 2.
2 Methods

For both of the works introduced in this study, dynamical as well as statistical features were available. Therefore, two hybrid simulation schemes have been chosen, as they were best adapted to the experimentally available parameters, a discrete-event simulation and the Glazier-Graner-Hogeweg model.

For the formulation of the DES, simulation events are defined and parametrized. These events can be split into morphogen related events and tissue related events. An introduction to current tissue simulation schemes is given along with their limitations to rationalize the exact choice of model. I introduce a grid-based simulation scheme, as none of the other schemes could be parametrized with the available experimental results. The parametrization of the model from experimental results is explained in detail.

Notogenesis is a result of immense cell rearrangements in the mesoderm, the convergence of the lateral cells, and the elongation of the axial cells. However, it is currently not known how these processes act together in a coordinated way. The parametrization of the system from relative cell motility and cell adhesion is possible through the CPM which is introduced in this chapter. An exact explanation for each of the terms in the Hamiltonian is given. As notogenesis relies on directed cohort cell migration the model needs to be modified into the GGH model. The existing theoretical background for modifying the CPM Hamiltonian is described in detail.

2.1. Morphogen Transport

The upkeeping of Moore's law [61] since its formulation up to the present day, and the subsequent falling prices have rendered computational power a ubiquitous resource for nowadays science. With the increasing power of these computational systems, more and more complex questions can be answered with computational *in silico* methods. Biological systems are by their very nature large systems of high complexity. They are composed of a large number, in a quantitative as well as a taxonomic way, of molecules or cells. Nevertheless, recent advances of computational power could render these problems within the reach of solvability.

The modeling of morphogenetic fields and organogenesis is faced with two different problems. The first is the correct distribution of the morphogens and molecules in question. The second is to correctly model tissue reshaping, cellular rearrangements, and cell motility. We are therefore faced with a twofold problem, first to correctly model our substrate, and second, with modeling the substance set free into this substrate. Furthermore, as morphogenetic changes will take place from the earliest embryo on up to the fully developed organism a large range of scales has to be covered. The scales can range from a few cell layers only, in an early tissue, up to several layers of tissue or macroscopic entities, i.e. limbs [52]. The last important problem is the resolution of experiments, the number of parameters a model has to capture and the experimental availability of these parameters.

For this large range of scales, different simulation schemes have been developed. An excellent review of the currently available models for substrate behavior and growth has been published by Tanaka [62]. The following paragraph will resume the most important points to further elucidate my exact choice of simulation schemes. For the projects of this thesis two schemes have been chosen as giving the best available insights with the least amount of parameters, they will be further explained in the following paragraphs.

2.2. Tissue Simulations

Several tissue simulation schemes have been developed recently as a new field of interest is emerging in science. These different methods all come at different resolutions and computational expense, ranging from continuous substrates or finite elements towards complete cells with molecular details. A great review of the current methods is found in [63] and the following short paragraph recapitulates the main points. Substrate simulations can be classified into the following categories: continuum models with finite elements, coarse-grained cellular models, vertex models, and continuous cell models in varying resolution.

The continuum model is a great model when the dispersal of a morphogen, or multiple morphogens, can be explained in an analytical way using diffusion. In this model, only the crude shape of the organism plays into the simulation. The organism is simply visualized as consisting of a homogeneous physical material. The substrate is represented as a soft incompressible and hyperelastic substance. As long as cellular rearrangements do not play a role, this method is the least expensive to produce valuable insights. It has been used to study many morphogenetic processes ranging from stress-dependent bone growth [64], to brain morphology development [65]. As our experimental procedures captured physical properties on the cellular level, I did not choose this method.

Spheroid models would be the next step to increase the resolution of the tissue simulation. In this type of simulation, the cells are represented by rigid spheres or ellipsoid shapes to incorporate cell polarity into the model. It has been shown that cells can be modeled by the Johnson-Kendall-Roberts (JKR) theory for adhesive spheres [66]. In this model, cells lose their mutual contact at a larger distance than the one where they engaged in a mutual contact. Nevertheless, the model has also been applied and yielded results with simpler potentials, like simple harmonic springs [67]. Not only has this model a higher resolution, but we have to keep in mind the way how it is computed is completely different from the prior method. The use of a force in simulation always results in the necessity for an integrator to advance the simulation from one time step to the next. While this model is computationally simple, the quantification of these forces is not always a trivial task

for an experimentalist. As we were unable to obtain absolute values for adhesive forces of the cell types involved in our notochord project, I chose another model that could be fully parametrized with the knowledge at hand. Spheroid models are a great way of getting insights at the tissue level of organogenesis, but you need to have a lab at hand that knows both how to handle the cell cultures and an atomic force microscope.

The continuous model was not suitable for simulating the filopodia related deposition of morphogens as this model lacks the explicit representation of cells. Furthermore, the spherical model was not suitable either as the parametrization for the cellular adhesion forces are missing at the current time. Therefore I chose to use a hybrid model by simulating rigid spheres on a fixed grid. This model is not a dynamic model, but it does have a time scale because of the DES. The exact model will be explained in more detail in chapter 2.4. For the formulation of this model, we need a probability for two cells to change place and a probability of tissue growth. These two parameters and the protocol of parametrization will be explained chapter 3.3 and chapter 4.2 respectively.

Computationally, any model has to deal adequately with the interactions between different cells and avoid overlaps in their representations. When raising the complexity of the cellular representation, and allowing for cellular motion, it is the easiest to give up the intercellular cavities and simply represent the tissue by a vertex model [68]. In this model, each cell is represented as a polygon or polyhedron where the vertices of each surface are shared between neighboring cells. This model is only suitable for densely packed tissues, as well as tissues that have high adhesiveness such that no cellular displacements will happen. Epithelial tissues are a good candidate for this model. As our systems did not qualify entirely as epithelial tissues, this method was not suitable.

Another method of avoiding overlaps, but increasing the resolution of the cell while keeping the intercellular cavities is to calculate on a grid. If we do this, it is also not an option to stick with dynamic integrators, but one has to abandon molecular dynamics completely and start sampling the model with statistical methods. The model in question is known as the cellular Potts model (CPM). This

model is also known as Glazier-Graner-Hogeweg model after its most important contributors. In this, cells are represented as occupying several grid spaces. A time step does not exist, but the statistics of the model is sampled by the Metropolis Algorithm. For this, a representative Hamiltonian is defined that assigns an energy to each state. The model is similar, but not identical to the Ising model [69, 70], and an adaptation of the Ising model's many spin formulation, the Potts model [71–73]. As this model was suitable to be formulated with our experimentally accessible quantities it was my model of choice to gain further insights into the questions raised for notogenesis. As such, it will be described in further detail, with a complete explanation of all its parameters in chapter 2.5.

2.3. Diffusion

As already introduced in chapter 1.2, several modes of transport exist for morphogens. Besides transport by filopodia there is a whole range of free diffusion with carrier proteins [40], exovesicles [43] or exosomes [22, 44]. For the filopodia simulations, it was essential to compare the obtained results with hypothetical results for the case of a diffusive transport. These results could show possible ambiguities in our results, or make a clear case for a transport by filopodia. These verifications have been done with the aid of Jakob Rosenbauer.

The diffusion equation for a concentration C at the place x and time t for a medium with non-growing domains reads as:

$$\frac{\partial C}{\partial t} - D\frac{\partial^2 C}{\partial x^2} = 0 \tag{2.1}$$

with the diffusion constant D. The diffusion constant depends on the geometrical properties of the morphogen.

Since the tissue is a growing and expanding medium, we have to alter equation 2.1. After Reynold's theorem, the diffusion equation for a growing domain [74, 75] is

$$\frac{\partial C}{\partial t} + u\frac{\partial C}{\partial x} + C\frac{\partial u}{\partial x} - D\frac{\partial^2 C}{\partial x^2} = 0 \tag{2.2}$$

with the growth field u. The growth field u describes the advection term. As our cells are incompressible we can disregard the term proportional to $\frac{\partial u}{\partial x}$. For our problem of a growing tissue with length $L(t)$ u is found by

$$u = \frac{dx}{dt} = \frac{\frac{\partial L(t)}{\partial t}}{L(t)} \tag{2.3}$$

The exact derivation is found in appendix A. These simulations were solved with a numerical solver that is also described in appendix A and provided the results for diffusion in chapter 3.3.1.

2.4. DES of Filopodia

Each and every of the aforementioned models requires a specific set of parameters. As the way the system is sampled varies in each of these models, i.e., statistical versus dynamical, some of them require time-resolved results, while others are fine with absolute values of force or even just relative values of force. Experimentally, it was possible for the group of Steffen Scholpp to resolve time-related parameters of morphogen deposition by filopodia [2]. The exact experimental procedures are introduced in more detail in chapter 3.1. The early zebrafish brain development takes places 30% to 80% epiboly. In this time frame, we had average results for the frequency of formation of filopodia, a distribution of their reach, and a distribution for their angle of formation. The nature of these results suggests the use of a discrete-event simulation as explained in chapter 1.7.

For each effect, the probability of occurrence per time step is required and drawn from the respective experimental distribution. The simulation proceeds by the Monte-Carlo algorithm, this means that a random number r $\in [0, 1]$ is taken

and compared to the desired probability p_{effect} of an effect, e.g., production of a filopodium. When r is smaller than p_{effect} the event is accepted, when r is larger or equal to p_{effect}, the event is discarded.

$$p_{\text{event}} = \begin{cases} 1 & \text{r} < p_{\text{effect}} \\ 0 & p_{\text{effect}} \leq \text{r} \end{cases} \tag{2.4}$$

Any further statistical measures linked to this effect are drawn from an experimentally measured distribution. For example, the formation of a filopodium is decided with the Monte-Carlo algorithm and $p_{\text{formation}}$, but the necessary length and angle of formation are drawn with the respective distribution from the experimentally measured distributions. The probability to produce a filopodium within a time step can be computed by

$$p_{\text{formation}} = \frac{C_p \cdot N_p}{T_{sim}} \tag{2.5}$$

with the number of contacts per producer C_p, the number of producing cells N_p, and the simulation time T_{sim}. After formation, the Wnt molecule is then attributed to the closest consumer cell, if the filopodia's length is long enough to reach the cunsumer cell's surface. As I chose to compute on a grid, sometimes unnaturally large cavities form far away from any cell. For this case, I introduced an additional *commitment length* that I set to roughly 10% of the total filopodium's length. A further argument in favor of the commitment length is that we have to keep in mind that the filopodium is not a static thing growing into a specific direction and way, but it will move and thus might reach a little longer than the actual distribution of actual deposition shown. Therefore, if an additional distance to the surface of a consumer cell does not exceed the limit of 2 μm, signaling will still occur. The numerical choice for this parameter only reflects the order of magnitude of the effect.

While the production of filopodia is straightforward in this model, the tissue simulation is not. A continuous model was not suitable for simulating the filopodia

related deposition of morphogens as this model lacks the explicit representation of cells. Furthermore, the spherical model was not suitable either as the parametrization for the cellular adhesion forces are missing at the current time. Therefore, I chose to use a hybrid model by simulating rigid spheres on a fixed precomputed grid. For the cell dynamics I had to parametrize the tissue growth and possible mixings of cells, as the density in a growing embryonal tissue is first of all not as high as to keep cells in fixed positions, and second, the initially very thick embryo will flatten and several tissue layers will compact to only a few layers. The model's success will, therefore, depend on the parametrizability of these two events, and the ability to bring them into a probability per time step.

Fortunately, the formulation of tissue growth in a probabilistic way is straightforward. During the simulation, the tissue is growing from a number of cells n_0 to a number of cells $n(t)$ within the time t. Furthermore, as we only consider the expansion from the animal pole to the vegetal pole, we will keep the tissue thickness perpendicular to the axis of spread as constant. Therefore, our tissue will simply expand from a thickness D_0 to a thickness $D(t)$ within the time t. I simplified the overall geometry of the problem by this approximation. I think that it is a safe assumption as the brain will only form at one side of the embryo, and one can disregard the circular shape of the tissue. Still, more elaborate simulations are planned, where the curvature and real shape of the embryo should be taken into consideration. The cellular growth is of exponential nature and we can relate the introduced parameters for the probability of growth p_{division} by

$$p_{\text{division}} = \frac{\ln(2) \cdot \log_2\left(\frac{D_F}{D_0}\right)}{T_{\text{sim}}} \tag{2.6}$$

with the complete simulation time T_{sim}, the initial tissue thickness D_0, and the final tissue thickness D_F. Furthermore, there are two different causes for growth in the early zebrafish embryo tissue during the 4.6 hpf and 8 hpf stages. The first one is a flattening of the early embryo that resides at the animal pole from several tissue layers to only two layers before gastrulation as shown in chapter 1.5. The second is the natural growth of the zebrafish tissue by cell division. The number of

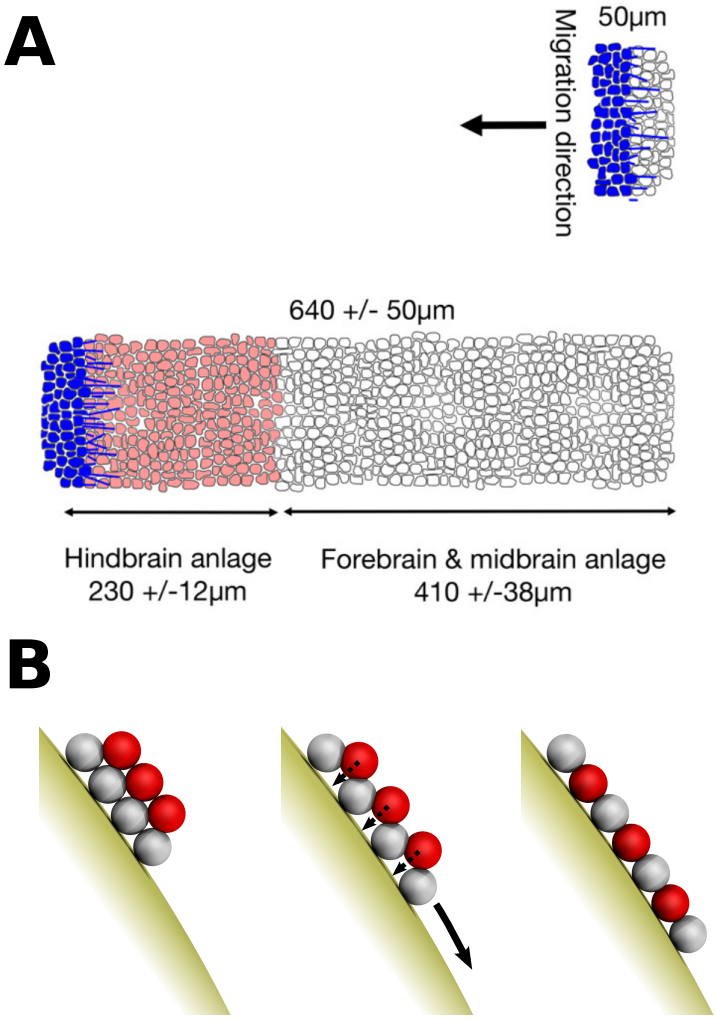

Figure 2.1.: (A) Tissue growth. *Our simulations cover the time from 4.6 hpf to 8 hpf. In this time, the tissue grows from a thickness of 50 µm to 600 µm.* **(B) Visualization of cell insertions.** *Initially the embryo consists of many cell layers. Here we show two example layers. Cells from the red cell layer insert into the tissue. A net growth of the tissue is observed. As both layers have the same distance from the source they will have similar Wnt contents.*

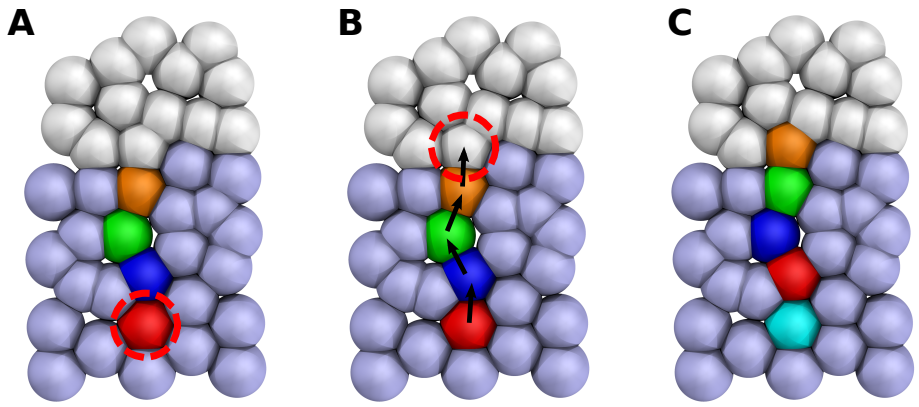

Figure 2.2.: Tissue growth algorithm. *Visualization of the tissue growth algorithm for an example path. The Wnt content is represented by different colors. The tissue is shown in light blue, with no specific information of the exact Wnt content, and empty grid positions by white cells. (A) First, a site where a cell will be introduced is chosen (red circle, and red cell). (B) All of these cells move across the shortest path to the nearest empty grid spot (red circle). (C) All the Wnt contents are moved accordingly, and a new cell (cyan) is introduced at the initial cell spot.*

cells is about 3 000 at 4.6 hpf (30% epiboly [13]) and about 13 000 at 8 hpf (80% epiboly [13]) [10]. For the simulation of the Wnt distribution, it is only important to look at the changes of cell fates that these two effects have. In the case of the intercalation of tissue layers, it is safe to assume that geometrically the introduced cell is at a similar distance to the source of Wnt and will have a similar morphogen content as the surrounding cells of the grid space where we introduce a new cell. In the case of cell division it is a safe assumption that the daughter cells will have the same fate as the parent cell, especially later on, when cell division becomes a more frequent and important effect than intercalation. Therefore, the Wnt content was always copied when introducing a new cell into the tissue regardless of the origin of the new cell. All of these simplifications have been done with the idea of producing the simplest and most effective model from a computational point of view.

After defining the probability for the introduction of a new cell, and explaining the microscopic origins of the new cells, along with their effect on the Wnt distribution, only one last thing is missing to understand the complete algorithm of tissue growth as employed in my DES: the algorithm to introduce new cells. First of all, I did not implement a refined algorithm that takes into account the meiosis cycle. If I had done so, each cell would cycle through the division cycle, and every twenty minutes within the simulation, a division would become more probable. For the aforementioned nondifferentiation between insertion and division, I have not implemented such an algorithm. The probability given in equation 2.6 is the probability per cell per time step. It effectively gives the number of divisions or insertions that have to happen in a given time step to keep up with the observed pattern of growth. Therefore, the simulation would cycle in each time step through every cell, and attempt one of these growth events to happen. This may not be the case for divisions, as already explained, but for the insertions, it is the correct description, as we do not know where an insertion will happen. They can happen anywhere in the tissue at any time. The differentiation between division and insertion, therefore, becomes kind of obsolete. After the growth event has been successful at a given place, the offsprings are placed at the locality of the parent cell and one of its neighbors. Subsequently, the shortest path to the closest empty cell spot is constructed to make room for the newly introduced cell. The neighboring

cells are driven from their initial localities in a cascading event and translocated towards the empty spot. In order to do so, a path is constructed that consists of a series of next neighbouring cells towards the empty spot. The Wnt content of each cell is passed on along this path until the final cell in the series occupies the empty cell spot. A graphic explanation of this algorithm is shown in figure 2.2.

Displacements of cells caused by tissue layer insertions are not the only cellular movements observed during early embryonic stages. As the tissue density is not high enough to compact tissues, and a certain flexibility is needed for these large-scale rearrangements, one will observe individual cell motility. This means that cells move around and lose their specific neighbors. Within my grid mechanics, this effect can be effectively described by a probability p_{motility} of two neighboring cells switching their respective grid places.

There are two ways of calculating this value. The first is to look at real cell motility and cell speeds v_{cell} within a tissue, and calculate from this speed an average velocity of the cell. This value needs to be refactored to cell diameters $d_{\text{cell}} = 16\mu m$ per time step, or basically, the probability of moving one cell further within a single type step:

$$p_{\text{motility}} = \frac{v_{\text{cell}}}{d_{\text{cell}}} \tag{2.7}$$

This only gives an estimation for the definition of this parameter. With high-resolution microscopy it is possible to find a more refined value for this parameter, the reasoning on how to do this are explained in the following. A recently published study by the research group of Prof. Nienhaus (CFN, KIT) [10] released a high-resolution time tracked light scan of a zebrafish in development. In this study, the placement of cellular centers was tracked in 500 individual scans. A collaboration at the (SCC, KIT) further refined these static results computationally to identify and map exact cellular movements and turn them into a dynamic dataset of the full early development [76, 77]. Every single cell was tracked in 50-second intervals from 40% epiboly up to the end of gastrulation and beyond (about 12 hpf). Figure 1.1 shows in panel A the 40%, in panel B the 80%, and in panel C the 50% epiboly

stages as calculated and rendered from these results.

With the knowledge of how cells move in a dynamic way from frame to frame, one is able to construct a next-neighbor tree. With this tree, it is possible to look at the time each of these contacts remains. In figure 2.3 I report the times for the neighborhood lifetime with a logarithmic plot and in minutes. In figure 2.4 I report the times for the neighborhood lifetime with a linear scale. If one considers these neighborhoods to act like independent entities that decay, an exponential decay can be fitted to these lifetimes. From the fit parameters, one obtains the half-life of the decay. This half-life can be transformed into a probability of decay. In figure 2.3 we see a strong difference between both fits. The red fit is taken along each of the lifetimes, in contrast to the green fit where I exclude the prominent first peak. In the absolute results in 2.4 one sees that the red fit mainly captures the initial peak, which is solely caused by short term neighbor losses and fluctuations. Neither these quick fluctuations, nor the long scale changes, should be included when determining the average motility. Therefore, preference was given to the green fit. From this one obtains a probability $p^{\text{exp.}}_{\text{motility}}$ for the loss of a neighbor in the experimental results.

The experimental motility that we observe and the probability $p^{\text{exp.}}_{\text{motility}}$ is influenced by two different base factors. We have to keep in mind that this parameter is a combination of neighborhood-loss due to true cell motility and motility caused by pushing tissue when cell insertions or cell divisions happen within the tissue. This plays an especially large role in our grid-based simulations as cell insertions or divisions push a large number of cells, and easily cause a large number of neighborhood losses. The true cell motility $p^{\text{sim.}}_{\text{motility}}$ that we are looking after is found by subtracting the neighborhood loss by tissue growth p_{pushing} from the experimental results:

$$p^{\text{sim.}}_{\text{motility}} = p^{\text{exp.}}_{\text{motility}} - p_{\text{pushing}} \tag{2.8}$$

The probability p_{pushing} cannot be disentangled in the experimental results, but it is possible to give an analytical derivation of p_{pushing} for my grid-based simu-

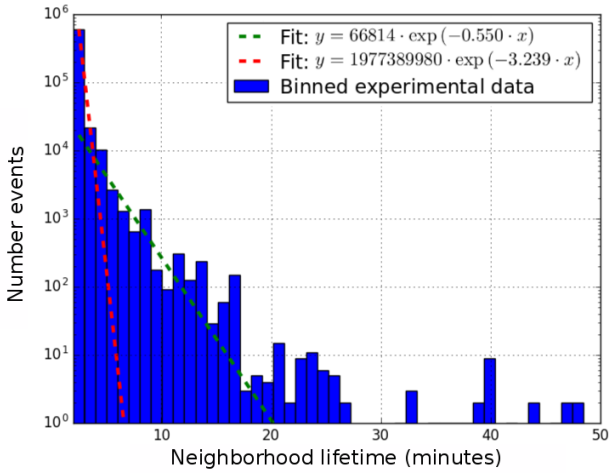

Figure 2.3.: Histogram of the neighborhood lifetimes in minutes with a logarithmic scale. *Histogram of the neighborhood lifetimes extracted from the time tracked light scan. [10]*

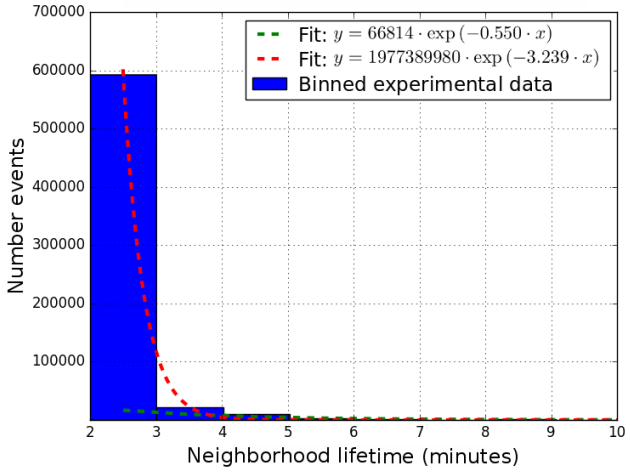

Figure 2.4.: Histogram of the neighborhood lifetimes in minutes with a linear scale. *Histogram of the neighborhood lifetimes extracted from the time tracked light scan. [10]*

lations. All of the following considerations are done for a line of cells of length L with L different cells. In each time step we know the probability for cell division to occur, which is as previously explained p_{division}. This value is constant throughout the simulation. The probability for neighborhood loss through pushing cells does not only depend on the probability of a cell to divide, but it also depends on where this division occurs. If the first cell of the sequence L is to divide, this cell and all the subsequent cells, i.e. L cells, lose their neighbors. If the second cell is to divide, this cell and all of the following $(L-2)$, i.e. $(L-1)$ lose their neighbors. In the first case we have L neighbouring loses with a probability p_{division}. In the second we have $L-1$ cells losing their neighbors, but there is the probability for this to occur by the first cell dividing or the second cell dividing. Therefore we have $L-1$ losses of neighbors with the probability $2 \cdot p_{\text{division}}$. We observe the pattern:

neighbor losses	**weight**
L	p_{division}
$L-1$	$2 \cdot p_{\text{division}}$
$L-2$	$3 \cdot p_{\text{division}}$
...	...
$L-(L-1)$	$(L-1) \cdot p_{\text{division}}$

These are the addends for obtaining the required probability p_{pushing}:

$$p_{\text{pushing}} = \frac{p_{\text{division}} \cdot \sum_{n=1}^{L-1} (L-n)(n+1)}{\sum_{n=1}^{L-1} n} \tag{2.9}$$

With the gaussian summation formula [1] we obtain:

[1] In this case: $\sum_{n=1}^{L-1} n = \frac{L \cdot (L+1)}{2}$ and $\sum_{n=1}^{L-1} n^2 = \frac{L \cdot (L-1) \cdot (2L-1)}{6}$

$$p_{\text{ pushing}} = p_{\text{ division}} \frac{(2+L)}{3} \tag{2.10}$$

Figure 2.5 recapitulates the different steps of the DES. During each simulation step that covers 1 s in real time, we cycle through different phases of the simulation. In the first, filopodia are produced with the probability of formation $p_{\text{ formation}}$ and an adequate angle and length from experimental distributions. After this step each occupied grid space tries to divide or insert a cell of similar Wnt content with $p_{\text{ formation}}$. After this, cells attempt to mix with next neighbours with a probability $p^{\text{ sim.}}_{\text{ motility}}$. Technically, there could also be morphogen decay, but as no experimental evidence was available for this to happen on the relevant simulation timescale I disregarded this step.

2.5. Cellular Potts Model

In 1992 Glazier and Graner published a work on the differential adhesion of cells [57, 78, 79] that extended prior studies of coarsening of foam to biological systems. In their work they introduce a formalism for the physics of cells that can, analogous to foam bubbles, be expressed by an extension of the large-q Potts model [71]. The formalism equally employs a grid, on which calculations are performed. The spins that aggregate for low temperatures into specific domains do not represent a different orientation of any intrinsic spin value, but each domain simply represents a specific cell with its spatial distribution [57].

Thus, one can introduce a cell $\sigma\left(\vec{x}\right)$ at the lattice site $\vec{x}$. For a tissue simulation one will not have an infinite amount of different cell types, but a biological system is made up of a large number of cells of the same type. Therefore we can simplify interactions between cells to interactions between cell types $\tau\left(\sigma\left(\vec{x}\right)\right)$. The most prominent, and for our intention only, cell interaction is the surface adhesion between different cell types $J_{\tau\left(\sigma\left(\vec{x}\right)\right)\tau\left(\sigma\left(\vec{x}'\right)\right)}$. J is a symmetric matrix defining the strength of surface adhesion between different cell types.

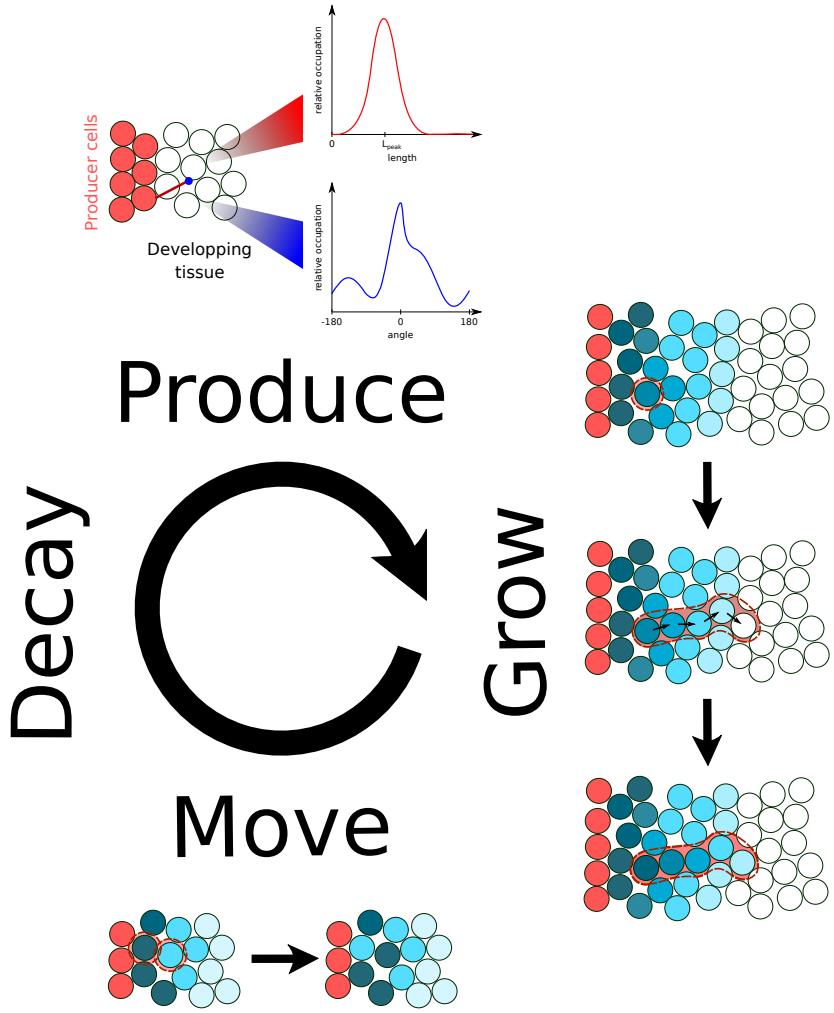

Figure 2.5.: Order of events in the DES. *The DES cycles through each possible event and accepts them with the given probabilites.*

Furthermore, we do not only have intercellular interactions, but we also have intercellular boundary conditions. In the early foam models, different domains would simply grow in size. The earliest model to impose a constraint on the growth of the domains would be the Weaire-Kermode model [79] for soap froths that introduced the Lagrangian multiplier

$$\lambda \sum_{cells} \left(V\left(\sigma\right) - V_0\left(\sigma\right)\right)^2 \tag{2.11}$$

with an inverse gas constant λ and the volume of a cell $V\left(\sigma\right)$ and the target volume $V_0\left(\sigma\right)$. Hence, the domains would not randomly grow but strive for a specific volume. Cells do not only try to keep a constant volume, they also try to minimize their surface. Therefore the CPM formulation adds a similar term with a target cell surface S_0.

The complete Hamiltonian of the grid, therefore, reads as

$$\begin{aligned} H = & \sum_{cells} \sum_{neighbors} J_{\tau\left(\sigma\left(\vec{x}\right)\right)\tau\left(\sigma\left(\vec{x}'\right)\right)} \left(1 - \delta_{\sigma\left(\vec{x}\right)\sigma\left(\vec{x}'\right)}\right) \\ & + \sum_{cells} \lambda_{\mathrm{V}} \left(V\left(\sigma\right) - V_0\left(\sigma\right)\right)^2 \\ & + \sum_{cells} \lambda_{\mathrm{S}} (S(\sigma) - S_0(\sigma))^2 \end{aligned} \tag{2.12}$$

with interaction constants λ_{V} and λ_{S} for volume and surface of the cells, and the Kronecker-delta[2] $\delta_{\sigma\left(\vec{x}\right)\sigma\left(\vec{x}'\right)}$ to exclude self interactions.

The model as written in equation 2.12 describes only a single state of the system in question. It does not describe any dynamics of the system, but this is what we are effectively interested in when running these simulations. An excellent introduction

[2] $\delta_{\sigma(\vec{x})\sigma(\vec{x}')} = \begin{cases} 1, & \text{if } \sigma(\vec{x}) = \sigma(\vec{x}'), \\ 0, & \text{if } \sigma(\vec{x}) \neq \sigma(\vec{x}'). \end{cases}$

to the dynamics of the CPM and the GGH model are found in [58] and I want to introduce the most important concepts at this point.

The Hamiltonian of equation 2.12 can be sampled by a simple Monte Carlo algorithm, but it is much more interesting to use the Metropolis acceptance criterion between different states γ and γ' to sample the states of the system:

$$p(\gamma \to \gamma') = \begin{cases} e^{-\frac{\Delta H_{\mathrm{Tot}}}{T}}, & \text{if } \Delta H_{\mathrm{Tot}} \geq 0, \\ 1, & \text{if } \Delta H_{\mathrm{Tot}} < 0. \end{cases} \tag{2.13}$$

In a Monte-Carlo scheme, the system hops randomly between any admissible state of the system. This is of computational interest if it is easy to generate a new conformation, but impossible to find the next lowest energy in rugged landscapes. One example for the application of Monte-Carlo sampling would be the use in protein folding [59]. If it is easy to find the next lowest conformation in very smooth landscapes, the Metropolis acceptance criterion can be used to construct a dynamic trajectory if the exponent in equation 2.13. For biological systems, this is the case.

First, we have to take a look at the rate of a single change of a lattice site from an initial configuration $\vec{S}$ to another configuration $\vec{S}'$. We obtain for the rate r with a small exponential argument:

$$\begin{aligned} r\left(\vec{S}_i \longrightarrow \vec{S}_{i+1}\right) &= p\left(\vec{S}_i \longrightarrow \vec{S}_{i+1}\right) - p\left(\vec{S}_{i+1} \longrightarrow \vec{S}_i\right) \\ &= 1 - \exp\frac{\left(-H_i + H_{i+1}\right)}{T} \\ &\sim \frac{\left(H_i - H_{i+1}\right)}{T} + \mathcal{O}\left(\left(\frac{\left(H_i - H_{i+1}\right)}{T}\right)^2\right) \end{aligned} \tag{2.14}$$

Practically this means:

$$r\left(\vec{S}_i \longrightarrow \vec{S}_{i+1}\right) \sim H_i - H_{i+1} \tag{2.15}$$

This result can now be transformed into a generalized velocity between different states, in which we assume the change of a single lattice site $\vec{S}_i \longrightarrow \vec{S}_{i+1}$ as our basic time step:

$$\vec{vel}\left(\vec{S}_i \longrightarrow \vec{S}_{i+1}\right) \equiv \frac{1}{T}\vec{\nabla}H \cdot \left(\vec{S}_i - \vec{S}_{i+1}\right) \tag{2.16}$$

This equation fulfills the requirements of a linear dynamic of Aristotelean form with

$$\vec{\nabla}H = \vec{F} = \mu \cdot \vec{vel} \tag{2.17}$$

relating the gradient to $\vec{\nabla}H$ a force $\vec{F}$ and linking it linearly with constant μ to the velocity $\vec{vel}$ for the case of overdamped dynamics.

Thus, the metropolis criterion will result in a slow sampling of the large phase space in a deterministic way. It gives us a dynamic trajectory of the system. The relation between the introduced time step and real time is a subject of controversial debate. Unfortunately, it was not possible to study and clarify this debate within my work. But, regardless of the exact relation between real time and the employed time step, this result permits us to expand the Hamiltonian 2.12 with further potentials to represent further sources of force in our simulations. When doing so, the CPM is generally referred to as the Glazier-Graner-Hogeweg model (GGH) [58]. The CPM and the GGH have numerous applications in studying biological systems, e.g. the dynamics of glioma [80], tumor growth [81], amd blood vessel growth [82]. I do keep in mind that an exact real-time scale is not given, therefore, in my results section, I refrain from interpreting results that would need to pinpoint a specific state to a specific point in time. For example, I can not decide with this model if the notochord becomes shorter or longer, but I can tell if the notochord has a concave or convex form.

2.6. Glazier-Graner-Hogeweg Model

For our notochord simulation, it is necessary to incorporate the effects of gastrulation into the simulation. During the gastrulation phase, cells move from the Spemann organizer up towards the animal pole. Thus, we have a border at the bottom of our simulation field where new cells enter the field, and they move in the upwards direction. For this, we use the extended CPM, the Glazier-Graner-Hogeweg model.

Several implementations for chemotaxis and force gradients have been formulated for the GGH model. I used a model in which the cell grid is extended by a further dimension in which each grid space can also hold a specific concentration of a signaling molecule, or simply a specific potential that acts as a force upon the individual cells. The basic Hamiltonian difference ΔH_B of equation 2.12 is extended by another Hamiltonian difference of the following form

$$\Delta H_{\mathrm{M}} = \mu\left(\tau\left(\vec{x}'\right)\right)\lambda_{\mathrm{M}}\left[c\left(\vec{x}'\right) - c\left(\vec{x}\right)\right] \tag{2.18}$$

with the concentration of a hypothetical signaling molecule $c(\vec{x})$ at a lattice site $\vec{x}$. $\mu\left(\tau\left(\vec{x}'\right)\right)$ is a type-dependent coupling constant as the premise of our simulation was that we want to investigate the effects of a small, faster cell cluster onto notochord formation. The potential I used was simply of linear form.

The GGH model that I implemented for this study, therefore, reads as:

$$\Delta H = \Delta H_{\mathrm{B}} + \Delta H_{\mathrm{M}} \tag{2.19}$$

Chapter 3.
3 Filopodia

In this chapter, I present my results from a joint experimental study targeting the transport and distribution of Wnt8a in the early phases of gastrulation. Experimental results suggested that this morphogen is actively transported through specialized cytonemes, namely filopodia, a class of cellular actin protrusions. Filopodia have a mean length of one cell diameter and transport the signaling molecule from Wnt active producer cells into the morphogenetic field. Subsequently, these cells transform into hindbrain, midbrain, and forebrain.

The goal of the computational study was to clarify if such a short-range mode of transport can result in the long-range effects and gradient necessary for brain development. The results have been published in a joint publication by the group of Steffen Scholpp [2]. By implementing a model with a minimal amount of parameters, I was able to gain further insights into the correlation between filopodia lengths and the hindbrain/midbrain axis. I concluded that, in this model, the flux of the first few Wnt active layers is the defining parameter, and that, contrary to trivial logic, it is important that the deposition of Wnt is imperfect. The predicted results for the deposition ratio matched experimental results. Furthermore, the results give further positive arguments for prepatterning in early morphogenetic fields.

3.1. Motivation

As laid out in chapter 1 the early phases of organism development are the results of a broad network of cellular signaling and tissue responses involving signaling molecules. One of the most notable classes of these signaling molecules is the highly conserved Wnt protein family. As explained in chapter 1.2 they are important regulators during tissue development, tissue regeneration, and stem cell regulation [32, 33]. These molecules are secreted in complexes and form a class of palmitoylated glycoproteins, vesicle-like agglomerations of a large number of these molecules. The response to these vesicles follows the French flag model, hence in a concentration-dependent manner [35]. The secretion and expression of Wnt depend on several factors, the most interesting one being a functional microtubule network [39]. While various modes of transport are known for Wnt, see chapter 1.2, it is of interest to find out the reason for a positive correlation between Wnts and the microtubule network. Furthermore, it is a key question of developmental biology to formulate and understand the principles that enable an organism to have a precise control over brain development.

Eliana Stanganello of the research group of Steffen Scholpp (ITG, KIT) used various methods of high-resolution fluorescence microscopy to elucidate the link between the actin network and the Wnt molecules. In her work, it became quite clear that specialized filopodia actively transport Wnt molecules [2, 83]. Experiments have been performed on single cells in vitro where different molecules were fluorescently labeled. Figure 3.1 displays a high-resolution static image of a cell with a cytoplasmic protrusion composed of actin, a filopodium. Two colors were used to discriminate and identify objects in this image. The actin network tagged in red and the Wnt8a molecules tagged with green fluorescent protein. It becomes apparent that Wnt is localized at the distal tip of the filopodium. Further experiments reported in figure 3.2 display the dynamic production of a filopodium with temporal resolution. Morphogens are localized at the distal tips of filopodia and grow outwards from Wnt active cells towards receiving epiboly cells. Finally, figure 3.3 unfolds the final steps of the proposed mechanism, the pruning of a filopodium. After successfully targeting the receiving cell, the contact between filopodium and

Wnt-producing cell breaks away. The transport of morphogens with filopodia has been reported in several distinct cases during organism development, e.g., fibroblast growth factor branchless [84], Notch-Delta ligands [85], and Dpp and Hh proteins [86]. The most recent cases of this transport were reported in the chick limb bud [87, 88] as well as in Drosophila during Hh signaling [89].

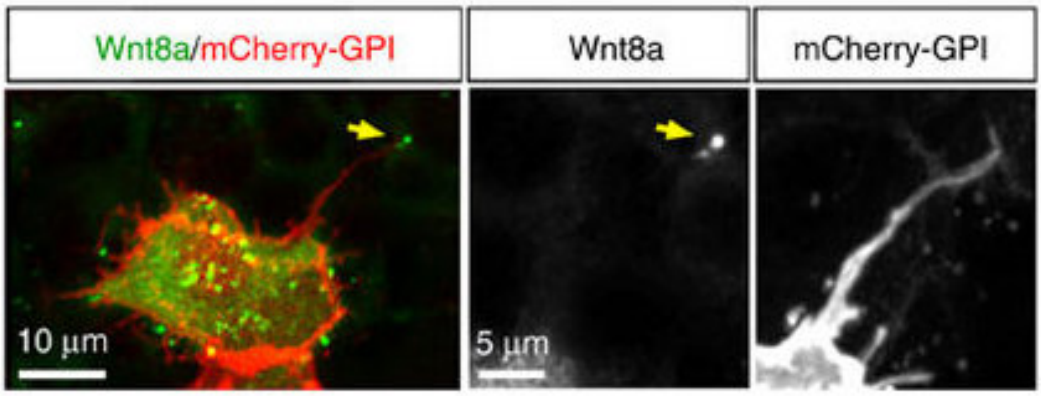

Figure 3.1.: Filopodium. *At the 16-cell stage, zebrafish embryos were microinjected in one blastomere with 0.1 ng of mRNA of Wnt8a-GFP and membrane-bound mCherry. Live cell imaging of a 15-min stack of mCherry expressed in single epiblast cells in a zebrafish embryo at 50% epiboly, highlighting a network of long cytoplasmic extensions. The high magnification pictures of single channels show Wnt8a-GFP localization to the distal tip (arrow). Text and figure [2].*

These previous experiments clearly indicate the transport of Wnt through filopodia, over a short distance. But, Wnt is as previously said the key component in the hindbrain, midbrain, and forebrain development, a differentiation that takes place over several cellular diameters. A whole range of mutagenesis experiments has been run to clarify the relation between filopodia and the hindbrain/midbrain axis. Fortunately, it was not only possible to localize Wnt through high-resolution fluorescence microscopy, but also to change the physical properties of these filopodia by altering factors that had a positive or negative effect on their formation. Figure 3.4 illustrates filopodia under the effects of different regulators that have been

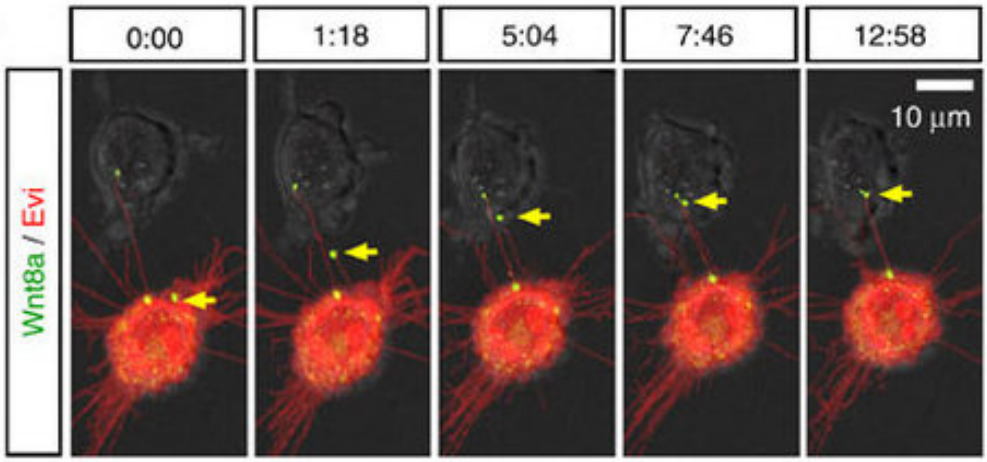

Figure 3.2.: Filopodium formation. *PAC2 fish fibroblast transfected with Wnt8a-GFP and Evi-mCherry containing multiple filopodia with Wnt8a present at the distal end (arrow) forming cell–cell contact with a neighboring PAC2 fibroblast by filopodia (min:s). Text and figure [2].*

identified as key components in filopodia formation. Regular filopodia are shown in the control (ctrl) panel, they have no branching and a mean length of 11.9 μm and a standard deviation of 2.89 μm which is in the range of one cellular diameter of 16 μm. Under the effect of Cdc42mRNA the length of filopodia is increased, with a mean length of 23.84 μm and a standard deviation of 10.61 μm. Cdc42a/c MOs deregulates the formation of filopodia and decreases the length substantially to 1.41 μm with a standard deviation of 0.82 μm.

The most interesting effect of these alterations are the immediate macroscopic effects upon brain development. In figure 3.5 the effects caused by longer filopodia are displayed. Under the influence of Cdc42, the hindbrain/midbrain axis is shifted and the hindbrain is larger. The hindbrain forms at the highest concentrations of Wnt8a, the forebrain at the lowest concentrations of the morphogen. The source of the morphogen, Wnt8a active cells are sitting next to the cells that later become the hindbrain. Adding Wnt8a increases the overall Wnt8a concentration and the gradient is shifted away from the producing cells. Embryos exposed to higher

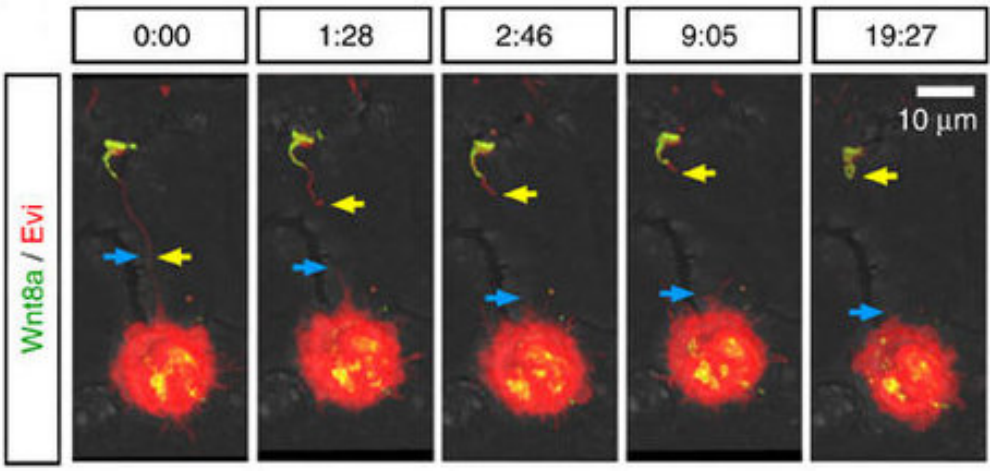

Figure 3.3.: Filopodium pruning process. *Filopodium pruning process after transfer of Wnt8a-GFP of PAC2 cells. After the cutting off, one part of the filopodium is retracted (blue arrows) and the other part shrinks and forms a Wnt8a-positive vesicle at the membrane of the contacted cell (yellow arrow). Scale bars as indicated. Time in min:s. Text and figure [2].*

Wnt8a concentration reacted with a similar shift and an enlarged hindbrain. The combination of both substances resulted in a completely malformed brain with only hindbrain present. Embryos with reduced filopodia lengths did not develop sufficiently to gain any comparative results.

As experiments do lack the necessary time resolution to track the exact spread of Wnt in the morphogenetic field, it is currently impossible to give a satisfactory answer to the exact causes of the above observations. Computer simulations can fill this gap by constructing a sufficient model from our current knowledge on filopodia formation and tissue growth. The exact simulation scheme is explained in chapter 2.4. In the following paragraph, I explain the complete parametrization of the model.

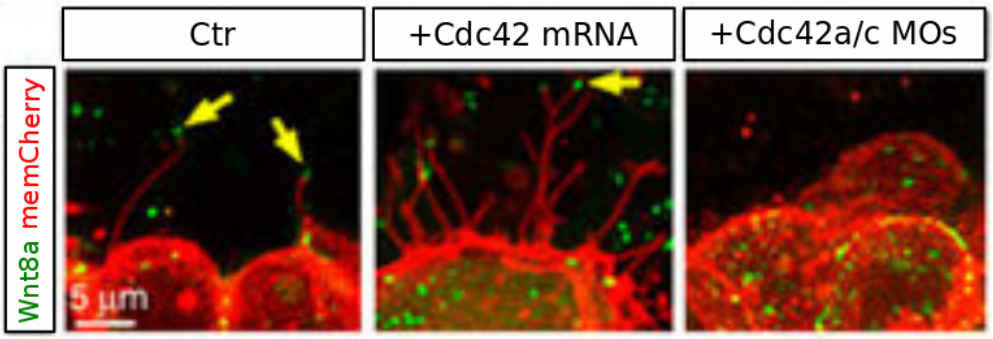

Figure 3.4.: Filopodia with varying length. *Live imaging of cell clones expressing indicated constructs in zebrafish. Regular filopodia are shown in the control (ctrl) panel. Under the effect of Cdc42mRNA the length of filopodia is increased. Cdc42a/c MOs deregulates the formation of filopodia and decreases the length substantially. Text and figure [2].*

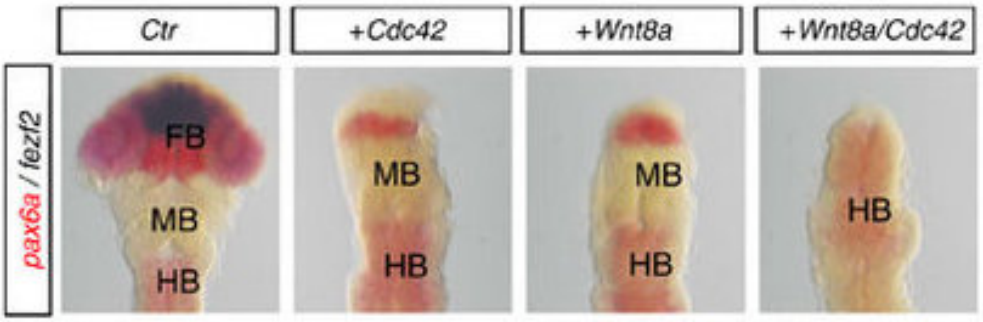

Figure 3.5.: Hindbrain/Midbrain border with varying filopodia lengths. *Embryos were microinjected with mRNA for the indicated constructs (Cdc42, 0.6 ng; Wnt8a, 0.2 ng; IRSp534 K, 1.2 ng) at the one-cell stage. Embryos were fixed at 26 hpf and subjected to in situ hybridization with probes for fezf2 and pax6a. Text and figure [2].*

3.2. Parametrization

To examine our hypothesis quantitatively, I developed a simulation of neural plate patterning as explained in chapter 2.4. The scheme reduces the process described in 3.1 to its core parameters. The simulation encompasses both a complete and sufficient characterization of filopodia and filopodia-external effects like the migration of epiblast cells. The parameters necessary for the description and simulation of filopodia, using the DES scheme as described in chapter 1.7 and 2.4, are based on the experimental results provided by the group of Steffen Scholpp. Key parameters for the description of filopodia are the angle of formation with respect to the producing cell, the filopodium's length in accordance to experimentally measured length distributions, and the frequency of production.

Experimentally, filopodia lengths could be determined by fixing a producing cell onto a substrate and measuring the distance of fluorescently labeled Wnt with respect to the cellular surface. For the wildtype, 391 filopodia have been measured. From the mean value and the standard deviation of this distribution, I constructed a gaussian distribution, from which in each simulation step filopodia lengths are drawn. I chose the gaussian distribution over any other distribution as the process of filopodia growth should comply with a random walk of the filopodia's distal tip. A non-gaussian, or non-random distribution, would imply that a filopodium's tip would exhibit guiding or would have means of chemical sensing. The process of guidance would make further claims about a necessary long-range interaction between filopodium and a hypothetical signaling molecule and the existence of receptors on the filopodium itself. None of these have been experimentally observed. Taking all this into consideration the best choice was to work with a gaussian distribution. For the wildtype variants, filopodia are characterized by a mean length of 11.9 μm and a standard deviation of 2.9 μm (standard error: 0.3 μm). For a further understanding of the relation between filopodia length and brain area development, two more distributions were measured and quantified. For the longer Cdc42mRNA mutants, we performed similar measurements resulting in a mean length of 23.8 μm with a standard deviation of 10.7 μm and for the shorter Cdc42a/c MOs we found a mean length of 1.4 μm with a standard deviation of 0.9

μm. In figure 3.6 the employed length distributions are illustrated.

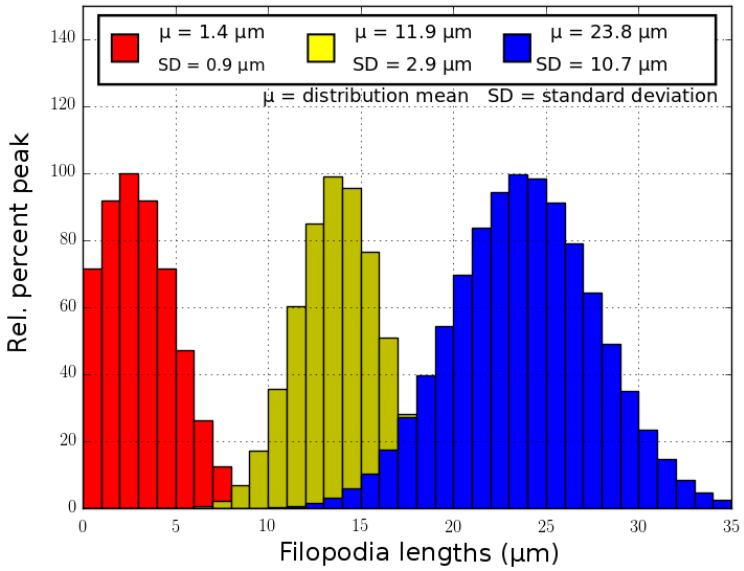

Figure 3.6.: Filopodia lengths distributions. *Length distributions for short (red), wildtype (yellow), and long (blue) filopodia.*

Unlike the distribution of lengths, the angle of formation is not determined by the filopodium itself but depends entirely on the producing cell. Through receptors, the cell has the means for directional sensing. The morphogenetic field is polarized towards the animal pole. This means that filopodia are preferentially generated at the cellular side facing towards the animal pole. Experimentally, angle distributions were obtained in the same manner as length distributions by fixing a producing cell on a substrate. The exact shape of the distribution relies on a multitude of factors. There is no way of analytical deduction that would not need the exact quantification of a multitude of additional factors. Given this, I rather chose an ad-hoc approach and interpolated a suitable distribution from our experimentally obtained empirical data. The interpolation[1] was done using a cubic spline. No further smoothening or symmetrification was applied to the function. The obtained function, as well as

[1] $f(x) = 2.08674726E+01 \cdot x^0 - 4.57694082E-01 \cdot x^1 + 1.58367755E-02 \cdot x^2 - 2.69223550E-04 \cdot x^3 + 2.22174751E-06 \cdot x^4 - 9.33019141E-09 \cdot x^5 1.92437954E-11 \cdot x^6 - 1.54624441E-14 \cdot x^7$

the experimentally determined distribution, have a strong peak towards the animal pole and are illustrated in figure 3.7.

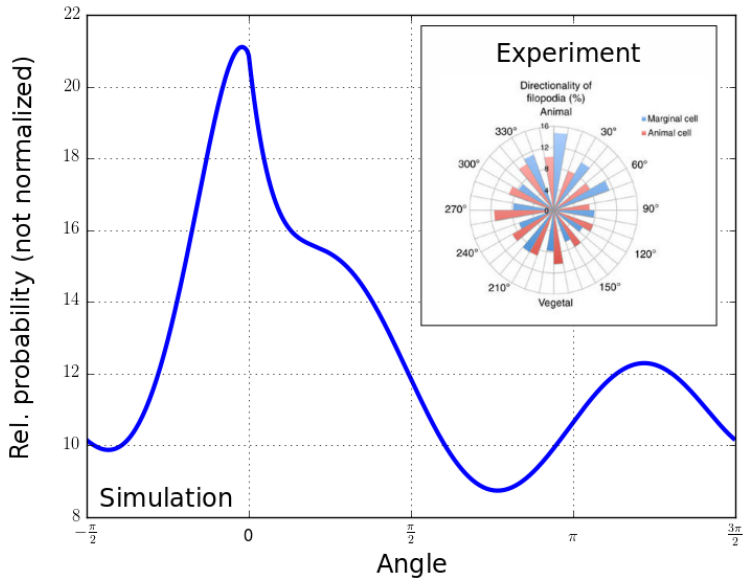

Figure 3.7.: Angular distribution of filopodia. *Experimental values are reported in the inset, the function as used in the simulation within the graph (blue).*

The last missing parameter for filopodia generation is the frequency of formation. The growth of filopodia is fast, and multiple filopodia can be produced at the same time. The experimental results on wildtype cells suggested a production rate of 10.8 per 10 minutes per cell, or 0.018 filopodia per cell per one-second timestep. The production and deposition of Wnt are within the simulation an instantaneous effect with the given rate. No explicit modeling of the growth of a filopodium was implemented. The rate of production has been kept constant in all three cases of filopodia, regardless of length. Newer experimental results suggest that Wnt has a self-controlling effect and that the rate of production should increase throughout the simulation.

Although the method explained in 2.4 could incorporate an explicit term for

ligand decay, it was disregarded for the given arguments. Experiments suggested that the ligand is stable over several hours, hence a larger time frame than the actual simulations and developmental phase. I, therefore, disregarded explicit ligand decay. Furthermore, the only net contribution would be a stronger gradient. The more interesting question was if this gradient can exist despite ligand stability.

The following paragraphs describe the parametrization of the tissue dynamics. The simulation is started from an initial 90 μm broad layer. The Wnt8a-positive marginal zone was set to a 40-μm broad layer ($\pm$ 3 densely packed cell rows) containing 650 ligand-producing cells and the receiving tissue - the neural plate anlage - was set to a 50-μm broad layer ($\pm$ 4 densely packed cell rows) containing 888 epiblast cells. This corresponded to the number of cell rows as measured by the group of Steffen Scholpp. The simulation is stopped after the field has grown to 600 μm. This corresponds to 8 hpf (75% epiboly stage) and 3.4 h of development. During the simulation, cells move according to the algorithm described in 2.4.

As explained in chapter 2.4, tissue growth depends on p_{division}. Due to the boundary conditions imposed by the problem, this parameter is not free. The boundary conditions of the embryonic development determine the size of the morphogenetic field at the beginning and the end of our simulation. This end thickness needs to be reached after 3.5h of development. These constraints set the precise value for the division rate. With initial tissue size D_0, final tissue D_F, and simulation time T_{sim} it evaluates to:

$$\begin{aligned} p_{Division} &= \frac{\ln(2) \cdot \log_2\left(\frac{D_F}{D_0}\right)}{T_{sim}} \\ &= 0.000156\frac{1}{\text{s}} \end{aligned} \tag{3.1}$$

The last parameter introduced in chapter 2.4 is the probability for cell moves, $p^{\text{sim.}}_{\text{motility}}$. The experimental probability can be obtained from the exponential fit in figure 2.3. With $f(x) = k_0 \cdot exp((-\kappa \cdot t))$ we identify κ as $0.550\frac{1}{s}$. With $T_{\frac{1}{2}} = \frac{\ln 2}{\kappa}$ and the relation between probability and half life $p = \frac{1}{2 \cdot T_{\frac{1}{2}}}$ we have the experimental motility

$$p^{\text{exp.}}_{\text{motility}} = 0.0066\frac{1}{\text{s}} \tag{3.2}$$

From this, we have to subtract the motility caused by tissue growth. With equation 2.10 and a length L of approximately 38 cellular layers we have

$$\begin{aligned} p_{\text{ pushing}} &= p_{\text{ division}}\frac{\big(2+L\big)}{3} \\ &= 0.0021\frac{1}{\text{s}} \end{aligned} \tag{3.3}$$

which finally yields the result

$$p^{\text{sim.}}_{\text{motility}} = 0.0045\frac{1}{\text{s}} \tag{3.4}$$

3.3. Results

The simulation results exhibit a highly dynamic behavior throughout the whole process. In the beginning, cell growth and tissue layer insertions, as explained in figure 2.1 panel (B), are slow. The deposition of Wnt8a is the dominant factor. My simulations show that the simulated concentration of the ligand peaked at 50μm from the body of the producing cells, forming a corona around the source tissue, consistent with our previous observations of Wnt8a-mCherry distribution. As cellular growth is not linear, the time intervals in which new cells enter the field and push older cells outwards become smaller and smaller. This deviates the initial gaussian from a simple gaussian to an elongated gradient in direction of the animal pole.

During the first simulation runs it became apparent that the commitment length introduced in chapter 1.7 became important for the process. As the endpoints of filopodia would not always lie within a target cell, but intercellular space, one has

to define what will happen to the morphogen in this case. In the first simulation runs, the commitment length was set to ∞ and targeting would always occur. In this case, no difference was observd between the gradients of longer and wildtype filopodia as displayed in figure 3.8. Not even the peak of the filopodia was shifted by the difference in filopodia length as the peak is only dependent on the ratio between cell growth and filopodia formation.

Biologically, an infinite commitment length does not make any sense. The growth of the filopodium is limited by the available resources. If the commitment length is set to a finite value, the model starts to exhibit interesting behaviors in regards to filopodia length. In the case of finite commitment length, the model becomes flux dependent. An incomplete deposition of the filopodia has a direct effect upon the peak value of the morphogen gradient. The decreased peak limits the amount of morphogen flowing into the morphogenetic field by advection and subsequently the gradient becomes shallower. Smaller absolute values of the gradient shift the concentration dependent tissue borders substantially.

I tested three scenarios with varying filopodia lengths, based on our clonal in vivo measurements. I found that ligand concentration within the entire morphogenetic field depends on the length of the filopodia, when filopodia that can't reach a cell are retracted without depositing any Wnt into the morphogenetic field. As the mean length of filopodia is in the order of one cell diameter, the flux is basically only dependent on the first three layers of producing cells. Even in the wildtype case, the flux towards the morphogenetic field is reduced. In the case of Cdc42mRNA the second layer, and the first layer can nearly fully deposit their Wnt content. For the Cdc42 knockout version, even the first layer is inhibited in its deposition capability. The results for predicted Wnt gradients and varying filopodia lengths are illustrated in figure 3.9.

After my prediction of this effect, the experimental group devised an experiment aimed to measure the frequency of deposition. Indeed, we observed low deposition frequencies with the epiblast cells resulting in lower Wnt8a concentrations for lower filopodia lengths [2].

Furthermore, it was not only possible to predict the frequency of deposition,

but also to relate them to the hindbrain/midbrain border. Experimentally it is possible to color the hindbrain and midbrain with different dyes, such that the hindbrain/midbrain axis can be measured. The position of the midbrain-hindbrain boundary (MHB) was measured in 15 representative embryos from wt, Cdc42 mRNA-injected and Cdc42-knockdown groups. In figure 3.10 the distance from either margin to the MHB is displayed. Axin2 measures the distance from the producing border, Oxt2 from the opposite border. These data were compared with values calculated from the simulation. The border in the wildtype was used to define the concentration levels for cell differentiation. The other two values predict the experimental results perfectly.

Not only did my simulations highlight the key components in morphogen transport by filopodia and the magnitude of control the early organism has over its development through them; they also have significant statements over a much-debated topic in developmental biology: *prepatterning*.

3.3.1. Prepatterning

A currently unsolved question in developmental biology is the question of scaling. Not every specimen of a specific organism grows to the same size, yet their organs display the correct proportions. If cellular fates are dependent on a specific concentration of a gradient, and if the spreading of these morphogens follows distance dependent laws, then how is it possible that the organism is able to scale correctly? One solution for this problem is known as prepatterning. In prepatterning cells do not take their final fates at the end of a developmental stage, but they take them as fast as possible. Hence, the faster cellular fates stabilize, the more this speaks in favor of prepatterning.

To solve the question if prepatterning plays a role in filopodia-based transport, and if the filopodia-based transport has any advantage over diffusion in regard to prepatterning, the previous results were further investigated. For this, we devised simulations that could transport the morphogen by diffusion and have preferential mixing. Generally, the migration by p_{motility} would be random and have no preferential direction. In preferential mixing, the Wnt content of the moving cell and

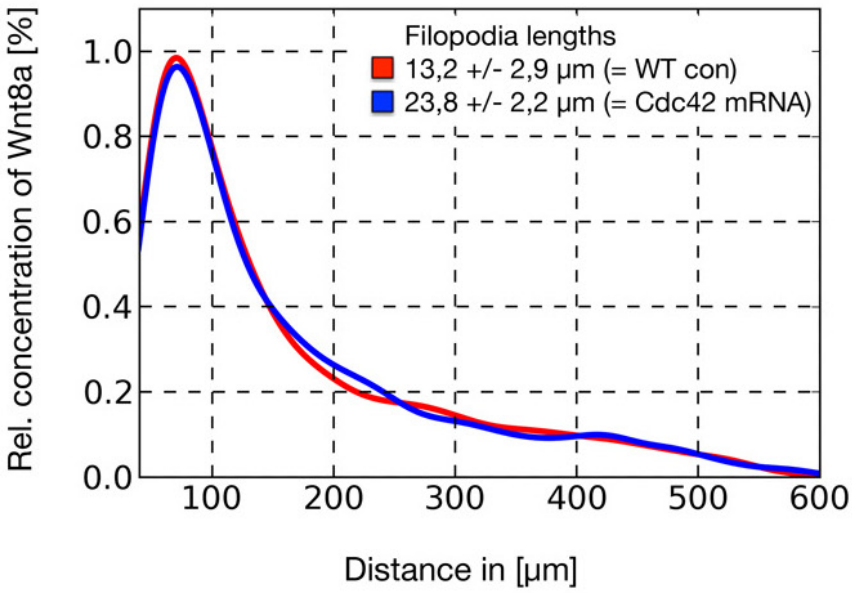

Figure 3.8.: Results for infinite commitment length. *With an infinite commitement length no difference is observed in the gradients. Figure [2]*

its neighbors are compared to define a gradient related preferential direction. With a probability of only 0.0002 $\frac{1}{\text{event}}$ the parent cell would preferentially switch places with a cell closer to the producing border if it had more Wnt, and move away from the producing border if it had less Wnt. In figures 3.11 to 3.18 four different cases are displayed: morphogen transport by diffusion with no preferential mixing, morphogen transport by diffusion with a low preferential mixing, morphogen transport by filopodia with no preferential mixing, and morphogen transport by filopodia with preferential mixing. Simulations were run with $p_{\text{motility}} = 0.0045\frac{1}{s}$ and a diffusion constant of $0.1\frac{\mu m^2}{s}$ [26, 90].

Figures 3.11, 3.13, 3.15, and 3.17 display in their A panel a spatial cellular fate map throughout the simulation time. Forebrain cells in red, midbrain cells in green, and hindbrain cells in blue. As the growth of the tissue is not linear in time, a cell

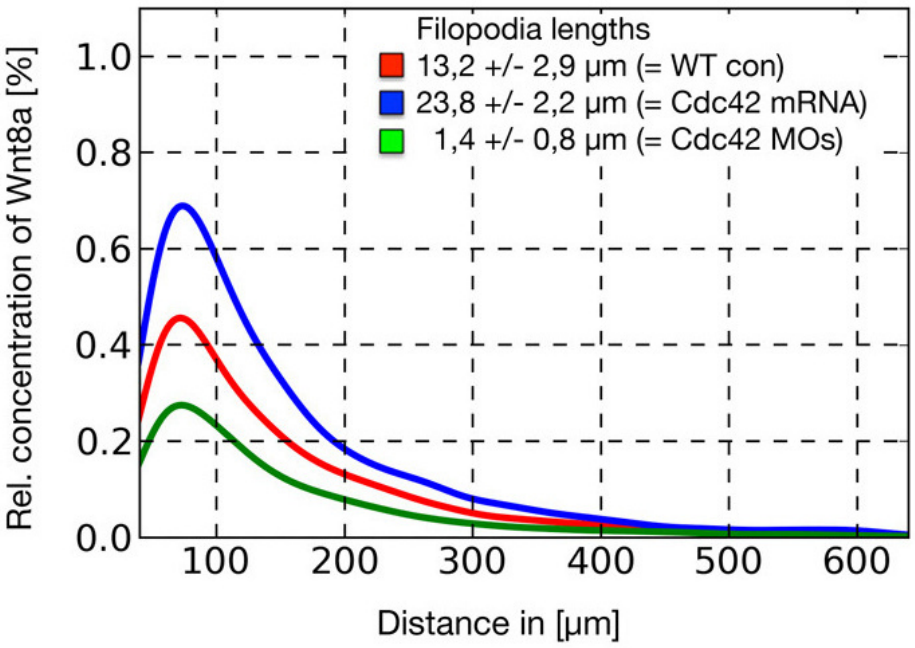

Figure 3.9.: Results for filopodia-based ligand distribution in morphogenetic field. *Wnt gradients for short, wildtype, and long filopodia. Figure [2]*

will move on a nonlinear trajectory in these plots. Two trajectories for two different cells are displayed in white in each plot. In the B panel of the respective figures, the time evolution of morphogen gradients is displayed.

Figures 3.12, 3.14, 3.16, and 3.18 take the results of the cellular fate map and display them on a more visual way. As each cell in the simulation divides and the number of cells increases through insertions, the number of daughter cells increases throughout the simulation. For each parent cell of the starting tissue, we show the relative number of daughter cells. Forebrain cells are colored in red, midbrain cells in white, and hindbrain cells in blue. Each thirty-minute interval is either displayed as a gray or white stripe.

For the case of morphogen transport by diffusion with no preferential mixing,

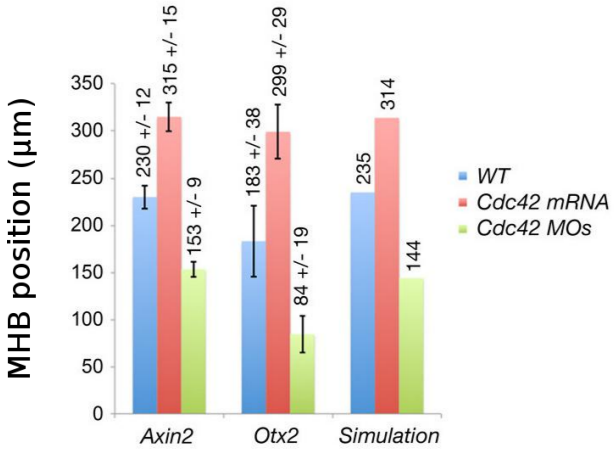

Figure 3.10.: Position of the MHB within the neural plate. *Position of the MHB as measured by Axin2 and Otx2 in experiment and simulation results. Figure [2]*

we see that the final patterning only takes place within the last 50 minutes of the simulation. Cells cycle through every cellular fate in a slow way. For the case of morphogen transport by diffusion with a low preferential mixing the final patterning happens earlier, but still relatively late. Also, cells have to cycle through many cell fates on a long time scale.

For the case of morphogen transport by filopodia with no preferential mixing we see that cell fates are very mixed, but the final cellular fates of the tissues are already found within the first hour.

Morphogen transport by filopodia with preferential mixing already determines the cellular fates within the first thirty minutes even though the rate of preferential mixing is very low. The cellular fate map in figure 3.17 exhibits a near perfect separation of cellular fates. This mode of transport can explain dynamic scaling entirely by prepatterning. These results are complementary to results in Drosophilia where pre-steady-state dynamics enable dynamic scaling [74, 91].

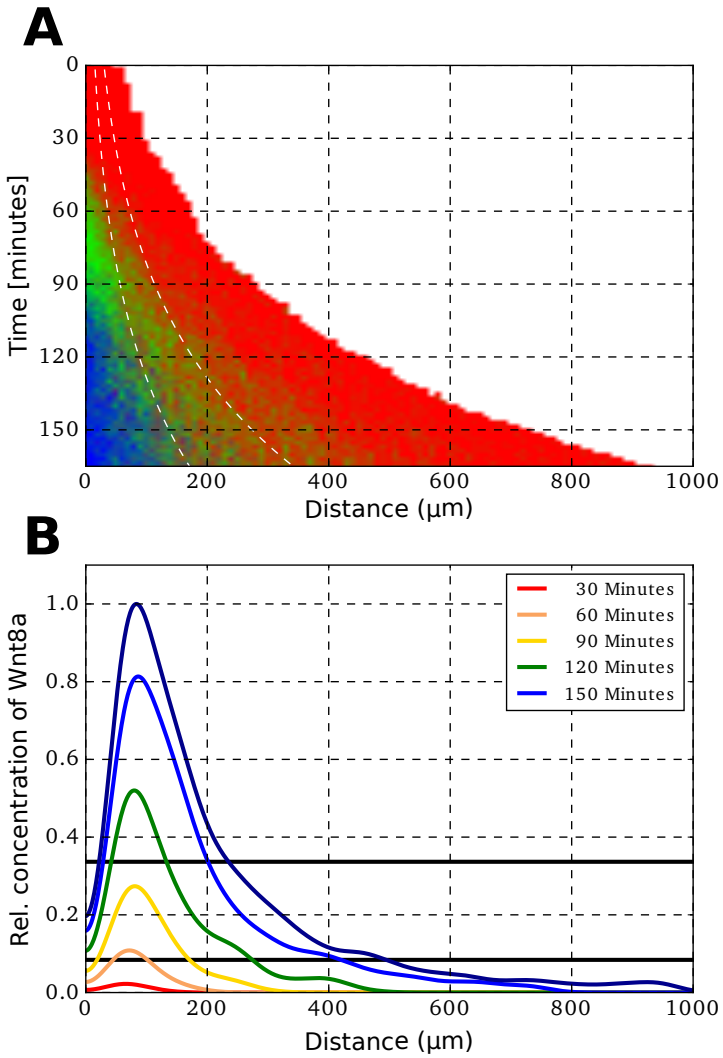

Figure 3.11.: Diffusion and no directed migration. *(A) A spatial cellular fate map throughout the simulation time. Forebrain cells in red, midbrain cells in green, and hindbrain cells in blue. Examplary cell trajectories in white. (B) Time evolution of morphogen gradients.*

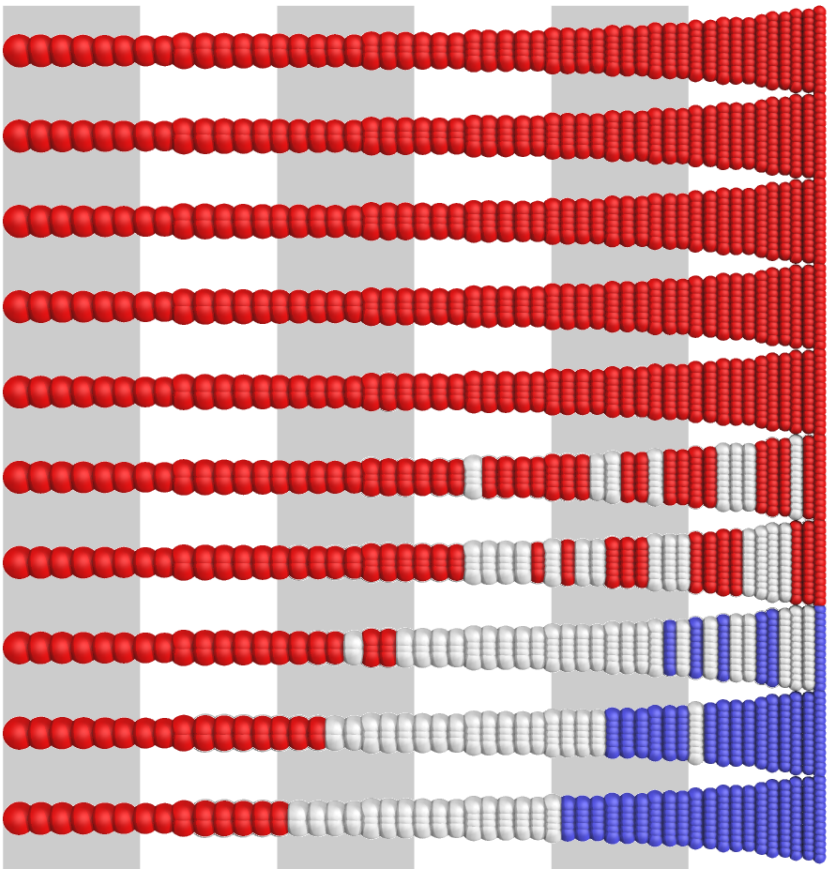

Figure 3.12.: Diffusion and no directed migration. *Fate map with initial tissue and relative number of daughter cells. Forebrain cells are colored in red, midbrain cells in white, and hindbrain cells in blue. Each thirty-minute interval is either displayed as a gray or white stripe.*

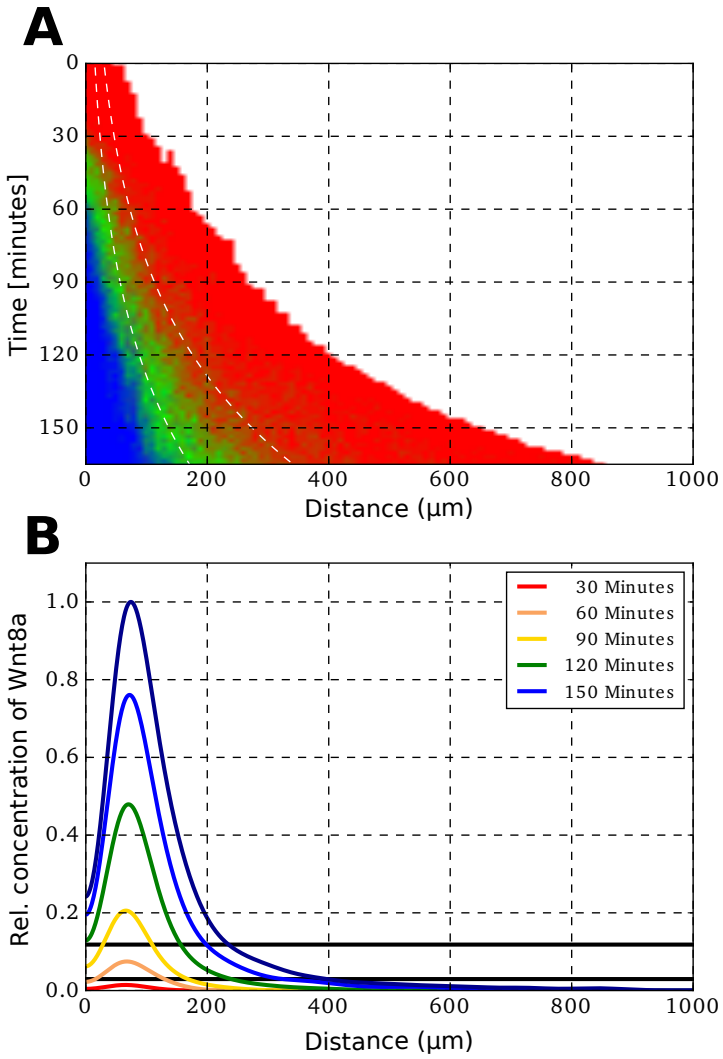

Figure 3.13.: Diffusion and directed migration. *(A) A spatial cellular fate map throughout the simulation time. Forebrain cells in red, midbrain cells in green, and hindbrain cells in blue. Examplary cell trajectories in white. (B) Time evolution of morphogen gradients.*

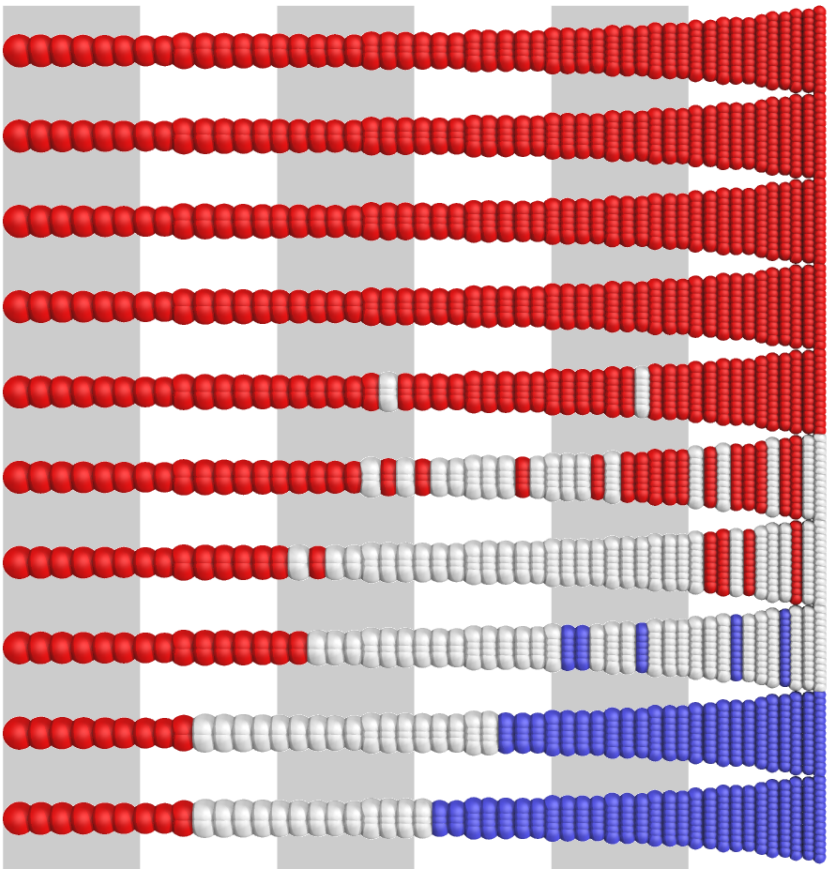

Figure 3.14.: Diffusion and directed migration. *Fate map with initial tissue and relative number of daughter cells. Forebrain cells are colored in red, midbrain cells in white, and hindbrain cells in blue. Each thirty-minute interval is either displayed as a gray or white stripe.*

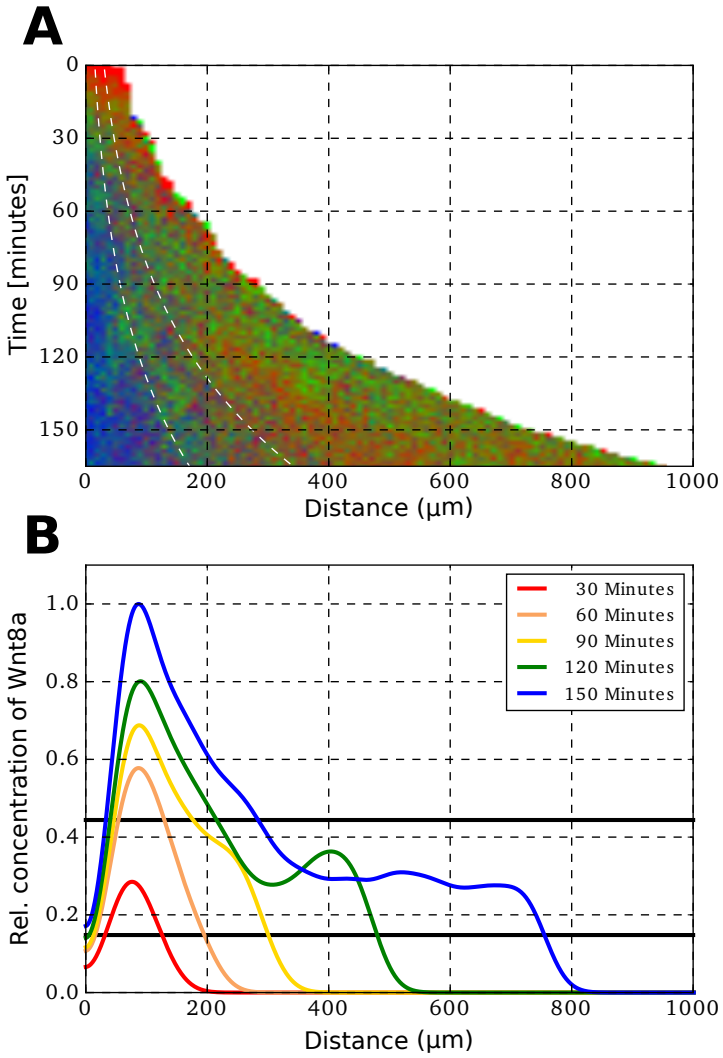

Figure 3.15.: Filopodia and no directed migration. *(A) A spatial cellular fate map throughout the simulation time. Forebrain cells in red, midbrain cells in green, and hindbrain cells in blue. Examplary cell trajectories in white. (B) Time evolution of morphogen gradients.*

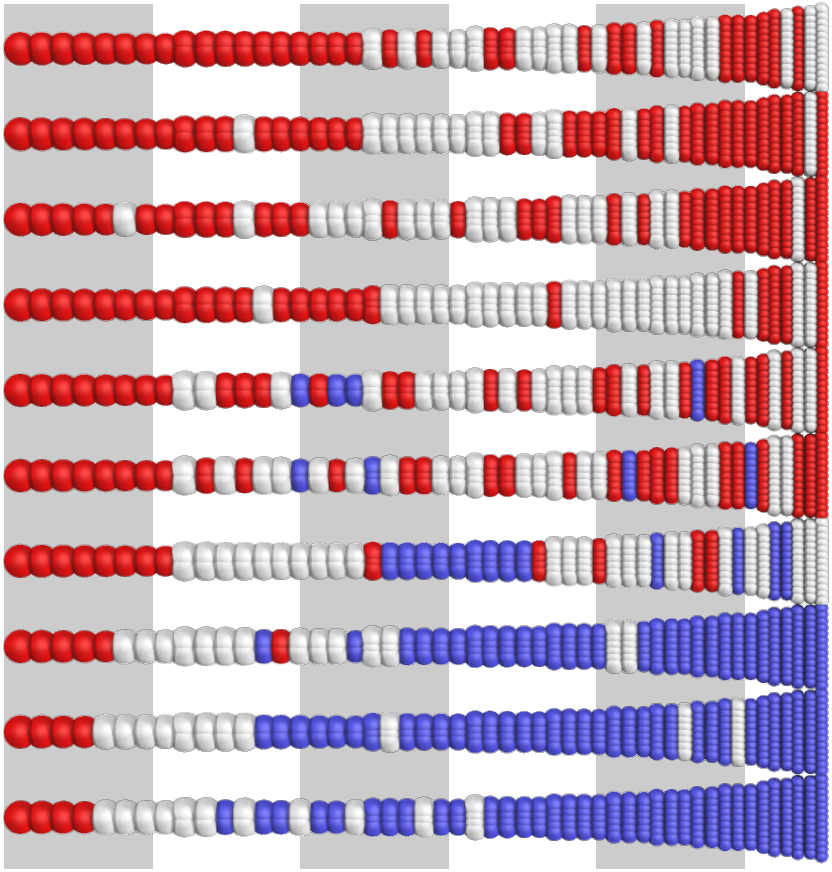

Figure 3.16.: Filopodia and no directed migration. *Fate map with initial tissue and relative number of daughter cells. Forebrain cells are colored in red, midbrain cells in white, and hindbrain cells in blue. Each thirty-minute interval is either displayed as a gray or white stripe.*

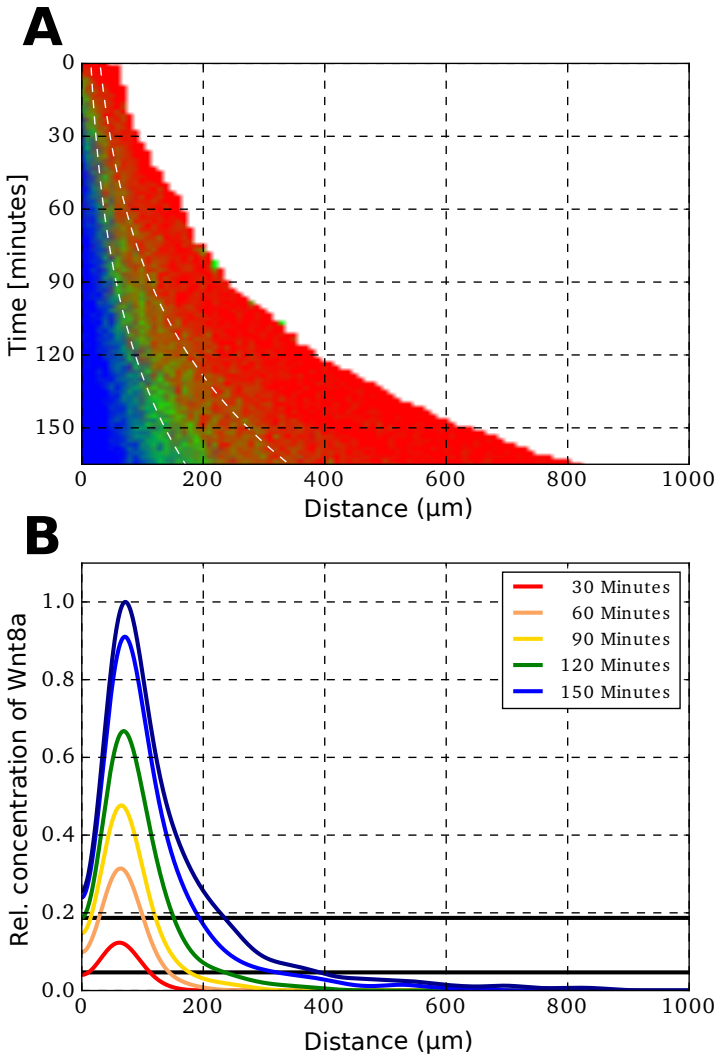

Figure 3.17.: Filopodia and directed migration. *(A) A spatial cellular fate map throughout the simulation time. Forebrain cells in red, midbrain cells in green, and hindbrain cells in blue. Examplary cell trajectories in white. (B) Time evolution of morphogen gradients.*

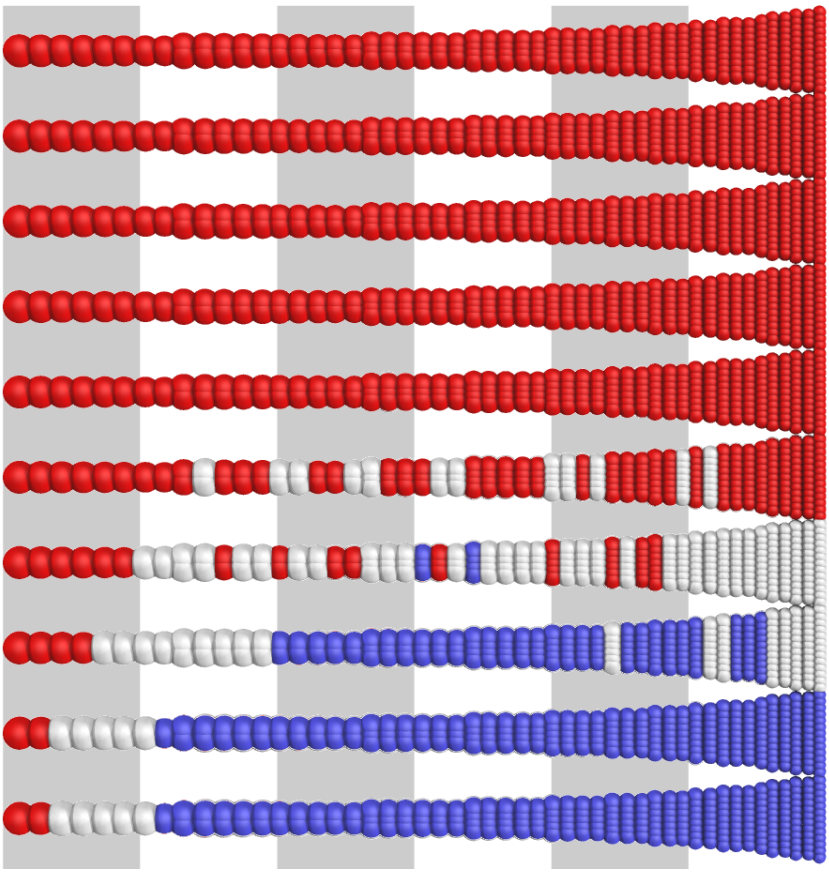

Figure 3.18.: Filopodia and directed migration. *Fate map with initial tissue and relative number of daughter cells. Forebrain cells are colored in red, midbrain cells in white, and hindbrain cells in blue. Each thirty-minute interval is either displayed as a gray or white stripe.*

Chapter 4.
4 Notochord

The following chapter introduces my results for the formation of the notochord. The notochord takes its origin during the gastrulation phase of the early zebrafish embryo. It is the common feature of Chordates and serves as a common embryonic midline structure for all of their members. It forms in the mesoderm from a highly interesting cellular system from a physical viewpoint. During notogenesis, the main interaction of these four cell types is not through cellular signaling, but mainly through their physical properties.

The notochord is an organ of rod-like structure. Experiments done by the group of Steffen Scholpp confirmed a group of highly adhesive and mobile cells in the formation of the notochord. These notochord tip cells (NTC) have a higher motility than any of the other groups, coupled with a higher cell adhesiveness. Therefore, we hypothesize that these cells are crucial for the exact formation of the notochord.

Computer simulations based on a Glazier-Graner-Hogeweg model are introduced and parametrized to make the best use of the experimentally available relative forces of the system in question. The simulations were able to clarify the effect of each cellular property on the shape of the newly forming notochord. The simulations give crucial results in regards to the current debate of the role of the LPM cells in notogenesis.

4.1. Motivation

As laid out in chapter 1.6 the notochord is the most prominent hallmark of the phylum Chordata and serves as common embryonic midline structure for all of their members, including humans. It plays a central role in the genesis of the vertebral body plan, as it serves as an embryonic scaffold for the surrounding mesoderm to subsequently form the skull, the membranes of the brain and, most importantly, the vertebral column [55]. Hence, among others, it is the progenitor of the vertebral column. As laid out in chapter 1.5 the notochord originates when cells break their cell-cell junctions and undergo single-cell ingression at the onset of gastrulation [92, 93]. This newly formed sheet of cells organizes into a coherent cell sheet, the mesoderm, and migrates from the embryonic margin towards the animal pole, using the overlying ectodermal cells as a substrate [94, 95].

The early mesoderm is our system of interest. As explained in chapter 1.6, and illustrated in figure 1.6, this sheet can be divided into four distinct regions: the prechordal plate mesoderm, the notochord tip cells, the axial notochordal plate, and the lateral plate mesoderm. The prechordal plate mesoderm serves as an outer epithelial layer. The adhesive forces of the PPM are the strongest and act as a skin layer. The PPM serves as a front towards the animal pole of the growing mesoderm. The notochord tip cells (NTC) have a higher motility than any of the other groups, coupled with a higher cell adhesiveness. The axial notochordal plate cells turn into the notochord.

The notochordal plate narrows and elongates in the migration directory of the cell sheet and finally transforms into the notochord, whereas the LPM cells migrate towards the midline to form the remaining mesodermal organs in the embryo. Up to date, it is not clear which process is the driving force behind the shaping of the notochord.

One possibility highlights the importance of the LPM and suggests that the notochordal plate compacts as a consequence of LPM pushing forces [96]. In this scenario, the outer cells push towards the midline and elongate the notochordal plate towards the animal pole as cells are being pushed and compressed into the

forward direction.

Another possibility is a cell-specific mechanisms in which a group of cells collectively reshapes to give rise to larger deformations in a tissue. The molecular mechanisms, generally known as convergence and extension, has been extensively studied in the LPM. Through cadherin-based junctions, neighboring cells are able to communicate with each other and mediate collective cell polarizations. This collective reshaping is able to elongate all cells of a tissue and produce an elongated structure [97]. Wnt-planar cell polarity (PCP) signaling controls the internalization of E-cadherin cell adhesion complexes. As explained in chapter 1.4, cadherins form the molecular basis for cell adhesion. The expression, or retraction, of these cell adhesion complexes, is able to guide cellular movement into a specific direction [98]. By lowering cellular adhesiveness at one pole of the cell, and increasing it at the other, cell motility in direction of the gradient is increased. Directed migration is a prerequisite for coordinated cohort movement of cellular clusters [99]. Therefore, a common hypothesis for notochord formation suggests that, similar to the LPM, Wnt-PCP-driven cell migration leads to the intercalation and elongation of the notochord plate cells to form the rod-shaped notochord [100].

The experimental group of Steffen Scholpp identified a possible key component in notogenesis. In experiments undertaken by Bernadett Bösze, the group mapped both the expression of key cell adhesion molecules and genes that are expressed in the axial mesoderm. With this protocol they were able to generate a map of strongly adhesive cell regions and the future notochord. Figure 4.1 identifies a peculiar cell cluster that expressed all of the relevant adhesion genes pcdh18a, e-cad, and fzd7a. This cell cluster contains approximately 70-80 cells and is localized in the axial mesoderm between the e-cad/gsc-positive PPM and the ntl-positive notochord. Strictly speaking, just below the outer epithelial layer, and in front of the future notochord. In the remainder of the text, this confined cell population is referred to as the notochord tip cells (NTC).

Not only was it possible to identify the location of this cell cluster, but it was also possible to identify the key element in the adhesive forces of the NTC. A Morpholino (MO)-based antisense approach [101] and a CRISPR/Cas9-based knockout

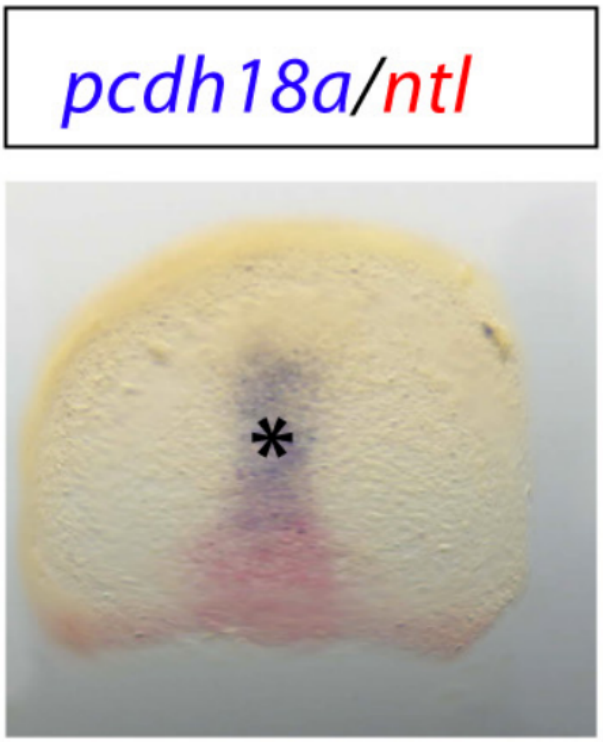

Figure 4.1.: Cellular map of key adhesion molecules and axial mesoderm. *Genes typical for the axial mesoderm are mapped in red, and Pcdh18a in blue at 8.5 hpf. Figure [11].*

strategy [102] suggested the levels of Pcdh18a to be the main components of cellular adhesiveness in the NTC [11]. The reduction of pcdh18a expression led to a wider axial mesoderm as illustrated in figure 4.2.

They were also able to investigate the shape of the notochord cells and found that the cells were less elongated and displayed a more circular form in embryos with reduced Pcdh18a levels, as shown in figure 4.3. From a physical viewpoint this suggests that there is less pressure in the cellular field, and less directionality in subsequent movements.

For complete verification of the importance of the NTCs, further experiments are

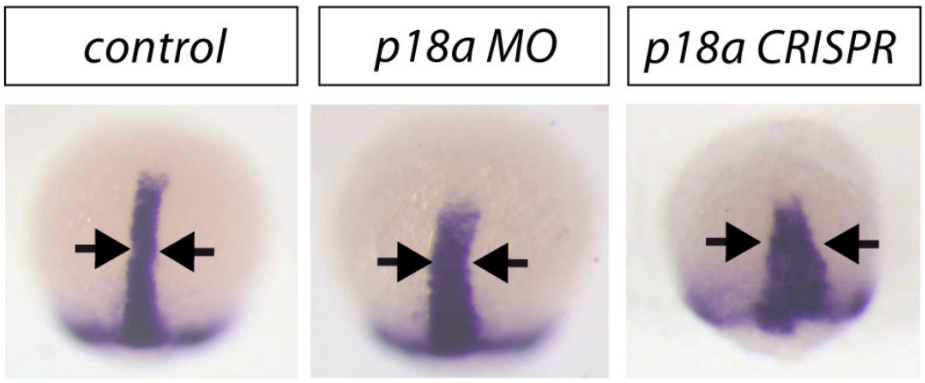

Figure 4.2.: Effects of Pcdh18a in notogenesis. *Notochord formation by reduction of Pcdh18a in the NTCs. NTL in blue. Figure [11].*

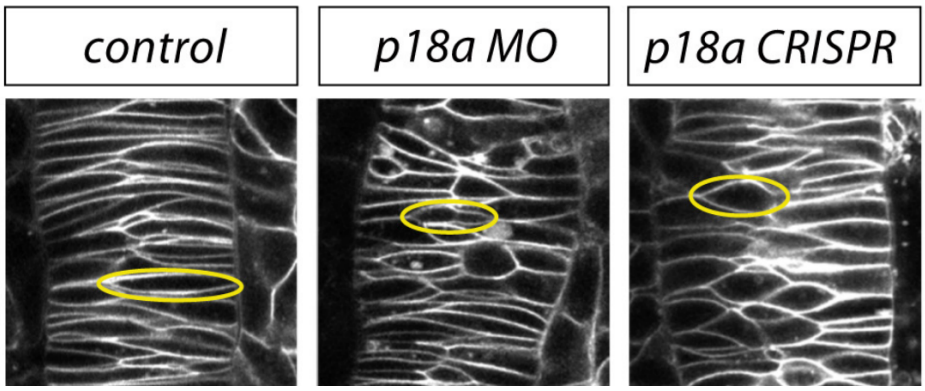

Figure 4.3.: Shape analysis of cells *At reduced levels of Pcdh18a cells become more circular. Figure [11].*

necessary. If we can alter the physical properties of these cells experimentally, it is possible to prove that these cells are sufficient to explain notogenesis when simulations in a minimal model display the same results. The most notable properties of the NTCs are adhesiveness and speed. In Xenopus explants, it is known that Fzd7 influences cadherin-mediated adhesion [103]. Fortunately, the experimental group observed a similar reduction of migration after co-expression of E-cad and Fzd7a.

Further experiments were undertaken to understand the exact role and interplay

of Pcdh18a, E-cad, and Fzd7a. In these experiments, it became apparent that E-cad leads to cell cluster compaction and decreases cell migration. The expression of Pcdh18a in the E-cad-positive cells sped up cell migration to levels comparable to wildtype cells. This result is in concordance with recently published data showing that Pcdh8 suppresses C-cadherin-mediated cell adhesion and promotes the Wnt-PCP pathway-dependent cell motility [104].

Experimentally, it was, therefore, possible to gain results for NTCs with increased cell adhesiveness, NTCs with increased cell motility but same cell adhesiveness, and wildtype cells with increased speed and cell adhesiveness. The simulation results are expressed for these three cases.

4.2. Parametrization

I implemented a lattice-based Glazier-Graner-Hogeweg model as explained in chapter 2.6 based on the cellular Potts model [57] to study the self-organization of the mesodermal tissue during gastrulation. I chose this model for several reasons. First, the number of parameters is minimal. Second, it recaptures our experimentally accessible cell properties and the model is sufficiently defined by intercellular adhesion energies, intracellular surface and volume constraints, and migration properties. Third, while it was impossible to quantitatively define cell adhesion properties, it was at least possible to define them in a relative manner for each cell type. The quantitative knowledge of the cellular adhesion force would have enabled the formulation of an explicit model, for example, the spheres model as introduced in chapter 2.2. Nevertheless, the available parameters in combination with this semi-statistical model are sufficient to address the important question: which properties of individual cells or cell groups are required to generate compaction of the migrating cell layer into a notochord-like structure?

In the modeling framework implemented in Python, every cell is represented in an object-oriented fashion by a physical location in the tissue, as well as cell-type-dependent physical properties such as cell-cell adhesiveness, relative migration speed, and migration direction. To reproduce the system, I specified four different

cell types: the leading PPM cluster, the central NTC, the trailing notochord plate and the surrounding LPM. The trailing notochord plate, and the surrounding LPM bear no physical difference, but their distinction was important for visual purposes and the purpose of clear representation of the results. It is this part of the LPM that can be experimentally tagged and highlighted in fluorescence microscopy.

The simulation runs on a grid in which each grid space only contains the index of the cell that currently occupies this spot. Each of these cells occupies several grid spaces. This defines the resolution of the system. The more grid spaces a cell occupies, the more refined the results will be, but also the higher the computational cost. I chose a cell size similar to other implementations of the GGH of $10 \cdot 15$ grid spaces in the initial state of the cell [82]. During the simulation, new cells ingress into the field as space permits, but none of the cells runs through cell division.

Every cell, together with its next neighbor interactions, gives an energetic contribution to the total energy of the system, as specified in the Hamiltonian function of the CPM (see equation 2.12). The system evolves from one state to the next by employing the Metropolis Monte-Carlo criterion as explained in chapter 2.5. The role of the parameter T of the Metropolis Monte-Carlo criterion for the biological simulations is debatable [58]. I express the following parameters for $T = 1$. The GGH has only four parameters: the coupling parameter λ_{V} for constant volume, the coupling parameter λ_{S} for constant surface, the cell adhesiveness matrix J, and the coupling to the underlying potential λ_{M}. The latter is the cause of cellular mobility. The first two parameters have not much of an effect on the other properties. By scaling λ_{V} to 1, λ_{S} has to be scaled such that cells do not increase their surface when moving, or experience weird shapes. A low parameter of λ_{S} will result in elongated cells, that only elongate instead of moving towards the animal pole. I have found that $\lambda_{\mathrm{S}} = 5$ results in a meaningful behaviour.

The strength of the coupling λ_{M} of the cellular field has to be weak enough that the ideas expressed in 2.5 hold true. If this is not the case, the cells display again a whole range of unphysical deformities and behaviors. The opposing factor of cell motility is the cell adhesiveness matrix J. The parameter needs to be sufficiently high to allow for cellular movement. I have chosen a parameter of $\lambda_{\mathrm{M}} = 120$. None

of the introduced parameters represents a physical unit as we calculate in units of spin changes as introduced in chapter 2.5.

The coupling matrix J defines a strength of cell adhesiveness between each cellular type and the medium (M). The magnitude of these parameters is similar to the parameters introduced in [82]. The coupling matrix J reads as

$$J_{\text{mobile}} = \begin{pmatrix} & \text{M} & \text{LPM} & \text{NTC} & \text{PPM} \\ \text{M} & 60 & 60 & 60 & 60 \\ \text{LPM} & 60 & 50 & 35 & 20 \\ \text{NTC} & 60 & 35 & 20 & 15 \\ \text{PPM} & 60 & 20 & 15 & 10 \end{pmatrix} \tag{4.1}$$

(4.2)

for the case of strong adhesion and

$$J_{\text{non mobile}} = \begin{pmatrix} & \text{M} & \text{LPM} & \text{NTC} & \text{PPM} \\ \text{M} & 60 & 60 & 60 & 60 \\ \text{LPM} & 60 & 50 & 50 & 30 \\ \text{NTC} & 60 & 50 & 50 & 30 \\ \text{PPM} & 60 & 30 & 30 & 10 \end{pmatrix} \tag{4.3}$$

for the case of weak adhesion. The PPM must exhibit a small differential adhesion to the other cell types, as otherwise, the NTC could freely pass this cellular layer. In the case of strong adhesion, the NTCs are bound twice as strong as the LPM.

The simulation started with cells ingressing from the epiblast and forming the mesendodermal cell layer, without any substrate curvature. The start of the simulation is shown in figure 4.4. Each simulation is started from the same equilibrated distribution that has been run until every cell was in maximal contact, and the tissue has not moved yet towards the animal pole. The NTC (green) has 31 cells in roughly 3 times 10 cells, and the PPM has three layers. The system is representative for cell distributions as found at the beginning of ingression.

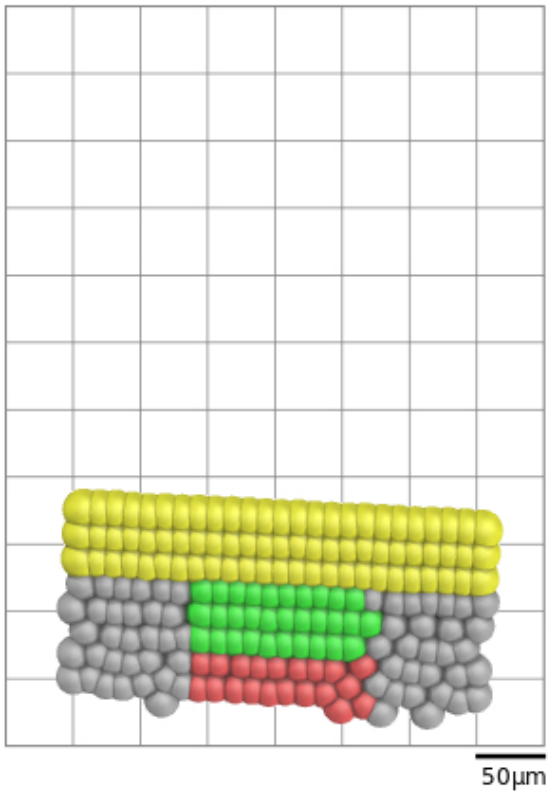

Figure 4.4.: Start conformation *Equilibrated distribution with NTC (green), three-layered PPM (yellow), axial mesoderm (red), and LPM (gray).*

We studied three different scenarios for the NTC - mobile leaders, adhesive leaders, and mobile & adhesive leaders - to answer the question which of these cell properties are important for notogenesis, and if a model without pushing forces of the LPM is sufficient to describe the experimentally observed patterns.

4.3. Results

Based on observations in vitro, I ran simulations in which I increased the cell motility μ of the mobile leading NTC by 100% compared to their neighbors. Results for this case of mobile leaders are reported in figure 4.6. One observes that the NTC exhibits an oblong shape that is perpendicular to the anteroposterior axis. This result suggested that the differential adhesion between the PPM and the NTC, along with the weak cell-substrate interaction, inhibited the elongation of the notochordal plate.

In the next experiment, I increased the adhesion of the NTC without altering the cell migration speed (adhesive leaders). Results are reported in figure 4.5. Again, one is able to observe an oblong shape and perpendicular orientation of the leading NTC. The trailing notochordal plate is broad and does not show any difference to newly inflowing cells. The broad notochordal plate agrees with the results of experiments with reduced Pcdh18a levels 4.2.

In the final simulation, I increased both the migration speed and adhesion (mobile & adhesive leaders). Results are reported in figure 4.7. The shape of the tissue changed. The E-cad-positive leading PPM forms a convex outline and thus resembles the curved shape of the prechordal plate in vivo as reported in figure 4.2. Furthermore, one observes that the centrally NTC-trailing cells of the notochordal plate condensed to a rod-shaped structure. This suggests the hypothesis that the transformation into a 3D condensed chord requires the stretching force of the NTC on the notochordal plate. As the GGH is exclusively next neighbour-based, stretching forces generated from the NTC will primarily operate on the trailing notochordal plate and secondarily on the adjacent LPM cells. The migration of the LPM should thus be generated by them being pulled towards the midline, and not of an active force that the LPM generates as the only direction of migration was in the anteroposterior direction. Remarkably, this simulation also reflects the changes in the expression pattern of Pcdh18a in the NTCs from a wide, round group into an elongated, stretched cell cluster. Thus far, the previous experiments and my simulations suggest that Pcdh18a expression in the NTC is required to organize the shape of a notochord either by regulating gene expression in the

notochord or by controlling the cellular mechanics of the rod-shaped organ. The means for answering this question are only found in the experiment.

Simulation alone of the system in question could not solve the exact mechanism of notogenesis. Nevertheless, it could elucidate key roles of the cellular functions and emergent behaviors. My simulations suggest that the condensation of the notochord facilitates movement of the LPM cells towards the midline. Consistent with this observation, there are no obvious convergent extension movements in the LPM in mice [105].

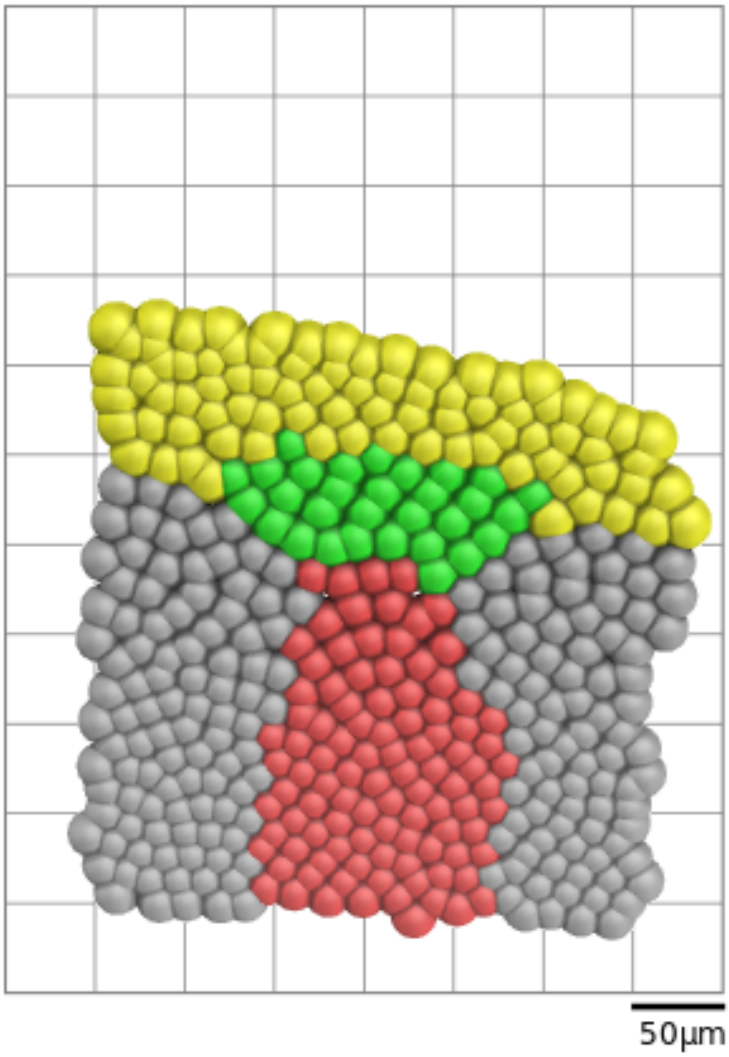

Figure 4.5.: Adhesive leaders. *Simulation results with NTCs twice as adhesive. An oblong shape forms and the notochord widens as the PPM inhibits forward motion. Rendering of the grid-based simulation results with spheres at each cell center using Pymol.*

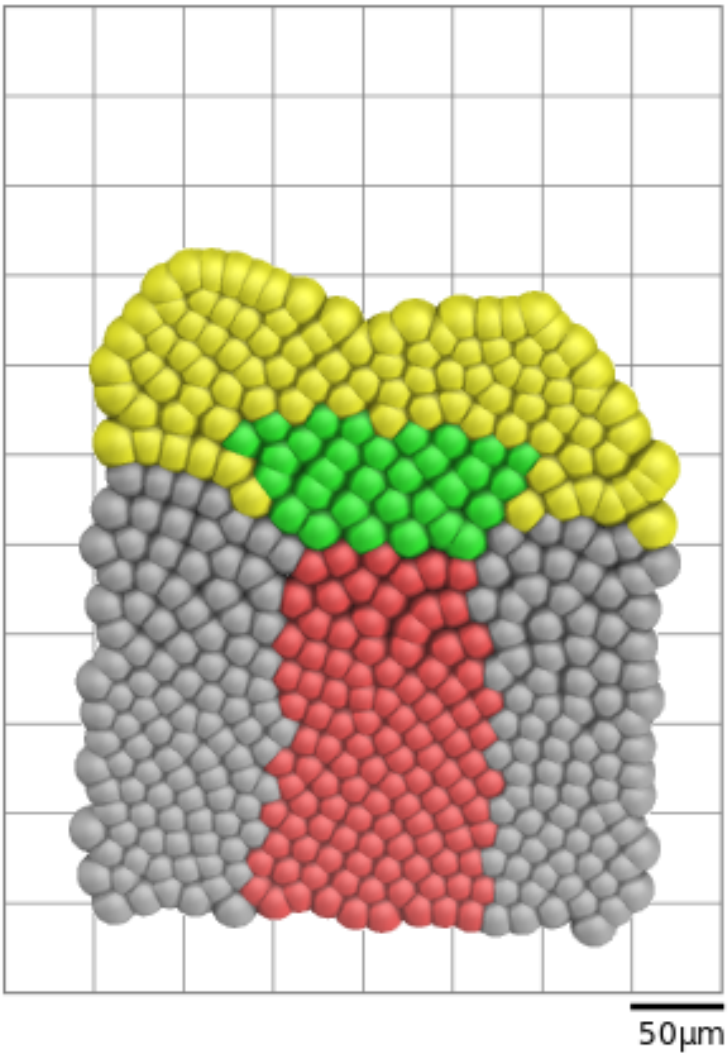

Figure 4.6.: Mobile leaders. *Simulation results with NTCs twice as motile. An oblong shape forms and the notochord widens as the PPM still inhibits forward motion. Rendering of the grid-based simulation results with spheres at each cell center using Pymol.*

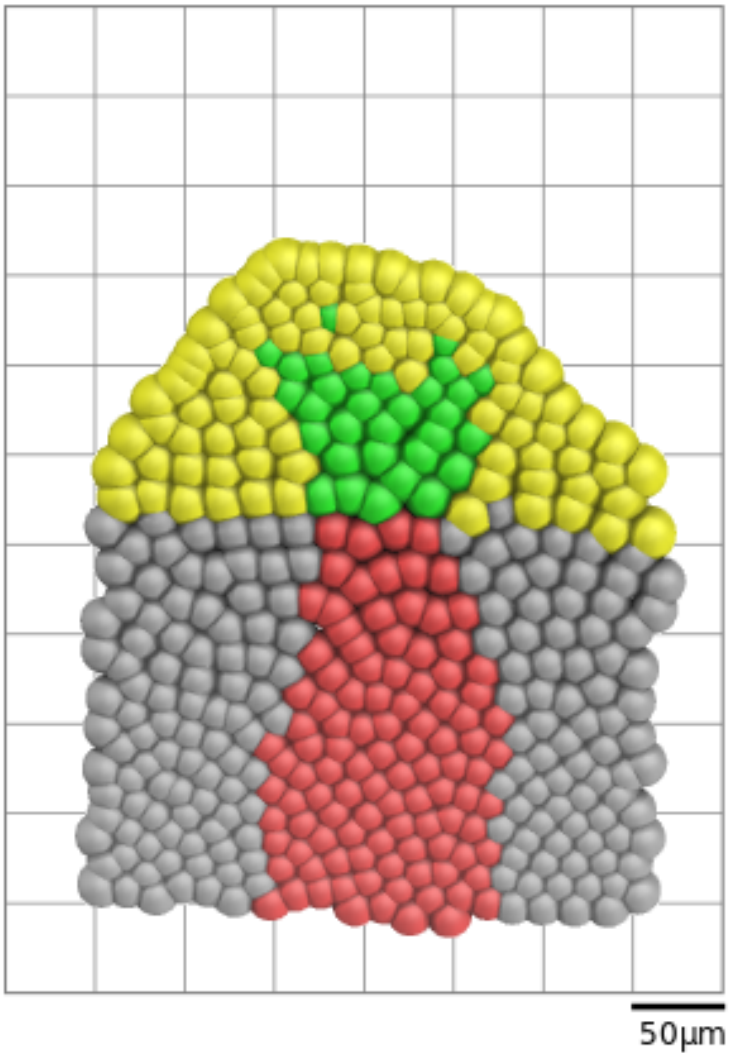

Figure 4.7.: Mobile and adhesive leaders. *Simulation results with NTCs twice as motile and adhesive. The PPM is deformed in a convex way due to the traction of the NTCs. The wildtype shape of the notochord is recovered. Rendering of the grid-based simulation results with spheres at each cell center using Pymol.*

Chapter 5.
5 Conclusions

The study of the physical limitations imposed on biological systems during the early embryonal stages has proven to be a fruitful collaboration between physics and developmental biology. The interplay of experiment and theory was able to clarify and identify key parameters in two important developmental stages. Here I give a brief summary of my findings, and an outlook to future work that can benefit from my results.

5.1. Summary

During this thesis I introduced results of my scientific work within the context of two applications that take place during the early phase of zebrafish gastrulation. They both employ Monte-Carlo based algorithms and minimal parameter simulations for highly complex biological applications in which physical factors are the key ingredients. The first application targets a novel transport mechanism for the morphogen Wnt during the early brain development of zebrafish [2, 83]. The second study is the application of a specialized cellular Potts model, the Glazier-Graner-Hogeweg, in the context of notochord formation [11].

In the context of morphogen transport, I presented my results from a joint experimental study targeting the transport and distribution of Wnt8a in the early phase

of gastrulation. Experimental results suggested that the respective morphogen is actively transported through specialized cytonemes, namely filopodia, a class of cellular actin protrusions. The goal of the computational study was to clarify if such a short-range mode of transport can result in the necessary long-range effects and gradient needed for brain development. The results are reported in a publication by the group of Steffen Scholpp [2].

By implementing a model with a minimal amount of parameters I was able to further study the correlation between filopodia length and the hindbrain/midbrain axis. The complicated tissue dynamics were covered with grid-based simulations for which I fully quantified the necessary parametrization. I concluded that in this model the flux of the first few Wnt active layers is the defining parameter, and that, contrary to trivial logic, it is important that the deposition of Wnt is not perfect. The predicted results for the deposition frequency, along with macroscopic changes for varying filopodia lengths, matched with experimental results.

I was not only able to explain these experimental findings, but also give further theoretical arguments for the role of prepatterning in dynamic scaling. A filopodia-based transport of morphogens determines the cellular fate on a very short time scale, and makes the transport mechanics independent of the spatial size of the individual embryo.

In the second work I used a modified cellular Potts model to study the role of the notochord tip cells within notogenesis. During embryogenesis, elaborate movements and cellular rearrangements take place to generate many organs. The notochord originates from cellular rearrangements in the mesoderm during the gastrulation phase of the embryo. The system is of physical interest as the cellular rearrangements are entirely dependent of the physical properties of three different cell types. I was able to fully parametrize my model from relative forces gained in experiment.

The simulations showed that the NTC marched towards the animal pole as a cohesive cell group during gastrulation. The NTC pushed the anteriorly located PPM ahead, leading to the formation of a convexly curved mesodermal cell sheet.

These results find further evidence in literature. A leading-edge mesodermal cell group to exert a pushing force on the PPM is reported from Xenopus [106]. Further insights from the simulation are that the NTC pulled the notochord plate cells towards the anterior, causing the notochordal plate to intercalate and elongate.

To date, there are two hypotheses explaining the transition of the axial mesodermal sheet into the elongated rod-shaped structure of the notochord. One hypothesis suggests that the notochordal plate cells actively migrate towards the animal pole and thereby extend their cell shape in the anteroposterior direction [107, 108]. However, the blockage of Pcdh18a function, which is equivalent to a speeding up cell motility without increasing cell adheviness, indicate that the inhibition of NTC migration results in a halt in the condensation of the notochordal plate and inhibition of its extension. Therefore, we conclude that highly mobile and adhesive NTCs are required to push against the resistance of the PPM [109]. Only then, the compressive force generated by the notochordal plate cells is released along the anteroposterior axis, leading to the elongation, alignment, and intercalation of the notochord cells.

An additional hypothesis suggests that the two mesodermal wings push the notochordal plate and help to generate the rod-shaped structure of the notochord [110]. This is contrary to the course of events in our simulations as no force or movement of the LPM towards the midline was implemented. Still, LPM cells moved towards the midline as cellular rearrangements condensed the cells of the axial plate. Therefore, simulations suggest that the condensation of the notochord facilitates movement of the LPM cells towards the midline. Consistent with this observation, there is no obvious convergent extension movements in the LPM in mice [105].

5.2. Outlook

While the introduced methods were able to gain a wealth of knowledge, modifications and new experimental setups are still possible. The ideas reported in this work do not only spark new ideas for investigations in physics, but also in biology. It would be interesting to know, what purpose the undeposited Wnt could serve, or if they are recycled.

The simulation scheme introduced for the filopodia-based morphogen transport only covered the basic case of linear and flat tissue growth. Modifications could investigate the role of curvature in the dynamics of the system, or even exact distributions of the ongrowing brain using the three-dimensional results obtained from high-resolution microscopy [10].

Future work could also tackle different patterning scenarios, some of which rely on multiple gradients. One example would be the dorsal-ventral patterning that further modifies the body plan of the embryo.

The Glazier-Graner-Hogeweg models pose interesting questions in non equilibrium thermodynamics. I think a further refinement of these efforts would be fruitful as they scale well on high-performance computing systems and contemporary cancer research is in dire need of models that can describe cell motility and growth.

As always in science, many questions have been solved, but more have been raised.

Acknowledgements

A wide number of people has supported me during the preparation of this thesis and my work.

I would like to thank Prof. Wolfgang Wenzel for accepting this thesis, and giving me the possibility to research these highly interesting interdisciplinary topics.

I would like to thank Prof. Nienhaus for freeing up precious time and being the co-examiner of my thesis.

Furthermore, I would like to thank my immediate supervisor Alexander Schug for the beneficial work environment and introducing me to Steffen Scholpp.

During this thesis I was able to travel to the United States of America with a KHYS Travel grant. I want to thank the KHYS for this amazing opportunity. I would like to thank Prof. José Onuchic for welcoming me in his research group. Even tough the travel had nothing to do with the topics presented in this work, I will always remember these months in the heat of Houston. In his research group I would like to thank in no particular order Heiko Lammert, Faruk Morcos, Mingyang Lu, Michele di Pierro, Lena Simine-Nicolin, Ana Mandić, Jeff Noel, Juliane Zimmermann, Xingcheng Lin, Davit Potoyan, and Mohit Raghunatan for the great time and fun we had. Special thanks go to Ryan Cheng for introducing me to cellular Potts models. Without him, half of this work would probably never have seen the light.

I would like to thank the immediate work group, past and present members. Benjamin Lutz, Shalini John Lovis, Ilaria Mereu, and Ines Reinartz. Although our meeting was brief at the time of writing this, I would also like to thank Jakob Rosenbauer, and Marie Weiel.

Further thanks go to the members of the partner group at INT. Again in no particular order, Prerna Sudera, Timo Strunk, Tobias Neumann, Priya Anand, Florian Gussmann, Thomas Koch, Pascal Friederich, Franz Symalla, Simon Kaiser, Velimir Meded, Manuel Rommel, Manuel Konrad, and Jana Holland-Cunz. Special thanks go to Nana Heilmann; I am grateful for our mutual friendship.

Especially, I would like to thank Steffen Scholpp. Together we were able to bring both physics and biology to their current limits. It was not always easy to find a common language, but we succeeded. Special thanks go to Eliana Stanganello and Bernadett Bösze for conducting the experiments. Further thanks go to our numerous collaborators, funding sources, and those that I have forgotten.

Appendix A.

A Appendix

The diffusion equation for a concentration C at place x at time t for a medium with non-growing domains reads as:

$$\frac{\partial C}{\partial t} - D\frac{\partial^2 C}{\partial x^2} = 0 \tag{A.1}$$

with diffusion constant D. The diffusion constant depends on the geometrical properties of the morphogen.

Since the tissue is a growing and expanding medium, we have to alter equation A.1. After Reynold's theorem, the diffusion equation for a growing domain [74, 75] is

$$\frac{\partial C}{\partial t} + u\frac{\partial C}{\partial x} + C\frac{\partial u}{\partial x} - D\frac{\partial^2 C}{\partial x^2} = 0 \tag{A.2}$$

with the growth field u. The growth field u describes the advection term. As our cells are incompressible, we can disregard the term proportional to $\frac{\partial u}{\partial x}$. For our problem of a growing tissue with length $L(t)$, u is found by

$$u = \frac{dx}{dt} = \frac{\frac{\partial L(t)}{\partial t}}{L(t)} \tag{A.3}$$

The length $L(t)$ of the exponentially growing tissue is found by

$$L(t) = L_0 \cdot e^{\kappa \cdot t} \tag{A.4}$$

Therefore we have

$$u = \kappa \tag{A.5}$$

So u is a constant determined by the growth of the tissue.

To solve this differential equation, numerical methods are available. For this we have to bring equation A.2 into matrix form. A Taylor expansion for the individual derivatives gives the system of equations

$$\frac{\partial C}{\partial t} = \frac{C(t + \Delta t) - C(t)}{\Delta t} \tag{A.6}$$

$$\frac{\partial^2 C}{\partial x^2} = \frac{C(x + \Delta x) - 2C(x) + C(x - \Delta x)}{\Delta x^2} \tag{A.7}$$

Combining equations A.6 and A.7 with equation A.2 leads to

$$\begin{aligned} C(t + \Delta t) = C(t) + \underbrace{D\frac{\Delta t}{\Delta x^2}}_{=s} \left[C(x + \Delta x) - 2C(x) + C(x - \Delta x)\right] - \\ - \underbrace{u\frac{\Delta t}{\Delta x}}_{=v} \left[C(x + \Delta x) - C(x)\right] \end{aligned} \tag{A.8}$$

The discretized version of equation A.8 with the time index n and the spatial index j reads as

$$\begin{aligned} C[n,j] = C[n+1,j+1](v-s) + C[n+1,j](1+2s-v) + \\ + C[n+1,j-1](-s) \end{aligned} \tag{A.9}$$

For five discrete sites the time propagation for one step would read as

$$C[0,1] = -s \cdot C[1,0] + (1+2s-v) \cdot C[1,1] + (v-s) \cdot C[1,2] + 0 \cdot C[1,3] + 0 \cdot C[1,4]$$
$$C[0,2] = 0 \cdot C[1,0] - s \cdot C[1,1] + (1+2s-v) \cdot C[1,2] + (v-s) \cdot C[1,3] + 0 \cdot C[1,4]$$
$$C[0,3] = 0 \cdot C[1,0] + 0 \cdot C[1,1] + -s \cdot C[1,2] + (1+2s-v) \cdot C[1,3] + (v-s) \cdot C[1,4]$$

or as

$$\begin{bmatrix} 1+2s-v & v-s & 0 \\ -s & 1+2s-v & v-s \\ 0 & -s & 1+2s-v \end{bmatrix} \begin{bmatrix} C[1,1] \\ C[1,2] \\ C[1,3] \end{bmatrix} = \begin{bmatrix} C[0,1] + sC[1,0] \\ C[0,2] \\ C[0,3] + (s-v)C[1,4] \end{bmatrix}$$

Larger systems can be parametrized in the same way. Linear algebraic solvers are readily available in most programing languages for soving these systems and evolve the system from one time step to the next.

Bibliography

[1] Claude Sinner, Benjamin Lutz, Abhinav Verma, and Alexander Schug. Revealing the global map of protein folding space by large-scale simulations. *Journal of Chemical Physics*, 143(24), 2015. ISSN 00219606. doi: 10.1063/1.4938172. URL `http://dx.doi.org/10.1063/1.4938172`.
(Not cited.)

[2] Eliana Stanganello, Anja I H Hagemann, Benjamin Mattes, Claude Sinner, Dana Meyen, Sabrina Weber, Alexander Schug, Erez Raz, and Steffen Scholpp. Filopodia-based Wnt transport during vertebrate tissue patterning. *Nature communications*, 6:5846, 2015. ISSN 2041-1723. doi: 10.1038/ncomms6846.
(Cited on pages xi, xiii, xiv, 4, 7, 24, 41, 42, 43, 44, 45, 46, 52, 54, 55, 56, 83, and 84.)

[3] Stefan Bozic, Jens Krüger, Claude Sinner, Benjamin Lutz, Alexander Schug, and Ivan Kondov. Integration of eSBMTools into the MoSGrid portal using the gUSE technology. *Proceedings - 6th International Workshop on Science Gateways, IWSG 2014*, pages 85–90, 2014. ISSN 978-1-4799-5819-1. doi: 10.1109/IWSG.2014.21.
(Not cited.)

[4] Benjamin Lutz, Claude Sinner, Stefan Bozic, Ivan Kondov, and Alexander Schug. Native structure-based modeling and simulation of biomolecular systems per mouse click. *BMC bioinformatics*, 15 (1):292, 2014. ISSN 1471-2105. doi: 10.1186/1471-2105-15-292. URL `http://www.pubmedcentral.nih.gov/articlerender.fcgi?artid=4162935{&}tool=pmcentrez{&}rendertype=abstract`.
(Not cited.)

[5] Claude Sinner, Benjamin Lutz, Shalini John, Ines Reinartz, Abhinav Verma, and Alexander Schug. Simulating biomolecular folding and function by native-structure-based/go-type models. *Israel Journal of Chemistry*, pages 1165–1175, 2014. ISSN 00212148. doi: 10.1002/ijch.201400012.
(Not cited.)

[6] Benjamin Lutz, Claude Sinner, Geertje Heuermann, Abhinav Verma, and Alexander Schug. ESBMTools 1.0: Enhanced native structure-based modeling tools. *Bioinformatics*, 29(21):2795–2796, 2013. ISSN 13674803. doi: 10.1093/bioinformatics/btt478.
(Not cited.)

[7] H M Berman, J Westbrook, Z Feng, G Gilliland, T N Bhat, H Weissig, I N Shindyalov, and P E Bourne. The Protein Data Bank. *Nucleic acids research*, 28(1):235–42, jan 2000. ISSN 0305-1048. URL `http://www.pubmedcentral.nih.gov/articlerender.fcgi?artid=102472{&}tool=pmcentrez{&}rendertype=abstract`.
(Cited on pages xi and 5.)

[8] C.Y. Janda, D. Waghray, A.M. Levin, C. Thomas, and K.C. Garcia. Crystal structure of XWnt8 in complex with the cysteine-rich domain of Frizzled 8. 2012. doi: 10.2210/pdb4f0a/pdb.
(Cited on pages xi and 5.)

[9] Lilianna Solnica-Krezel. Conserved patterns of cell movements during vertebrate gastrulation. *Current Biology*, 15(6):213–228, 2005. ISSN 09609822. doi: 10.1016/j.cub.2005.03.016.
(Cited on pages xii and 12.)

[10] Andrei Y. Kobitski, Jens C. Otte, Masanari Takamiya, Benjamin Schäfer, Jonas Mertes, Johannes Stegmaier, Sepand Rastegar, Francesca Rindone, Volker Hartmann, Rainer Stotzka, Ariel García, Jos van Wezel, Ralf Mikut, Uwe Strähle, and G. Ulrich Nienhaus. An ensemble-averaged, cell density-based digital model of zebrafish embryo development derived from light-sheet microscopy data with single-cell resolution. *Scientific Reports*, 5(i):8601, 2015.

ISSN 2045-2322. doi: 10.1038/srep08601. URL `http://www.nature.com/doifinder/10.1038/srep08601`.
(Cited on pages xiii, 4, 29, 30, 32, and 86.)

[11] Bernadett Bösze, Claude Sinner, Kathrin Stricker, Victor Gourain, Thomas Thumberger, Sabrina Weber, Joachim Wittbrodt, Uwe Strähle, Alexander Schug, and Steffen Scholpp. Pcdh18a-positive tip cells orchestrate notochord formation. *Submitted, to be published in*, 2017.
(Cited on pages xvi, 4, 70, 71, and 83.)

[12] C B Kimmel, W W Ballard, S R Kimmel, B Ullmann, and T F Schilling. Stages of embryonic development of the zebrafish. *Dev Dyn*, 203(3):253–310, 1995. ISSN 1058-8388. doi: 10.1002/aja.1002030302. URL `http://www.ncbi.nlm.nih.gov/pubmed/8589427`.
(Cited on page 2.)

[13] M. Westerfield. *The zebrafish book. A guide for the laboratory use of zebrafish (Danio rerio)*. Univ. of Oregon Press, Eugene, 4 edition, 2000.
(Cited on pages 2, 11, and 29.)

[14] Carl Philipp Heisenberg and Yohanns Bellaïche. XForces in tissue morphogenesis and patterning. *Cell*, 153(5), 2013. ISSN 00928674. doi: 10.1016/j.cell.2013.05.008.
(Cited on page 3.)

[15] Satoshi Kurosaka and Anna Kashina. Cell biology of embryonic migration. *Birth Defects Research Part C - Embryo Today: Reviews*, 84(2):102–122, 2008. ISSN 1542975X. doi: 10.1002/bdrc.20125.
(Cited on page 3.)

[16] A. M. Turing. The chemical basis of morphogenesis. *Philosophical Transactions of the Royal Society of London. Series B, Biological Sciences.*, 237 (641):37–72, 1952. ISSN 00928240.
(Cited on page 4.)

[17] Richard Harland and John Gerhart. Formation and Function of Spemann

' S Organizer. *Annual Reviews of Cellular andDevelopmental Biology*, 13: 611–667, 1997.
(Cited on pages 4 and 11.)

[18] Edward M De Robertis. Spemann's organizer and self-regulation in amphibian embryos. *Nature Reviews Molecular Cell Biology*, 7(4):296–302, 2006. ISSN 1471-0072. doi: 10.1038/nrm1855. URL `http://www.nature.com/doifinder/10.1038/nrm1855`.
(Cited on page 4.)

[19] Patrick Müller and Alexander F. Schier. Extracellular Movement of Signaling Molecules. *Developmental Cell*, 21(1):145–158, 2011. ISSN 15345807. doi: 10.1016/j.devcel.2011.06.001.
(Cited on page 5.)

[20] Ortrud Wartlick, Anna Kicheva, and Marcos González-Gaitán. Morphogen gradient formation. *Cold Spring Harbor perspectives in biology*, 1(3), 2009. ISSN 19430264. doi: 10.1101/cshperspect.a001255.
(Cited on page 5.)

[21] Patrick Müller, Katherine W Rogers, Shuizi R Yu, Michael Brand, and Alexander F Schier. Morphogen transport. *Development (Cambridge, England)*, 140(8):1621–38, 2013. ISSN 1477-9129. doi: 10.1242/dev.083519. URL `http://www.ncbi.nlm.nih.gov/pubmed/23533171`.
(Cited on pages 5 and 6.)

[22] Julia Christina Gross, Varun Chaudhary, Kerstin Bartscherer, and Michael Boutros. Active Wnt proteins are secreted on exosomes. *Nature Cell Biology*, 14(10):1036–1045, 2012. ISSN 1465-7392. doi: 10.1038/ncb2574. URL `http://dx.doi.org/10.1038/ncb2574`.
(Cited on pages 6, 8, and 23.)

[23] Liang Zhang and Jeffrey L. Wrana. The emerging role of exosomes in Wnt secretion and transport. *Current Opinion in Genetics and Development*, 27: 14–19, 2014. ISSN 18790380. doi: 10.1016/j.gde.2014.03.006. URL `http://dx.doi.org/10.1016/j.gde.2014.03.006`.

(Cited on page 6.)

[24] Clotilde Théry, Laurence Zitvogel, and Sebastian Amigorena. Exosomes: composition, biogenesis and function. *Nature reviews. Immunology*, 2(8): 569–579, 2002. ISSN 1474-1733. doi: 10.1038/nri855.
(Cited on page 6.)

[25] Marina Colombo, Graça Raposo, and Clotilde Théry. Biogenesis, Secretion, and Intercellular Interactions of Exosomes and Other Extracellular Vesicles. *Annu. Rev. Cell Dev. Biol*, 30(August):255–89, 2014. ISSN 1081-0706. doi: 10.1146/annurev-cellbio-101512-122326.
(Cited on page 6.)

[26] Shaohua Zhou, Wing Cheong Lo, Jeffrey L. Suhalim, Michelle A. Digman, Enrico Gratton, Qing Nie, and Arthur D. Lander. Free extracellular diffusion creates the Dpp morphogen gradient of the Drosophila wing disc. *Current Biology*, 22(8):668–675, 2012. ISSN 09609822. doi: 10.1016/j.cub.2012.02.065. URL `http://dx.doi.org/10.1016/j.cub.2012.02.065`.
(Cited on pages 6 and 54.)

[27] Shuizi Rachel Yu, Markus Burkhardt, Matthias Nowak, Jonas Ries, Zdenek Petrásek, Steffen Scholpp, Petra Schwille, and Michael Brand. Fgf8 morphogen gradient forms by a source-sink mechanism with freely diffusing molecules. *Nature*, 461(7263):533–6, 2009. ISSN 1476-4687. doi: 10.1038/nature08391. URL `http://www.ncbi.nlm.nih.gov/pubmed/19741606`.
(Cited on page 6.)

[28] F. A. Ramírez-Weber and Thomas B. Kornberg. Cytonemes: Cellular processes that project to the principal signaling center in Drosophila imaginal discs. *Cell*, 97(5):599–607, 1999. ISSN 00928674. doi: 10.1016/S0092-8674(00)80771-0.
(Cited on page 6.)

[29] T B Kornberg and S Roy. Cytonemes as specialized signaling filopodia. *Development*, 141(4):729–736, 2014. ISSN 0950-1991. doi: 10.1242/dev.086223. URL `http://www.ncbi.nlm.nih.gov/pubmed/24496611`.

(Cited on page 6.)

[30] J Miller, S E Fraser, and D McClay. Dynamics of thin filopodia during sea urchin gastrulation. *Development (Cambridge, England)*, 121(8): 2501–2511, 1995. ISSN 0950-1991. URL papers2://publication/uuid/0B52E584-6D6F-4554-8793-1AD486189855.
(Cited on page 6.)

[31] Pieta K. Mattila and Pekka Lappalainen. Filopodia: molecular architecture and cellular functions. *Nature Reviews Molecular Cell Biology*, 9(6):446–454, 2008. ISSN 1471-0072. doi: 10.1038/nrm2406. URL http://www.nature.com/doifinder/10.1038/nrm2406.
(Cited on page 6.)

[32] Stephane Angers and Randall T Moon. Proximal events in Wnt signal transduction. *Nature reviews. Molecular cell biology*, 10(7):468–77, 2009. ISSN 1471-0080. doi: 10.1038/nrm2717. URL http://www.ncbi.nlm.nih.gov/pubmed/19536106.
(Cited on pages 8 and 42.)

[33] Hans Clevers and Roel Nusse. Wnt/β-catenin signaling and disease. *Cell*, 149(6):1192–1205, 2012. ISSN 00928674. doi: 10.1016/j.cell.2012.05.012.
(Cited on pages 8 and 42.)

[34] A J Mikels and R Nusse. Wnts as ligands: processing, secretion and reception. *Oncogene*, 25(57):7461–7468, 2006. ISSN 0950-9232. doi: 10.1038/sj.onc.1210053. URL http://www.ncbi.nlm.nih.gov/pubmed/17143290.
(Cited on page 8.)

[35] Fillip Port and Konrad Basler. Wnt Trafficking: New Insights into Wnt Maturation, Secretion and Spreading. *Traffic*, 11(10):1265–1271, 2010. ISSN 13989219. doi: 10.1111/j.1600-0854.2010.01076.x.
(Cited on pages 8 and 42.)

[36] Kerstin Bartscherer, Nadège Pelte, Dierk Ingelfinger, and Michael Boutros. Secretion of Wnt Ligands Requires Evi, a Conserved Transmembrane Protein.

Cell, 125(3):523–533, 2006. ISSN 00928674. doi: 10.1016/j.cell.2006.04.009.
(Cited on page 8.)

[37] Carla Bänziger, Davide Soldini, Corina Schütt, Peder Zipperlen, George Hausmann, and Konrad Basler. Wntless, a Conserved Membrane Protein Dedicated to the Secretion of Wnt Proteins from Signaling Cells. *Cell*, 125 (3):509–522, 2006. ISSN 00928674. doi: 10.1016/j.cell.2006.02.049.
(Cited on page 8.)

[38] Damien Y. M. Coudreuse, Giulietta Roel, Marco C. Betist, and Olivier Destree Hendrik C. Korswagen. References and Notes 1. *Science*, 312(5775): 921–924, 2006. ISSN 0036-8075. doi: 10.1126/science.1124856.
(Cited on page 8.)

[39] Tatjana Holzer, Katrin Liffers, Karolin Rahm, Benjamin Trageser, Suat Özbek, and Dietmar Gradl. Live imaging of active fluorophore labelled Wnt proteins. *FEBS Letters*, 586(11):1638–1644, 2012. ISSN 00145793. doi: 10.1016/j.febslet.2012.04.035. URL `http://dx.doi.org/10.1016/j.febslet.2012.04.035`.
(Cited on pages 8 and 42.)

[40] Kimberly A Mulligan, Christophe Fuerer, Wendy Ching, Matt Fish, Karl Willert, and Roeland Nusse. Secreted Wingless-interacting molecule {(Swim)} promotes long-range signaling by maintaining Wingless solubility. *Proc. Natl. Acad. Sci. {U.S.A.}*, 109(2):370–377, 2012. ISSN 0027-8424. doi: 10.1073/pnas.1119197109.
(Cited on pages 8 and 23.)

[41] Shinya Matsuda and Osamu Shimmi. Directional transport and active retention of Dpp/BMP create wing vein patterns in Drosophila. *Developmental Biology*, 366(2):153–162, 2012. ISSN 00121606. doi: 10.1016/j.ydbio.2012.04.009. URL `http://dx.doi.org/10.1016/j.ydbio.2012.04.009`.
(Not cited.)

[42] A Sawala, C Sutcliffe, and H L Ashe. Multistep molecular mechanism for bone morphogenetic protein extracellular transport in the

Drosophila embryo. *Proc Natl Acad Sci U S A*, 109(28):11222–11227, 2012. ISSN 0027-8424. doi: 10.1073/pnas.1202781109. URL http://www.ncbi.nlm.nih.gov/pubmed/22733779$\delimiter"026E30F$nhttp://www.pnas.org/content/109/28/11222.full.pdf.
(Cited on page 8.)

[43] Valentina Greco, Michael Hannus, and Suzanne Eaton. Argosomes. *Cell*, 106(5):633–645, 2001. ISSN 00928674. doi: 10.1016/S0092-8674(01)00484-6. URL http://linkinghub.elsevier.com/retrieve/pii/S0092867401004846.
(Cited on pages 8 and 23.)

[44] Karen Beckett, Solange Monier, Lucy Palmer, Cyrille Alexandre, Hannah Green, Eric Bonneil, Graca Raposo, Pierre Thibault, Roland Le Borgne, and Jean Paul Vincent. Drosophila S2 cells secrete wingless on exosome-like vesicles but the wingless gradient forms independently of exosomes. *Traffic*, 14 (1):82–96, 2013. ISSN 13989219. doi: 10.1111/tra.12016.
(Cited on pages 8 and 23.)

[45] Katherine W. Rogers and Alexander F. Schier. Morphogen Gradients: From Generation to Interpretation. *Annual Review of Cell and Developmental Biology*, 27(1):377–407, 2011. ISSN 1081-0706. doi: 10.1146/annurev-cellbio-092910-154148.
(Cited on page 8.)

[46] L. Wolpert. Positional information and the spatial pattern of cellular differentiation. *Journal of Theoretical Biology*, 25(1):1–47, 1969. ISSN 00225193. doi: 10.1016/S0022-5193(69)80016-0. URL http://www.sciencedirect.com/science/article/pii/S0022519369800160.
(Cited on page 8.)

[47] Anja I H Hagemann, Jennifer Kurz, Silke Kauffeld, Qing Chen, Patrick M Reeves, Sabrina Weber, Simone Schindler, Gary Davidson, Tomas Kirchhausen, and Steffen Scholpp. In-vivo analysis of formation and endocytosis of the Wnt/β-Catenin signaling complex in zebrafish embryos. *Journal of cell*

science, (July):3970–3982, 2014. ISSN 1477-9137. doi: 10.1242/jcs.148767. URL `http://www.ncbi.nlm.nih.gov/pubmed/25074807`.
(Cited on page 8.)

[48] Daniela Peukert, Sabrina Weber, Andrew Lumsden, and Steffen Scholpp. Lhx2 and Lhx9 determine neuronal differentiation and compartition in the caudal forebrain by regulating Wnt signaling. *PLoS Biology*, 9(12), 2011. ISSN 15449173. doi: 10.1371/journal.pbio.1001218.
(Cited on page 8.)

[49] S a Sandersius, C J Weijer, and T J Newman. Emergent cell and tissue dynamics from subcellular modeling of active biomechanical processes. *Physical biology*, 8(4):045007, 2011. ISSN 1478-3975. doi: 10.1088/1478-3975/8/4/045007.
(Cited on page 10.)

[50] Shuichi Hayashi and Masatoshi Takeichi. Emerging roles of protocadherins: from self-avoidance to enhancement of motility. *Journal of cell science*, 128 (8):1455–1464, 2015. ISSN 1477-9137. doi: 10.1242/jcs.166306. URL `http://jcs.biologists.org/content/128/8/1455.full`.
(Cited on page 10.)

[51] Jean Léon Maître and Carl Philipp Heisenberg. Three functions of cadherins in cell adhesion. *Current Biology*, 23(14):626–633, 2013. ISSN 09609822. doi: 10.1016/j.cub.2013.06.019.
(Cited on page 10.)

[52] Shinichi Hayashi, Koji Tamura, and Hitoshi Yokoyama. Yap1, transcription regulator in the Hippo signaling pathway, is required for Xenopus limb bud regeneration. *Developmental Biology*, 388(1):57–67, 2014. ISSN 1095564X. doi: 10.1016/j.ydbio.2014.01.018. URL `http://dx.doi.org/10.1016/j.ydbio.2014.01.018`.
(Cited on pages 10 and 20.)

[53] Xuejun Chen, Eunjin Koh, Michael Yoder, and Barry M. Gumbiner. A protocadherin-cadherin-FLRT3 complex controls cell adhesion and morpho-

genesis. *PLoS ONE*, 4(12), 2009. ISSN 19326203. doi: 10.1371/journal.pone.0008411.
(Cited on page 10.)

[54] Lila Solnica-Krezel and Diane S Sepich. Gastrulation: Making and Shaping Germ Layers. *Annu. Rev. Cell Dev. Biol*, 28:687–717, 2012. ISSN 1081-0706. doi: 10.1146/annurev-cellbio-092910-154043.
(Cited on page 11.)

[55] Derek L Stemple. Structure and function of the notochord: an essential organ for chordate development. *Development (Cambridge, England)*, 132 (11):2503–2512, 2005. ISSN 0950-1991. doi: 10.1242/dev.01812.
(Cited on pages 13 and 68.)

[56] David Kimelman and Kevin JP Griffin. Vertebrate mesendoderm induction and patterning. *Current Opinion in Genetics and Development*, 10(4):350–356, 2000. ISSN 0959437X. doi: 10.1016/S0959-437X(00)00095-2.
(Cited on page 13.)

[57] François Graner and James A. Glazier. Simulation of biological cell sorting using a two-dimensional extended Potts model. *Physical Review Letters*, 69 (13):2013–2016, 1992. ISSN 00319007. doi: 10.1103/PhysRevLett.69.2013.
(Cited on pages 15, 34, and 72.)

[58] J.A. Glazier, A. Balter, and Poplawski N.I. *Single-Cell Based Models in Biology and Medicine*. Birkhäuser, 2007. ISBN 978-3-7643-8101-1.
(Cited on pages 15, 37, 38, and 73.)

[59] T. Strunk, M. Wolf, M. Brieg, K. Klenin, a. Biewer, F. Tristram, M. Ernst, P. J. Kleine, N. Heilmann, I. Kondov, and W. Wenzel. SIMONA 1.0: An efficient and versatile framework for stochastic simulations of molecular and nanoscale systems. *Journal of Computational Chemistry*, 33:2602–2613, 2012. ISSN 01928651. doi: 10.1002/jcc.23089.
(Cited on pages 17 and 37.)

[60] Nicholas Metropolis and S Ulam. The Monte Carlo Method, 1949. ISSN 0162-

1459. URL http://www.tandfonline.com/doi/abs/10.1080/01621459.1949.10483310.
(Cited on page 17.)

[61] G E Moore. Cramming more components onto integrated circuits (Reprinted from Electronics, pg 114-117, April 19, 1965). *Proceedings Of The Ieee*, 86(1):82–85, 1965. ISSN 1098-4232. doi: 10.1109/N-SSC.2006.4785860. URL papers3://publication/uuid/8E5EB7C8-681C-447D-9361-E68D1932997D.
(Cited on page 20.)

[62] Simon Tanaka, David Sichau, and Dagmar Iber. LBIB Cell: A cell-based simulation environment for morphogenetic problems. *Bioinformatics*, 31(14): 2340–2347, 2015. ISSN 14602059. doi: 10.1093/bioinformatics/btv147.
(Cited on page 20.)

[63] Simon Tanaka. Simulation Frameworks for Morphogenetic Problems. *Computation*, 3(2):197–221, 2015. ISSN 2079-3197. doi: 10.3390/computation3020197. URL http://www.mdpi.com/2079-3197/3/2/197/.
(Cited on page 21.)

[64] Edward K. Rodriguez, Anne Hoger, and Andrew D. McCulloch. Stress-dependent finite growth in soft elastic tissues. *Journal of Biomechanics*, 27 (4):455–467, 1994. ISSN 00219290. doi: 10.1016/0021-9290(94)90021-3.
(Cited on page 21.)

[65] Benjamen A. Filas, Alina Oltean, David C. Beebe, Ruth J. Okamoto, Philip V. Bayly, and Larry A. Taber. A potential role for differential contractility in early brain development and evolution. *Biomechanics and Modeling in Mechanobiology*, 11(8):1251–1262, 2012. ISSN 16177959. doi: 10.1007/s10237-012-0389-4.
(Cited on page 21.)

[66] Yeh Shiu Chu, Sylvie Dufour, Jean Paul Thiery, Eric Perez, and Frederic Pincet. Johnson-Kendall-Roberts theory applied to living cells. *Physical Review Letters*, 94(2):1–4, 2005. ISSN 00319007. doi: 10.1103/PhysRevLett.

94.028102.
(Cited on page 21.)

[67] D. Drasdo, R. Kree, and J. S. McCaskill. Monte Carlo approach to tissue-cell populations. *Physical Review E*, 52(6):6635–6657, 1995. ISSN 1063651X. doi: 10.1103/PhysRevE.52.6635.
(Cited on page 21.)

[68] Hisao Honda and Goro Eguchi. How much does the cell boundary contract in a monolayered cell sheet? *Journal of Theoretical Biology*, 84(3):575–588, 1980. ISSN 10958541. doi: 10.1016/S0022-5193(80)80021-X.
(Cited on page 22.)

[69] Ernst Ising. Beitrag zur Theorie des Ferromagnetismus. *Zeitschrift für Physik*, 31(1):253–258, 1925. ISSN 00443328. doi: 10.1007/BF02980577.
(Cited on page 23.)

[70] Lars Onsager. Crystal statistics. I. A two-dimensional model with an order-disorder transition. *Physical Review*, 65(3-4):117–149, 1944. ISSN 0031899X. doi: 10.1103/PhysRev.65.117.
(Cited on page 23.)

[71] R.B. Potts and C. Domb. Some generalized order-disorder transformations. *Mathematical Proceedings of the Cambridge Philosophical Society*, 48(1):106–109, 1952. ISSN 0305-0041. doi: 10.1017/S0305004100027419. URL `http://www.journals.cambridge.org/abstract{_}S0305004100027419`.
(Cited on pages 23 and 34.)

[72] F. Y. Wu. The Potts model. *Reviews of Modern Physics*, 54(1):235–268, jan 1982. ISSN 0034-6861. doi: 10.1103/RevModPhys.54.235. URL `http://link.aps.org/doi/10.1103/RevModPhys.54.235`.
(Not cited.)

[73] J. Ashkin and E. Teller. Statistics of two-dimensional lattices with four components. *Physical Review*, 64(5-6):178–184, 1943. ISSN 0031899X. doi: 10.1103/PhysRev.64.178.

(Cited on page 23.)

[74] Patrick Fried and Dagmar Iber. Read-out of dynamic morphogen gradients on growing domains. *PLoS ONE*, 10(11):1–12, 2015. ISSN 19326203. doi: 10.1371/journal.pone.0143226. URL `http://dx.doi.org/10.1038/ncomms6077`.
(Cited on pages 23, 56, and 91.)

[75] Dagmar Iber, Simon Tanaka, Patrick Fried, Philipp Germann, and Denis Menshykau. *Simulating Tissue Morphogenesis and Signaling*, pages 323–338. Springer New York, New York, NY, 2015. ISBN 978-1-4939-1164-6. doi: 10.1007/978-1-4939-1164-6_21. URL `http://dx.doi.org/10.1007/978-1-4939-1164-6{_}21`.
(Cited on pages 23 and 91.)

[76] Johannes Stegmaier, Jens C. Otte, Andrei Kobitski, Andreas Bartschat, Ariel Garcia, G. Ulrich Nienhaus, Uwe Strähle, and Ralf Mikut. Fast segmentation of stained nuclei in terabyte-scale, time resolved 3D microscopy image stacks. *PLoS ONE*, 9(2):1–11, 2014. ISSN 19326203. doi: 10.1371/journal.pone.0090036.
(Cited on page 30.)

[77] Johannes Stegmaier, Fernando Amat, William C. Lemon, Katie McDole, Yinan Wan, George Teodoro, Ralf Mikut, and Philipp J. Keller. Real-Time Three-Dimensional Cell Segmentation in Large-Scale Microscopy Data of Developing Embryos. *Developmental Cell*, 36(2):225–240, 2016. ISSN 18781551. doi: 10.1016/j.devcel.2015.12.028. URL `http://dx.doi.org/10.1016/j.devcel.2015.12.028`.
(Cited on page 30.)

[78] Lynn White. Sc Ie : Nce :. 155(3767):1203–1207, 1967.
(Cited on page 34.)

[79] J a Glazier and D Weaire. The kinetics of cellular patterns. *Journal of Physics: Condensed Matter*, 4(8):1867–1894, 1999. ISSN 0953-8984. doi: 10.1088/0953-8984/4/8/004.

(Cited on pages 34 and 36.)

[80] Brenda M Rubenstein and Laura J Kaufman. The role of extracellular matrix in glioma invasion: a cellular Potts model approach. *Biophysical journal*, 95(12):5661–80, 2008. ISSN 1542-0086. doi: 10.1529/biophysj.108.140624. URL `http://www.pubmedcentral.nih.gov/articlerender.fcgi?artid=2599859{&}tool=pmcentrez{&}rendertype=abstract`.
(Cited on page 38.)

[81] S Turner and J A Sherratt. Intercellular adhesion and cancer invasion: a discrete simulation using the extended Potts model. *Journal of theoretical biology*, 216(1):85–100, 2002. ISSN 0022-5193. doi: 10.1006/jtbi.2001.2522. URL `papers://26be3d2d-f137-49d6-b32d-2a0d64de49bd/Paper/p2520`.
(Cited on page 38.)

[82] R. M H Merks, Erica D. Perryn, Abbas Shirinifard, and James A. Glazier. Contact-inhibited chemotaxis in de novo and sprouting blood-vessel growth. *PLoS Computational Biology*, 4(9), 2008. ISSN 1553734X. doi: 10.1371/journal.pcbi.1000163.
(Cited on pages 38, 73, and 74.)

[83] Eliana Stanganello and Steffen Scholpp. Role of cytonemes in Wnt transport. *Journal of cell science*, 129(4):665–72, 2016. ISSN 1477-9137. doi: 10.1242/jcs.182469. URL `http://www.ncbi.nlm.nih.gov/pubmed/26823607`.
(Cited on pages 42 and 83.)

[84] Makoto Sato and Thomas B. Kornberg. FGF is an essential mitogen and chemoattractant for the air sacs of the Drosophila tracheal system. *Developmental Cell*, 3(2):195–207, 2002. ISSN 15345807. doi: 10.1016/S1534-5807(02)00202-2.
(Cited on page 43.)

[85] Cyrille De Joussineau, Jonathan Soule, Marianne Martin, Christelle Anguille, and Philippe Montcourrier & Daniel Alexandre. Delta-promoted filopodia mediate long-range lateral inhibition in Drosophila. *Nature*, 426(December):555–559, 2003. ISSN 1476-4687. doi: 10.1038/nature02143.1.

(Cited on page 43.)

[86] Sougata Roy, Hai Huang, Songmei Liu, and Thomas B Kornberg. Cytoneme-mediated contact-dependent transport of the Drosophila decapentaplegic signaling protein. *Science (New York, N.Y.)*, 343(6173): 1244624, 2014. ISSN 1095-9203. doi: 10.1126/science.1244624. URL `http://www.pubmedcentral.nih.gov/articlerender.fcgi?artid=4336149{&}tool=pmcentrez{&}rendertype=abstract`.
(Cited on page 43.)

[87] Timothy a Sanders, Esther Llagostera, and Maria Barna. Specialized filopodia direct long-range transport of SHH during vertebrate tissue patterning. *Nature*, 497(7451):628–32, 2013. ISSN 1476-4687. doi: 10.1038/nature12157. URL `http://www.ncbi.nlm.nih.gov/pubmed/23624372`.
(Cited on page 43.)

[88] Corinne L. Fairchild and Maria Barna. Specialized filopodia: At the 'tip' of morphogen transport and vertebrate tissue patterning. *Current Opinion in Genetics and Development*, 27:67–73, 2014. ISSN 18790380. doi: 10.1016/j.gde.2014.03.013. URL `http://dx.doi.org/10.1016/j.gde.2014.03.013`.
(Cited on page 43.)

[89] Marcus Bischoff, Ana-Citlali Gradilla, Irene Seijo, Germán Andrés, Carmen Rodríguez-Navas, Laura González-Méndez, and Isabel Guerrero. Cytonemes are required for the establishment of a normal Hedgehog morphogen gradient in Drosophila epithelia. *Nature cell biology*, 15(11):1269–81, 2013. ISSN 1476-4679. doi: 10.1038/ncb2856. URL `http://www.pubmedcentral.nih.gov/articlerender.fcgi?artid=3840581{&}tool=pmcentrez{&}rendertype=abstract`.
(Cited on page 43.)

[90] A. Kicheva, P. Pantazis, T. Bollenbach, Y. Kalaidzidis, T. Bittig, F. Julicher, and M. Gonzalez-Gaitan. Kinetics of Morphogen Gradient Formation. *Science*, 315(5811):521–525, jan 2007. ISSN 0036-8075. doi: 10.1126/science.1135774. URL `http://www.sciencemag.org/cgi/doi/10.1126/science.`

1135774.
(Cited on page 54.)

[91] Patrick Fried, Máximo Sánchez-Aragón, Daniel Aguilar-Hidalgo, Birgitta Lehtinen, Fernando Casares, and Dagmar Iber. A Model of the Spatio-temporal Dynamics of Drosophila Eye Disc Development. *PLOS Computational Biology*, 12(9):e1005052, 2016. ISSN 1553-7358. doi: 10.1371/journal.pcbi.1005052. URL http://dx.plos.org/10.1371/journal.pcbi.1005052.
(Cited on page 56.)

[92] Claudio D Stern. Neural induction: old problem, new findings, yet more questions. *Development (Cambridge, England)*, 132(9):2007–21, 2005. ISSN 0950-1991. doi: 10.1242/dev.01794. URL http://www.ncbi.nlm.nih.gov/pubmed/15829523.
(Cited on page 68.)

[93] Cornelis J Weijer. Collective cell migration in development. *Journal of cell science*, 122(Pt 18):3215–3223, 2009. ISSN 1477-9137. doi: 10.1242/jcs.036517.
(Cited on page 68.)

[94] R M Warga and Charles B Kimmel. Cell movements during epiboly and gastrulation in zebrafish. *Development*, 108(4):569–580, 1990. ISSN 0950-1991. URL http://www.ncbi.nlm.nih.gov/pubmed/2387236$\delimiter"026E30F$nhttp://www.ncbi.nlm.nih.gov/entrez/query.fcgi?cmd=Retrieve{&}db=PubMed{&}dopt=Citation{&}list{_}uids=2387236.
(Cited on page 68.)

[95] Juan-Antonio Montero, Lara Carvalho, Michaela Wilsch-Bräuninger, Beate Kilian, Chigdem Mustafa, and Carl-Philipp Heisenberg. Shield formation at the onset of zebrafish gastrulation. *Development (Cambridge, England)*, 132 (6):1187–1198, 2005. ISSN 0950-1991. doi: 10.1242/dev.01667.
(Cited on page 68.)

[96] M. Tada and C.-P. Heisenberg. Convergent extension: using collective cell migration and cell intercalation to shape embryos. *Development*, 139(21): 3897–3904, 2012. ISSN 0950-1991. doi: 10.1242/dev.073007.
(Cited on page 68.)

[97] Eric Theveneau and Roberto Mayor. Neural crest delamination and migration: From epithelium-to-mesenchyme transition to collective cell migration. *Developmental Biology*, 366(1):34–54, 2012. ISSN 00121606. doi: 10.1016/j.ydbio.2011.12.041. URL `http://dx.doi.org/10.1016/j.ydbio.2011.12.041`.
(Cited on page 69.)

[98] Florian Ulrich, Michael Krieg, Eva Maria Schötz, Vinzenz Link, Irinka Castanon, Viktor Schnabel, Anna Taubenberger, Daniel Mueller, Pierre Henri Puech, and Carl Philipp Heisenberg. Wnt11 functions in gastrulation by controlling cell cohesion through Rab5c and E-Cadherin. *Developmental Cell*, 9 (4):555–564, 2005. ISSN 15345807. doi: 10.1016/j.devcel.2005.08.011.
(Cited on page 69.)

[99] I. Roszko, D. S. Sepich, J. R. Jessen, a. Chandrasekhar, and L. Solnica-Krezel. A dynamic intracellular distribution of Vangl2 accompanies cell polarization during zebrafish gastrulation. *Development*, 142(14):2508–2520, 2015. ISSN 0950-1991. doi: 10.1242/dev.119032. URL `http://dev.biologists.org/cgi/doi/10.1242/dev.119032`.
(Cited on page 69.)

[100] Paul Skoglund and Ray Keller. Integration of planar cell polarity and ECM signaling in elongation of the vertebrate body plan. *Current Opinion in Cell Biology*, 22(5):589–596, 2010. ISSN 09550674. doi: 10.1016/j.ceb.2010.07.012. URL `http://dx.doi.org/10.1016/j.ceb.2010.07.012`.
(Cited on page 69.)

[101] Emil Aamar and Igor B. Dawid. Protocadherin-18a has a role in cell adhesion, behavior and migration in zebrafish development. *Developmental Biology*, 318 (2):335–346, 2008. ISSN 00121606. doi: 10.1016/j.ydbio.2008.03.040.

(Cited on page 69.)

[102] Alexa Burger, Helen Lindsay, Anastasia Felker, Christopher Hess, Carolin Anders, Elena Chiavacci, Jonas Zaugg, Lukas M Weber, Raul Catena, Martin Jinek, Mark D Robinson, and Christian Mosimann. Maximizing mutagenesis with solubilized CRISPR-Cas9 ribonucleoprotein complexes. *Development*, 143(11):2025–2037, 2016. ISSN 0950-1991. doi: 10.1242/dev.134809. URL `http://www.ncbi.nlm.nih.gov/pubmed/27130213$\delimiter"026E30F$nhttp://dev.biologists.org/lookup/doi/10.1242/dev.134809`.
(Cited on page 70.)

[103] a Medina and H Steinbeisser. Interaction of Frizzled 7 and Dishevelled in Xenopus. *Developmental dynamics : an official publication of the American Association of Anatomists*, 218(4):671–80, 2000. ISSN 1058-8388. doi: 10.1002/1097-0177(2000)9999:9999<::AID-DVDY1017>3.0.CO;2-9. URL `http://www.ncbi.nlm.nih.gov/pubmed/10906785`.
(Cited on page 71.)

[104] Jianyong Chen, Sin Park Chang, and Shao Jun Tang. Activity-dependent synaptic Wnt release regulates hippocampal long term potentiation. *Journal of Biological Chemistry*, 281(17):11910–11916, 2006. ISSN 00219258. doi: 10.1074/jbc.M511920200.
(Cited on page 72.)

[105] Patricia Ybot-Gonzalez, Dawn Savery, Dianne Gerrelli, Massimo Signore, Claire E Mitchell, Clare H Faux, Nicholas D E Greene, and Andrew J Copp. Convergent extension, planar-cell-polarity signalling and initiation of mouse neural tube closure. *Development (Cambridge, England)*, 134(4):789–99, 2007. ISSN 0950-1991. doi: 10.1242/dev.000380. URL `http://dev.biologists.org/content/134/4/789.short`.
(Cited on pages 77 and 85.)

[106] Yusuke Hara, Kazuaki Nagayama, Takamasa S. Yamamoto, Takeo Matsumoto, Makoto Suzuki, and Naoto Ueno. Directional migration of leading-

edge mesoderm generates physical forces: Implication in Xenopus notochord formation during gastrulation. *Developmental Biology*, 382(2):482–495, 2013. ISSN 00121606. doi: 10.1016/j.ydbio.2013.07.023. URL `http://dx.doi.org/10.1016/j.ydbio.2013.07.023`.
(Cited on page 85.)

[107] Ray Keller. Shaping the vertebrate body plan by polarized embryonic cell movements. *Science (New York, N.Y.)*, 298(5600):1950–1954, 2002. ISSN 00368075. doi: 10.1126/science.1079478.
(Cited on page 85.)

[108] Ray Keller. Cell migration during gastrulation. *Current Opinion in Cell Biology*, 17(5 SPEC. ISS.):533–541, 2005. ISSN 09550674. doi: 10.1016/j.ceb.2005.08.006.
(Cited on page 85.)

[109] J. G. Dumortier, S. Martin, D. Meyer, F. M. Rosa, and N. B. David. Collective mesendoderm migration relies on an intrinsic directionality signal transmitted through cell contacts. *Proceedings of the National Academy of Sciences*, 109 (42):16945–16950, 2012. ISSN 0027-8424. doi: 10.1073/pnas.1205870109.
(Cited on page 85.)

[110] Sophie Balmer, Sonja Nowotschin, and Anna Katerina Hadjantonakis. Notochord morphogenesis in mice: Current understanding and open questions. *Developmental Dynamics*, 245(5):547–557, 2016. ISSN 10970177. doi: 10.1002/dvdy.24392.
(Cited on page 85.)

List of publications and contributions

2015

- Revealing the global map of protein folding space by large-scale simulations; **C. Sinner**, B. Lutz, A. Verma, A. Schug; *The Journal of Chemical Physics 143 (24)*: 243154.
- Filopodia based Wnt transport during vertebrate tissue patterning; E. Stanganello, A.I.H. Hagemann, B. Mattes, **C. Sinner**, D. Meyen, S. Weber, A. Schug, E. Raz, S. Scholpp; *Nature communications 6*: article number 5846.

2014

- [**Proceedings**] Integration of eSBMTools into the MoSGrid portal; S. Bozic, J. Krüger, **C. Sinner**, B. Lutz, A. Schug, I. Kondov, 2014; *6th International Workshop on Science Gateways(IWSG 2014)*: 85-90.
- Native structure-based modeling and biomolecular systems per mouse click; B. Lutz, **C. Sinner**, S. Bozic, I. Kondov, A. Schug; *BMC Bioinformatics 15*: 292.
- Simulating Biomolecular Folding and Function by Native-Structure-Based/Go-Type Models; **C. Sinner**, B. Lutz, S. John, I. Reinartz, A. Verma, A. Schug, 2014; *Israel Journal of Chemistry 54(8-9)*: 1165-1175.

2013

- esbmtools 1.0: enhanced structure-based modeling tools; B. Lutz, **C. Sinner**, G. Heuermann, A. Verma, A. Schug, 2013; *Bioinformatics 29(21)*: 2795-2796.

2012

- Agrotis puta (Hübner, 1803), a species of Macroheterocera new to the fauna of Luxembourg (Insecta, Lepidoptera, Noctuidae); **C. Sinner**, 2012; *Bulletin de la Société des naturalistes luxembourgeois 113*: 165-166.